Dual catalytic systems for cross dehydrogenative coupling toward donor-acceptor conjugated polymer synthesis

Liwen Xing

A dissertation

submitted in partial fulfillment of the

requirements for the degree of

Doctor of Philosophy

University of Washington

2022

Reading Committee:

Christine K. Luscombe, Chair

Gojko Lalic

Alshakim Nelson

Program Authorized to Offer Degree:

Molecular Engineering: Data Science

University of Washington

Abstract

Dual catalytic systems for cross dehydrogenative coupling toward donor-acceptor conjugated polymer synthesis

Liwen Xing

Chair of the Supervisory Committee:
Professor Christine K. Luscombe
Materials Science & Engineering

Donor-acceptor (D-A) conjugated polymers, as one type of organic semiconducting materials, have drawn lots of attention for the application in organic electronics due to their lowered band gaps and high charge mobility. The polymerization based on cross dehydrogenative coupling (CDC) is an atom-economic synthetic method for D-A polymers as it significantly simplifies the overall synthetic routes by applying C-H bond activation during the polymerization. Two different dual catalytic systems – Au/Ag and Pd/Ag for CDC polymerizations were investigated here. Despite both transformations occurring by a similar mechanistic sequence, dramatically different kinetic behaviors and polymerization results were discovered. The Pd/Ag system produced unexpectedly low homocoupling defects and high molecular weight polymers despite the small molecule coupling reaction proceeding inefficiently. Conversely, Au/Ag system produced low molecular weight polymers with lots of homocoupling defects while catalyzing an efficient small molecule coupling reaction. While the findings in this work provide valuable insight for future studies in obtaining high-molecular weight D-A polymers via CDC, these findings could affect the design of substrates in late-stage C−H functionalization.

ACKNOWLEDGMENTS

This work would not have been possible without the guidance and support of my advisor Prof. Christine Luscombe. She showed me patience and encouragement throughout the duration of my PhD. I learned tremendously from her in terms of being a good scientist, researcher, writer, and a human being.

I would like to express my deepest appreciation to all Luscombe group members. They generously shared their expertise when I encountered difficulties in my research and helped me editing my manuscripts. I am also so grateful for the friendship we built over the years at UW together, which is one of the most valuable experiences in my life.

This work would not have been possible without the amazing work done by the collaborators, Dr. Lauren Kang who was a former Luscombe group member, Prof. Kendall Houk from University of California, Los Angeles, Ji-Ren Liu, and Prof. Xin Hong from Zhejiang University, China.

I sincerely thank the Molecular Engineering & Sciences Institute of UW for giving me the opportunity to pursue a PhD degree. I also gratefully acknowledge The Clean Energy Institute and the NSF Center for Selective C-H Functionalization for creating communities for academic communications, which enriched my scientific and professional insights.

Thank you to my Master's advisor, Prof. Coleen Pugh, and my mentor, Dr. Ajay Amrutkar for bringing me on board as a new researcher in the polymer chemistry field.

I also wish to thank my family, especially my parents, and friends who supported my decision to pursue a PhD at the beginning and have been there for me for the entire process. Special thanks to Samantha, who has been a great friend and colleague to me, for always listening to my problems. I would also like to thank my cat, Sebastian for being so cute and comforting. I adopted him when I first started at UW, and he kept me company and witnessed all the achievements and struggles of my PhD life.

There are many people I am so grateful for who made me the scientist I am today. I would not have made it here without them.

TABLE OF CONTENTS

LIST OF ABBREVIATIONS

Ac	Acetyl
Ar	Arene
Alt	Alternation
BBT	Benzo[1,2-b;3,4-b]dithiophene
CDC	Cross dehydrogenative coupling
CMD	Concerted-metalation deprotonation
CTP	Catalyst transfer polymerization
Đ	Dispersity
D-A	Donor-Acceptor
DArP	Direct arylation polymerization
DAST	Diethylaminosulfur trifluoride
DCM	Dichloromethane
DMAc	N,N-Dimethylacetamide
DMF	N,N-Dimethylformamide
DMSO	Dimethyl sulfoxide
DP	Number-average degree of polymerization
DPP	Diketopyrrolopyrrole
EDTA	Ethylenediaminetetraacetic acid
EI	Electron ionization
Eq	equivalence
Et	Ethyl
EtOH	Ethanol

GC-MS	Gas chromatography-mass spectrometry
GPC	Gel permeation chromatography
H	Hour
Hex	n-Hexyl
3-HET	3-hexylesterthiophene
3-HT	3-hexylthiophene
HOMO	Highest occupied molecular orbital
I	Intergration
i-Pr	isopropyl
KIE	Kinetic isotope effect
L	Ligand
LUMO	Lowest occupied molecular orbital
M	Metal
Me	Methyl
MeOH	Methanol
MHz	Megahertz
M_n	Number average molecular weights
Mol	Mole
NMR	Nuclear magnetic resonance

Abbreviations for NMR splitting patterns:

s: singlet

d: doublet

t: triplet

q: quartet

p: pentet

m: multiplet

br: broad

dd: doublet of doublets

dt: doublet of triplets

ddt: doublet of doublet of triplets

OFET	Organic field-effect transistor
OLED	organic light-emitting diode
OPiv	Pivalate
OPV	Photovoltaics
Oxi-DArP	Oxidative direct arylation polymerization
p	Conversion to polymer
P3HT	Poly(3-hexylthiophene)
PBX	1-Pivaloyloxy-1,2-benziodoxol-3(1*H*)-one
PEG	Polyethylene glycol
PEO	Polyethylene oxide
PEPPSI	Pyridine-enhanced precatalyst preparation stabilization and initiation
Ph	Phenyl
PivOH	Pivalic acid
ppm	Parts per million
r	Stoichiometric ratio of reactants
RDS	Rate-determining step

R_f	Retention factor
RR	Regioregularity
R.T.	Room temperature
SEC	Size-exclusion chromatography
TBAF	Tetrabutylammonium fluoride
t-Bu	Tert-butyl
THF	Tetrahydrofuran
TMEDA	Tetramethylethylenediamine
TM	Transition Metal
TMS	Tetramethylsilane
TS	Transition State

LIST OF FIGURES

LIST OF SCHEMES

LIST OF TABLES

Chapter 1. Introduction

*Sections within Chapter 1 have been adapted from previously published articles: *J. Mater. Chem. C,* **2021**, *9*, 16391–16409; DOI: 10.1039/d1tc04128b and *J. Am. Chem. Soc.* **2022***, 144,* 2311–2322; DOI: 10.1021/jacs.1c12599.

1.1 Donor-Acceptor (D-A) Semiconducting Polymers

Semiconducting polymers, also referred as π-conjugated polymers, are a class of polymers that possess semiconducting properties. The alternation of single and double bonds along their polymer backbones creates an extended π-conjugation, where the electrons are delocalized. Since the discovery and development of the first semiconducting polymer, polyacetylene, by Heeger, MacDiarmid, and Shirakawa in 1970s, for which they were jointly awarded The Nobel Prize in Chemistry 2000, semiconducting polymers have received significant scientific and industrial interests and studies.[1–3] Nowadays, semiconducting polymers have become promising materials for organic electronics in many applications, such as organic photovoltaics (OPVs),[4,5] organic light-emitting diodes (OLEDs),[6–8] organic field-effect transistors (OFETs),[9–12] and biomedical electronic devices.[13,14] They are intrinsically more flexible and stretchable compared to inorganic semiconducting materials, such as silicon. In addition, their solution processibility makes them accessible to inexpensive and efficient manufacturing processes, such as roll-to-roll printing, while their biocompatibility allows them to be applied as implantable medical devices in living organisms. The various chemical structures of semiconducting polymers enable their wide range of electronic and optical tunability.

Donor-acceptor (D-A) semiconducting polymers consist of alternating electron-rich and electron poor units along the polymer backbone. They have drawn a lot of attention as their backgrounds demonstrate a "push-pull" electronic effect, leading to lowered bandgaps compared to the homo semiconducting polymers. The lowered bandgaps enable improved charge mobility and broader ranges for light absorption of the D-A semiconducting polymers.[4,5] Moreover, their band gaps are tunable by adjusting their chemical structures.[15,16] The mechanism responsible for the low bandgaps of D-A semiconducting polymers is called molecular orbital hybridization.[4,5,17] The hybridization of frontier molecular orbitals (highest occupied molecular orbital (HOMO) and the lowest unoccupied molecular orbital (LUMO)) of the donor and acceptor units occurs and generates a new set of hybridized molecular orbitals with a new bandgap (E_g) that is narrower than either bandgap of the donor or acceptor (Figure 1.1). D-A semiconducting polymers are particularly useful in OPV devices as electron donors. Compared to the classic electron donor material in OPV devices, homopolymer poly-(3-hexylthiophene), the D-A semiconducting polymers can increase the power conversion efficiency to over 10 %, which is often considered as the benchmark for commercial viability.[5,18] In order to acquire the D-A semiconducting polymers with high electronic device performance, the synthesized D-A semiconducting polymers need to have perfectly alternating donor and acceptor chemical structures and high molecular weights. Any homo-coupling defect on the polymer backbone limits the material's optical and electronic performance.[19,20]

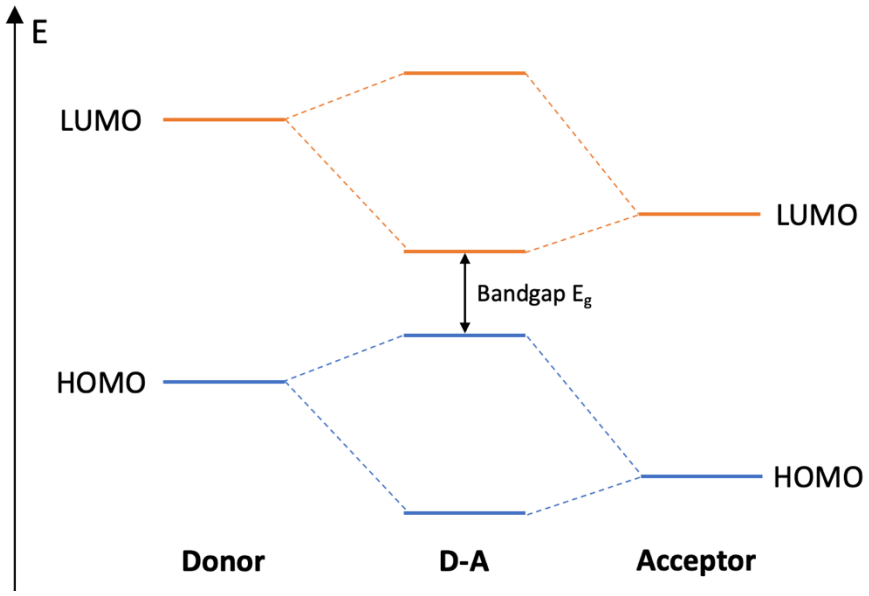

Adapted from ref. 5.

Figure 1.1 Diagram of molecular orbital hybridization in D-A semiconducting polymers.

1.2 Atom-Economical Syntheses of D-A Semiconducting Polymers

There are some obstacles that hinder large-scale manufacture and commercial viability of D-A semiconducting polymers. One severe obstacle is the amplified negative environmental impacts associated with their conventional synthetic methods in industrial scales. The conventional synthetic methods for D-A semiconducting polymers, including Suzuki and Stille couplings, are often multi-step processes which involve pre-functionalization of the starting molecules.[21,22] Scheme 1.1 shows two examples of D-A semiconducting polymers and their conventional synthetic routes.[23,24] The pre-functionalization steps include halogenation, boronation, stannylation, and other metalation reactions depending on the type of coupling. The long synthetic process of D-A semiconducting polymers results in waste of time and money and generation of a large amount of hazardous chemical waste and toxic byproducts, particularly the organotin byproducts generated from Stille coupling are virulent to humans.[25–27]

Scheme 1.1 a) Synthesis of poly[4,4-bis(2-ethylhexyl)-4Hcyclopenta[2,1-b;3,4-b']dithiophene-2,6-diyl-alt-2,1,3-benzothiadiazole-4,7-diyl] (PCPDTBT) via Suzuki coupling.[24] b) Synthesis of DPP containing copolymers (TDPP-BBT) via Stille coupling[23]

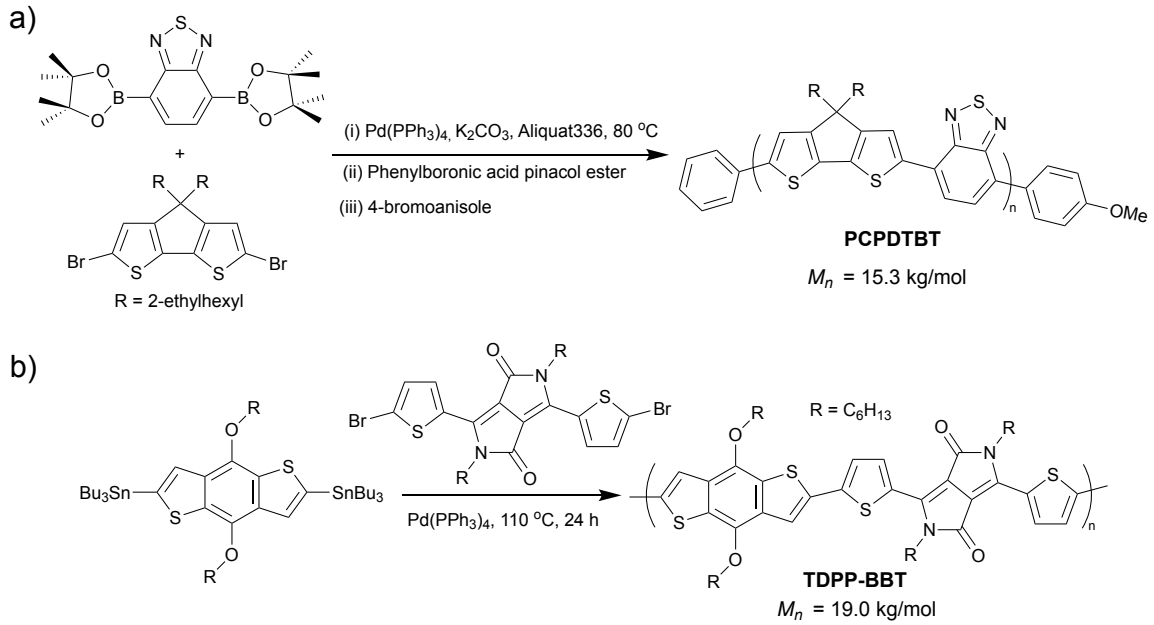

The concept of atom economy was first proposed by Trost in Science in 1991.[28] The atom economy of a chemical process is measured by the ratio of mass of the desired product to the total mass of all the products generated, including byproducts. The lower the weight of byproduct(s) a chemical process generates, the more atom-economical the process is. The optimal atom economy is 100 %. Atom-economy has become an important factor when determining if a chemical process is environmentally friendly. Reducing the number of steps and avoiding using large functional groups in a synthetic process are effective ways to decrease the generation of wasted byproducts. C-H activation on sp^2 carbons of aromatic rings has become a promising tool to synthesize semiconducting polymers, in which the C-H bonds are activated, and subsequently C-C bonds are formed in situ. The development of aryl-aryl coupling via C-H activation was first driven by pharmaceutical industry, because biaryl structures are very

common in many drug compounds. Direct arylation and cross dehydrogenative coupling (CDC) are the two C-H activation involved synthetic routes for D-A semiconducting polymers as green alternatives to the conventional synthetic methods, due to their high atom economy (Scheme 1.2). However, compared to the conventional coupling methods, it is more challenging for direct arylation and CDC to obtain high molecular weight polymers with desired chemo- and regioselectivity due to the inert nature of C-H bonds.

Scheme 1.2 Comparison among the conventional cross coupling polymerization, direct arylation and cross dehydrogenative coupling polymerizations

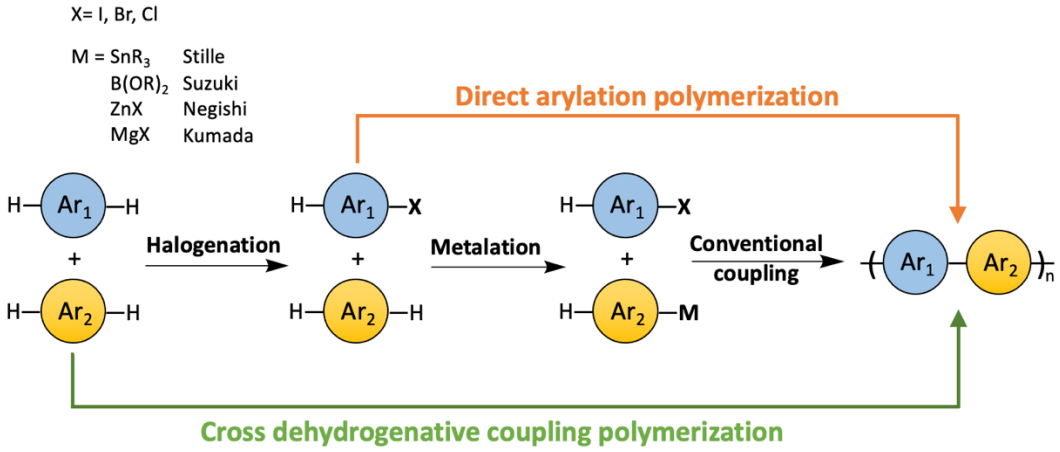

1.2.1 *Direct Arylation Polymerization (DArP)*

In the direct arylation coupling reaction, only one of the two coupling partners needs to be pre-halogenated, and the necessity of pre-metalation step of the other coupling partner is avoided. Direct arylation polymerization (DArP) has been widely studied for the synthesis of defect-free D-A semiconducting polymers.[29–33] Most direct arylation reactions are catalyzed by palladium catalysts in presence of a base, such as Cs_2CO_3 and K_2CO_3, and a carboxylic acid which acts as a proton shuttle. Direct arylations are usually carried out under inert gas atmosphere, at an elevated temperature from ~60 °C to ~120 °C, and in aprotic organic solvents such as DMAc, DMF, NMP, toluene, etc.[34] A typical direct arylation catalytic cycle includes the

following four major steps (Scheme 1.3): i) Oxidative addition, where the Pd(0) catalyst reacts with the C-X bond to form a Pd(II) complex; ii) Ligand exchange, where X^- on the Pd(II) complex is replaced by a carboxylate anion ($RCOO^-$); iii) C-H bond activation by the Pd(II) complex; iv) Reductive elimination to form the C-C bond and regenerate the Pd(0) catalyst.[34–36] The C-H activation step in the direct arylation catalytic cycle normally goes through a concerted metalation-deprotonation (CMD) mechanism, and the bases and carboxylic acids are known to assist this process.[37]

Scheme 1.3 A plausible catalytic cycle of direct arylation

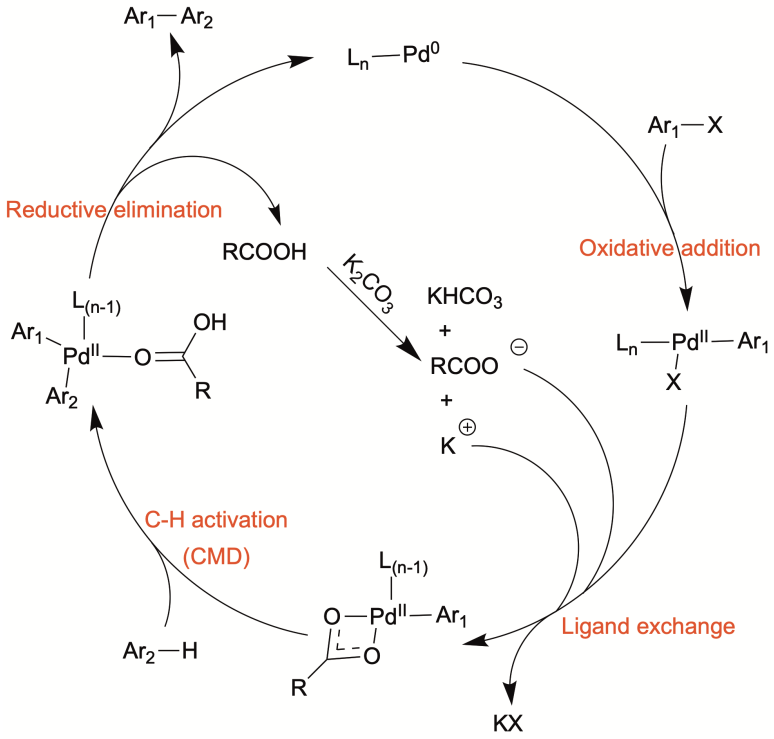

1.2.2 *Cross Dehydrogenative Coupling (CDC) Polymerization*

CDC has received a lot of attention in the organic materials space since its initial report by Fagnou et al.[38] CDC polymerization is a more ideal synthetic route for D-A semiconducting polymers than DArP in terms of atom economy, because neither of the coupling partners needs

to be pre-functionalized. The C-H bonds on both coupling partners will be activated and form a C-C bond subsequently during the polymerization. The application of CDC polymerization towards D-A semiconducting polymer synthesis have been reviewed considerably in the past few years.[39–44] However, unlike DArP, the mechanisms of CDC reactions have not been studied extensively yet. It is particularly challenging to synthesize defect-free D-A semiconducting polymers via CDC, due to the difficulty in achieving high chemo- and regioselectivities when multiple possible reactive sites, in this case C-H bonds, are present. Moreover, the catalysts often have insufficient selectivity to distinguish the donor and acceptor monomers.[38] Another challenge when synthesizing D-A semiconducting polymers via CDC is to obtain high molecular weight polymers. High molecular weight is required for a polymer to be useful as a material. The CDCs are normally driven by the discrepancy in electronic properties of the coupling partners (electron-rich and electron-poor comonomers).[45] The small oligomers (dimers, trimers, etc.) formed at the beginning of the polymerization are less electron-rich or less electron-poor compared to their corresponding monomers. Therefore, further coupling reactions with these oligomers becomes relatively unfavored, hence inhibiting the chain propagation process that forms long polymer chains.[46]

In 2018, the Kanbara group and the Chen group both independently reported successful syntheses of highly alternating D-A conjugated poly(arylene)s with large molecular weights via CDC for the first time.[47,48] Kanbara et al. conducted a palladium/silver dual catalyzed CDC polymerization (Scheme 1.4a).[47,49] The D-A semiconducting polymer they synthesized, a copolymer of 2,2′,3,3′,5,5′,6,6′-octafluorobiphenyl and 3,3′-dihexyl-2,2′-bithiophene, was applied as a light emitting material in OLEDs. Chen and co-workers accomplished CDC polymerization of various D-A semiconducting polymers with a similar palladium catalytic

system to Kanbara's (Scheme 1.4c).[48] The highly alternating and regioregular structures of the copolymers were demonstrated by comparing the ^{1}H NMR spectra of the same copolymers synthesized by Stille coupling, showing the robustness of the CDC method compared to the conventional method. Three years later, Lu et al. expanded the monomer scope of Kanbara's palladium/silver catalytic CDC polymerization by preparing a series of fluorinated benzotriazole-based D-A semiconducting copolymers (Scheme 1.4b).[50]

Scheme 1.4 a) Palladium/silver catalyzed CDC polymerization; b) Synthesis of fluorinated benzotriazole containing D-A semiconducting polymers via CDC; c) The CDC polymerizations of various D-A semiconducting polymers

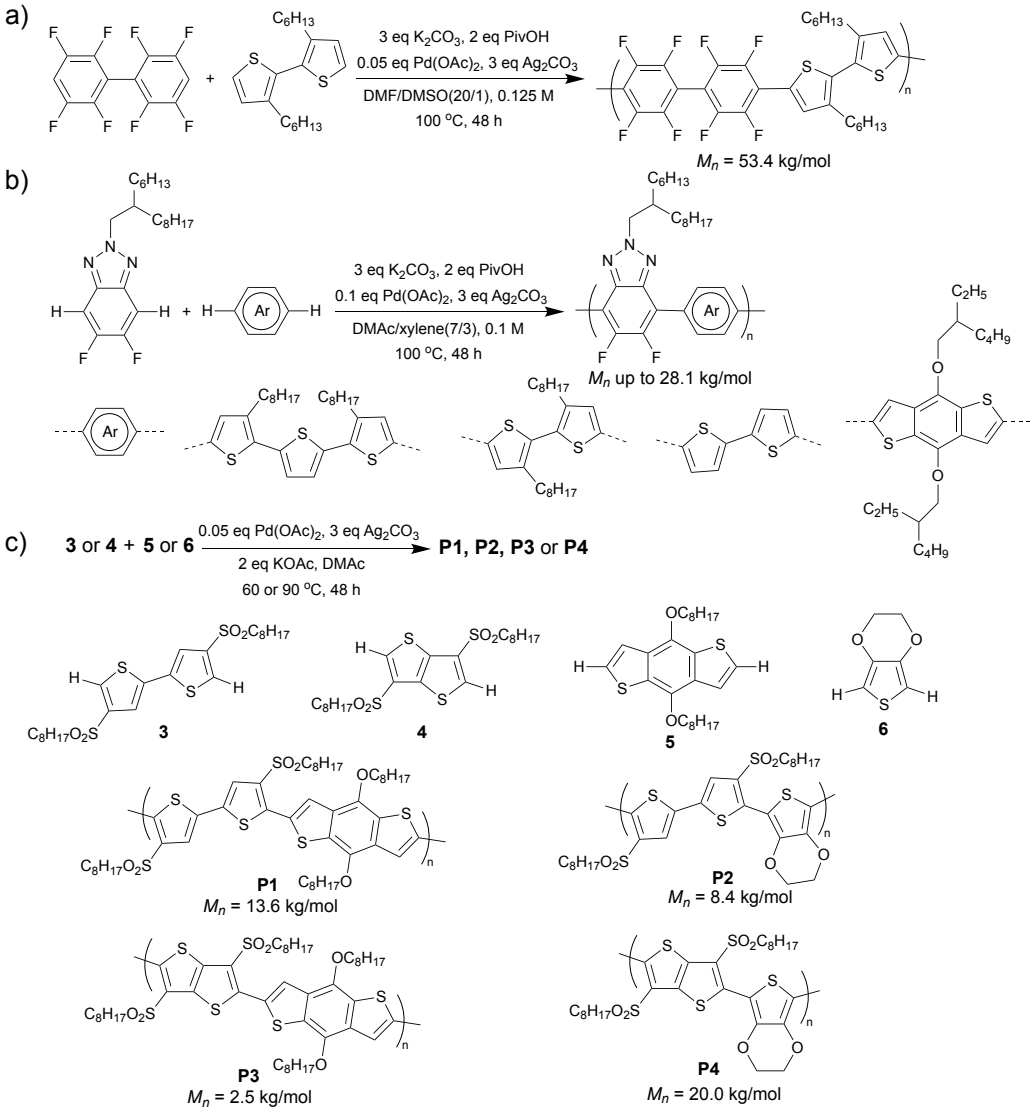

Apart from poly(arylene)s, another type of promising D-A semiconducting polymers which was successfully synthesized via CDC are luminescent poly(arylene-vinylene)s.[51,52] In 2016, the Kanbara group depicted the first CDC polymerization of a diethenyl aromatic monomer and an arene monomer, also referred as dehydrogenative direct alkenylation polymerization, to synthesize several 1-(2-pyrimidinyl)pyrrole-based poly(arylene-vinylene)s with a rhodium catalyst (Scheme 1.5, top).[51] After that, they reported a palladium catalyzed dehydrogenative direct alkenylation polymerization of polyfluoroarylene-based poly(arylene-vinylene)s (Scheme 1.5, bottom).[52] In this report, they eliminated the necessity of installing the directing 2-pyrimidinyl group.

Scheme 1.5 Rhodium- and palladium catalyzed dehydrogenative direct alkenylation polymerizations to synthesize poly(arylene-vinylene)s

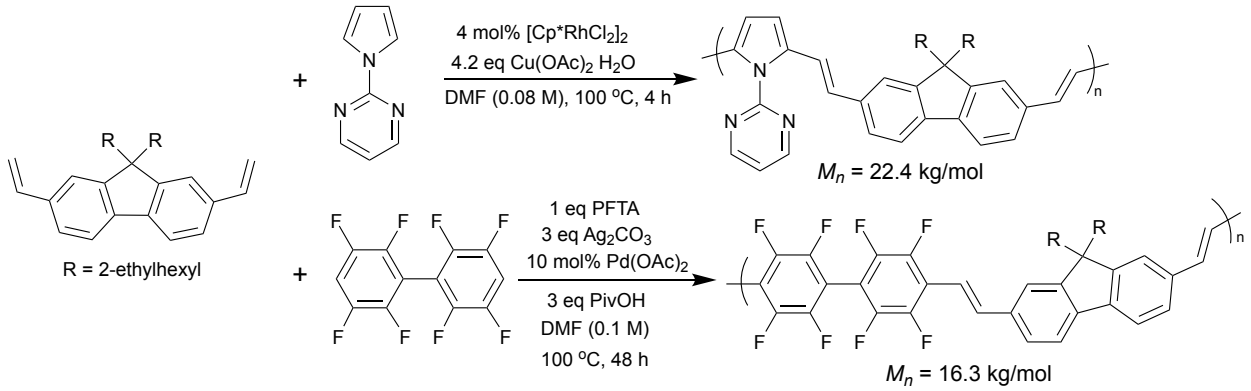

1.2.3 *The Carothers Equation*

Since the polymerizations we are discussing about here are all based on small molecule condensation reactions, it is safe to assume that these polymerizations are step-growth polymerizations. In step-growth polymerizations, bi-functional or multi-functional monomers react with reaction to form dimers, trimers, tetramers, and eventually long polymer chains. Molecules of any degree of polymerization (n-mer) can couple with one another during the step-

growth polymerization (Figure 1.2). In step-growth polymerizations using AA+BB type of monomers, the number-average degree of polymerization (DP) can be expressed as DP = (1 + r)/(1 + r − 2rp), where p is the extent of the polymerization and r is the stoichiometric ratio between the comonomers. This equation was originally proposed by Carothers and is often referred to as the Carothers equation.[53,54] This equation is graphically depicted in Figure 1.3. According to the Carothers equation, to obtain a high molecular weight, namely high DP, the polymerization must be driven close to completion (p = 1), and equal molar monomers are required (r = 1), because any small deviation of the p or r value from 1 can cause a large drop in DP. For example, when r =1 and p = 95 %, DP is only 20. However, a reaction extent of >95 % is considered high enough for most small molecule condensations, and perfectly equal molar monomers is hard to achieve due to the existence of impurities in monomers. Therefore, developing a step-growth polymerization that produces high molecular weight polymers is more difficult than developing the corresponding small molecule condensation reaction.

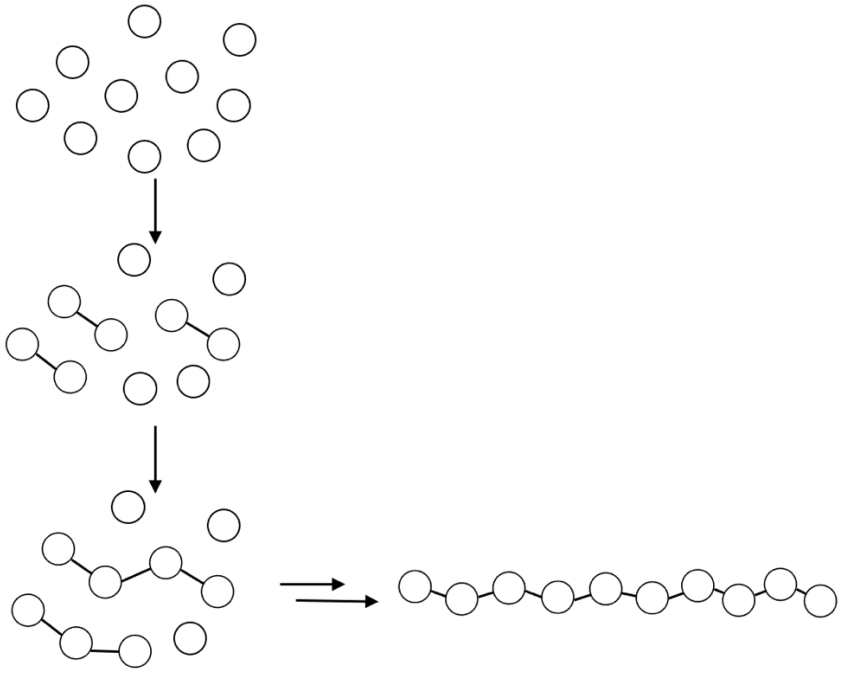

Figure 1.2 A diagrammatic representation of step-growth polymerizations.

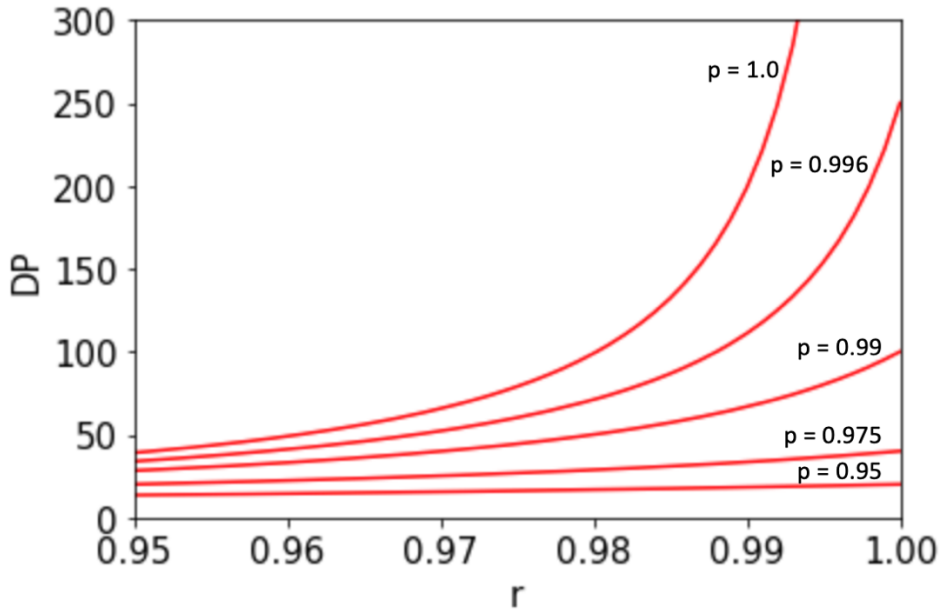

Figure 1.3 Graphic depiction of the Carothers equation.

The Carothers equation was proposed based on the assumption of equal reactivity of functional groups, meaning that the reactivity of one functional group of a bifunctional monomer is the same irrespective of whether the other functional group has reacted, and the reactivity of a functional group is independent of the size of the molecule to which it is attached. This is not always true in step-growth polymerizations. For polymerizations such as polyesterifications or polycondensation to synthesize nylon, the molecular weights of the product can be accurately predicted using the Carothers equation, since the reactivity of the functional groups in these polymerizations does not change significantly (the change of the rate constant is within 3 folds) with the size of the reactants.[53] In some polycondensations, however, the molecular weight of the polymer products can be significantly higher than predicted by the Carothers equation.[55–59] For example, Endo et al. reported a polycondensation between 2,2-dichloro-1,3-benzodioxole and 4,4'-isopropylidenediphenol.[58] A number-average molecular weight (M_n) of 120 kg/mol was obtained when 5 equivalents of dioxole and 3 equivalents of diphenol were used, when an M_n of

0.693 kg/mol was predicted by the Carothers equation. This was ascribed to the rate acceleration during the polycondensation, where the rate of the 1st condensation reaction to form the dioxole-diphenol dimer was 27 times slower than that of the 2nd condensation reaction between the dioxole-diphenol dimer and another diphenol. Conversely, significantly lower molecular weights than predicted by Carothers equation can be observed if the reactivity of the functional groups decreases as the polymerization proceeds.[46]

1.3 Conclusions

In conclusion, to facilitate the industry-scale production and improve the commercial viability of D-A semiconducting polymers, it is needed to replace the conventional synthetic strategies with more atom-economical synthetic strategies, for instance CDC polymerizations. As it was mentioned in the section 1.2.2, one of the challenges for CDC polymerizations to synthesize high molecular weight and defect-free D-A semiconducting polymers is that the metal catalysts used in the CDCs often have insufficient selectivity to distinguish the electron-rich and electron-poor coupling partners, causing homo-coupling side reactions to occur. Weix et al. envisioned that the dual catalytic systems where two distinct metal catalysts work synergistically together could be promising for cross-coupling reactions to achieve high cross-coupling yields and suppress the homo-coupling side reactions.[60] Therefore, herein, two different dual catalytic systems – Au/Ag and Pd/Ag for CDC polymerizations were investigated. The findings in this work provide valuable insight for future studies in obtaining high-molecular weight and defect-free D-A semiconducting polymers via CDC. Additionally, these findings could affect the design of substrates in late-stage C−H functionalization.

Chapter 2. Au/Ag dual catalytic cross dehydrogenative coupling for donor-acceptor semiconducting polymer synthesis

*The work in Chapter 2 is adapted from a previously published article: *Polym. Chem.,* **2019***,10,* 486-493; DOI: 10.1039/c8py01162a

2.1 Introduction

In 2015, Larrosa et al. reported a gold-catalyzed small molecule CDC between an electron-rich TIPS-protected indole and an electron-poor fluorinated benzene. In their study, high yields of the cross-coupling product were obtained with almost stoichiometric ratios of the cross-coupling partners and without utilization of directing groups.[61] Whereas in the previously reported CDCs catalyzed by Pd, a large excess of one of the coupling partners was usually added in order to reach high cross-coupling yields and suppress homo-coupling.[62–64] The proposed mechanism of this Au catalyzed CDC by Larrosa et al. is shown in Scheme 2.1. C-H bonds of electron-rich and electron-poor substrates were activated by Au(III) and Au(I) respectively, and that pivaloyloxy-1,2-benziodoxol-3(1H)-one (PBX) acted as an oxidant. However, the function of silver pivalate (AgOPiv) was not elucidated in their paper, which as we speculated was very likely to play a role of C-H activation reagent based on the previous reports[65–68] and the fact that AgOPiv was essential for the Au catalyzed CDC reaction to proceed. With decently high reactivity and high chemo-selectivity, this Au catalyzed CDC seemed to be promising for D-A semiconducting polymer synthesis. Therefore, in this chapter, polymerizations via the Au-catalyzed CDC to synthesize D-A semiconducting polymers using 3,3'-dihexyl-2,2'-bithiophene as the electron-rich monomer and 1,2,4,5-tetrafluorobenzene or 2,2',3,3',5,5',6,6'-

octafluorobiphenyl as the electron-poor monomer were attempted. Meanwhile, a series of small molecule studies were performed to investigate the role of the AgOPiv in the Au catalyzed CDC.

Scheme 2.1 Proposed mechanism for Au(I) and Au(III) catalyzed CDC. A represents the electron-poor acceptor and D represents the electron-rich donor

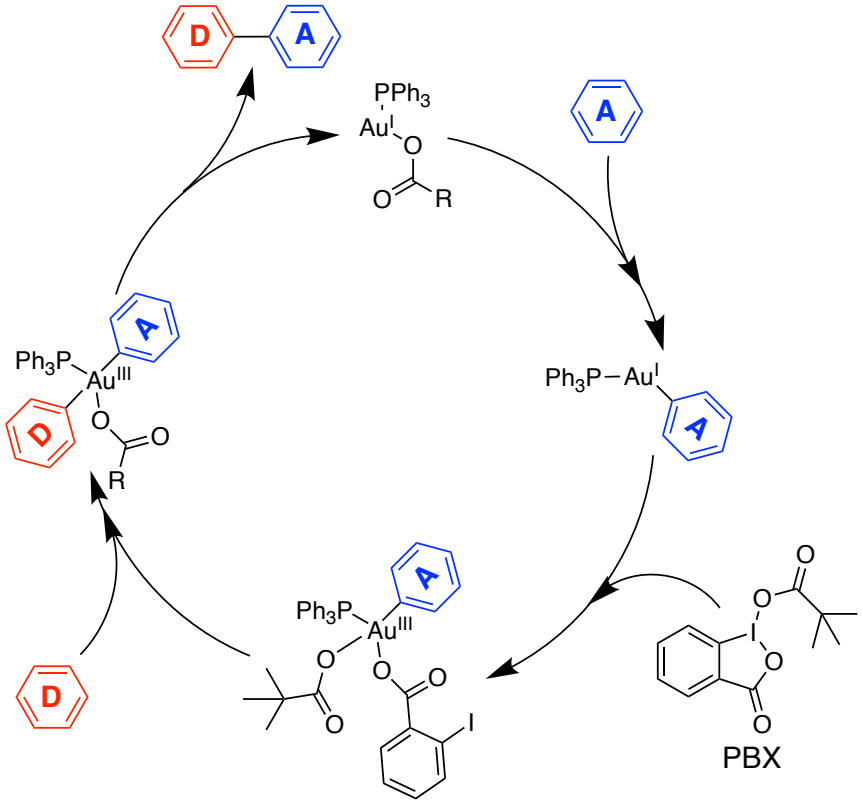

Adapted from ref. 61.

2.2 Results and Discussion

2.2.1 *Preliminary Condition Screening and Polymerizations*

Firstly, a condition screening study was performed by a former lab member, Dr. Lauren Kang, to obtain the conditions that provide the highest cross-coupling yield (Table 2.1). We chose to use a model system comprising of 2-methylthiophene (**A**) and pentafluorobenzene (**B**), serving as the electron-rich and electron-poor coupling partners, respectively (Scheme 2.2) to

mimic the subsequent synthesis of D-A semiconducting polymers (poly(thiophene-alt-fluorobenzene)). These two distinct aromatic compounds were coupled in the presence of AgOPiv, triphenylphosphinegold(I) catalyst (PPh_3AuL), and PBX as the oxidant (Table 2.1, representative ^1H NMR spectrum used for analysis shown in Section 2.4.2, Figure 2.4). Overall, cross-coupling yields increased with the increasing AgOPiv loading (Table 2.1, compare entries 2, 4, 5 and 7, 9, 10) regardless of the **A**:**B** ratio used. There was no measurable presence of homo-coupled product of **B** by GC-MS for all entries.

Scheme 2.2 Small molecule CDC model reaction using 2-methythiophene (A) and pentafluorobenzene (B)

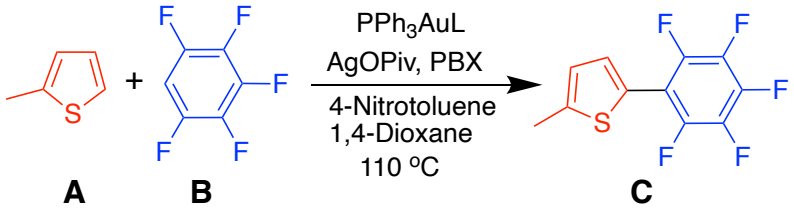

Table 2.1 Optimization of small molecule cross-coupling reaction. Reactions were run on 0.1 mmol scale of **A**, using 5 mol % Au-catalyst and PBX (1.5 eq). Reported yields are averages of 3 runs per reaction. The yields were determined by ^1H NMR using 4-nitrotoluene as an internal standard. There was no measurable presence of homo-coupled product of **B**. Yields of homo-coupled product of **A** were up to 13 % for entries 6-11 and 5 % for entries 1-5.

Entry	Eq. of A	Eq. of B	L	Eq. of AgOPiv	% Yield of C	Rxn time (h)
1	1	5	Cl	0.35	36±7	20
2	1	5	OAc	0.35	59±5	20
3	1	5	OAc	0.35	82±2	40
4	1	5	OAc	0.7	87±2	20
5	1	5	OAc	1	94±6	20
6	1	1	Cl	0.35	27±8	20
7	1	1	OAc	0.35	20±7	20
8	1	1	OAc	0.35	52±5	40
9	1	1	OAc	0.7	41±9	20
10	1	1	OAc	1	66±12	20
11	1	1	OAc	1	66±3	40

Using optimized conditions with increased AgOPiv and PBX loadings, polymerizations were attempted using 3,3'-dihexyl-2,2'-bithiophene as the electron-rich monomer and 1,2,4,5-tetrafluorobenzene (Scheme 2.3, top) or 2,2',3,3',5,5',6,6'-octafluorobiphenyl (Scheme 2.3 bottom) as the electron-poor monomer. All polymerizations were run on a 1 mmol scale with 1:1 comonomer ratios. 3,3'-Dihexyl-2,2'-bithiophene was chosen to increase polymer solubility as the polymer grew by incorporating alkyl chains along the polymer backbone, and to eliminate any regioselectivity issues by using a symmetrical monomer that would otherwise arise using a 3-alklythiophene monomer. ^{1}H NMR assignment (Figure 2.1 and Section 2.4.3, Figure 2.5) of the peaks were made by referencing the literature and our small molecule model reactions.[47] Previous work had indicated that the aromatic peak from the terminal fluorinated aromatic group could be observed at 7.3 ppm. However, in our spectra (Figure 2.1), we observe a doublet in this region, which we assign to terminal thiophenes suggesting that our polymer chains are terminated by thiophene units on both chain ends. For **Polymer B**, there are overlapping signals in the nearby region. As such, we cannot entirely eliminate the possibility of fluorinated aromatic end-groups. However, given the greater incorporation of the bithiophene monomer into the polymer chain (discussed further below), statistically, there is a greater probability that the polymers are terminated by thiophenes.

Scheme 2.3 Polymerization schemes with 1,2,4,5-tetrafluorobenzene (top) and with 2,2',3,3',5,5',6,6'-octafluorobiphenyl (bottom) as the electron-poor monomer

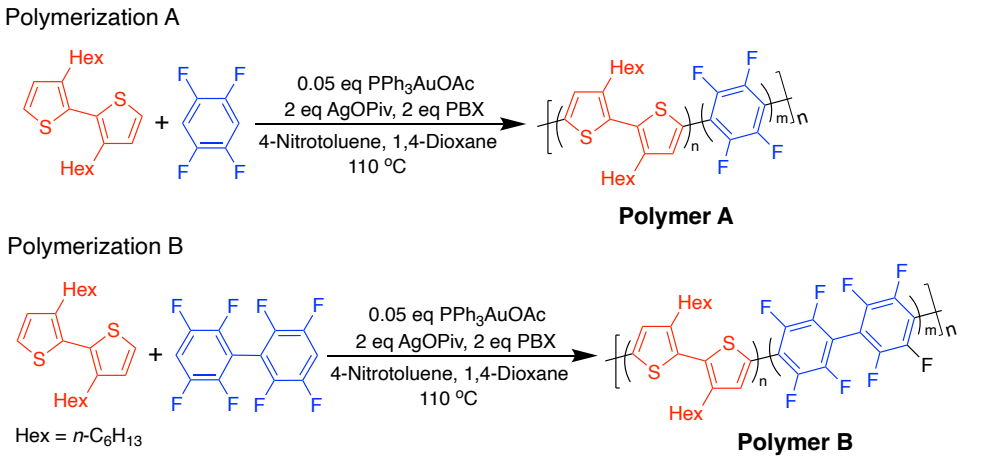

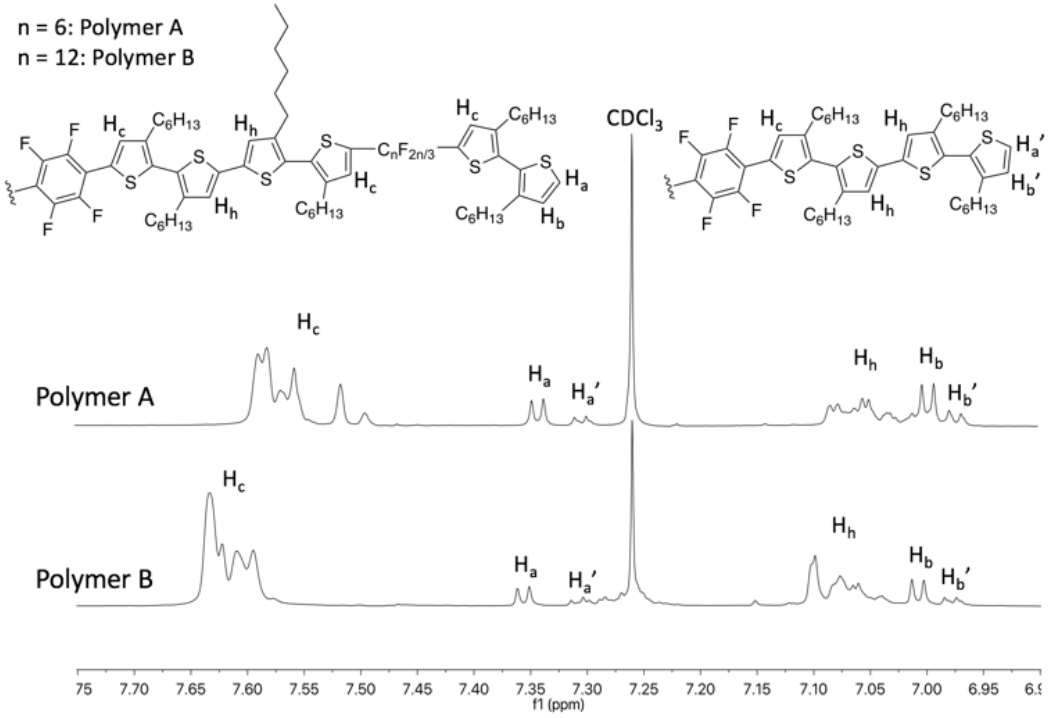

Figure 2.1 Example ^{1}H NMR spectra showing the regions used for Mn, DP, and % alt calculation. The ^{1}H NMR spectra correspond to aliquots at 168 h time point.

The number-average degree of polymerization (DP) and thus number-average molecular weight (M_n) values were determined using end-group analysis via ^{1}H NMR spectroscopy (Section 2.4.5, Equations 2.2 and 2.3, respectively), and dispersity (Đ) values were determined

using size-exclusion chromatography (SEC). The resonances of thiophene aromatic protons positioned between two thiophenes (e.g., -T**T**-**T**T-, where T = thiophene) appear at 7.01-7.09 ppm for **Polymer A** and 7.04-7.10 ppm for **Polymer B** (labelled H_h in Figure 2.1), while the resonance of thiophene aromatic proton located between a fluorinated benzene and a thiophene (e.g., -F-**TT**-F-, where F = tetrafluorobenzene) appears at 7.50-7.59 ppm for **Polymer A** and 7.59-7.63 ppm for **Polymer B** (labelled H_c in Figure 2.1). The presence of the H_h peaks indicate that there is a higher degree of homo-coupling observed in the polymerization than was observed in the small molecule reactions. We also see two different thiophene end-group peaks depending on whether or not the end-group is adjacent to a fluorinated benzene or a bithiophene as a result of homo-coupling. Specifically, the proton signals from the end-groups of bithiophenes adjacent to a fluorinated benzene appear as doublets at ~7.35 (H_a) and ~7.00 ppm (H_b), while those adjacent to another bithiophene appear as doublets at ~7.3 ($H_{a'}$) and ~6.98 ppm ($H_{b'}$). The ratio of the H_c peaks vs. all end-group peaks gives us the number of alternating units along the polymer backbone. Multiplying this value by two provides the total number of both bithiophene and fluorinated benzene units that make up the alternating units. Furthermore, the ratio of the H_h peaks vs. all end-group peaks gives us the number of additional bithiophene units that were incorporated into the polymer chain. The sum of these provides a value for DP and the equation is shown in the Section 2.4.5, Equation 2.2. This analysis was then be used to calculate M_n (Equation 2.3).

Based on this analysis, the resulting M_n of **Polymer A** and **Polymer B** were calculated to be 5.1 kg/mol and 9.4 kg/mol at 192 h time point, respectively, with DPs of 18 and 28, respectively (Table 2.2). The yields for **Polymer A** and **Polymer B** were 47% and 63%, respectively, with the Đ for both measured to be 1.2. The percentage of alternating units in the

polymer sequence (% alt) was calculated by comparing the ratio of the number of alternating units (H_c) vs. all repeat unit peaks in the aromatic region of the ^{1}H NMR (Section 2.4.5, Equation 2.4, and Figure 2.1). A homo-coupling defect free polymer would have a % alt of 100 %. Noticeably, the % alt of both polymers remained constant at around 70 % throughout the polymerization process (Table 2.2) regardless of reaction time. The presence of multiple peaks in the ^{19}F NMR (Section 2.4.3, Figure 2.6) of the polymers also reflect the fact that 100% alternation was not achieved.[47] The lower than expected % alt showed that the selectivity observed in the small molecule reaction did not transfer to the polymer synthesis, suggesting three possibilities: (i) The terminal protons at the polymer chain-ends would become more electronically similar due to increased conjugation thereby reducing selectivity as the polymer grew; (ii) The previously proposed mechanism as shown in Scheme 2.1 was not occurring in the current polymerizations and required further investigation; (iii) the dimers generated at the early stages of the polymerization are less distinguishable to the catalyst than the monomers due to the substrate driven electronic effect. We believe that the first possibility can be ruled out for two reasons. Firstly, the two adjacent hexyl groups of the bithiophene unit in polymers would cause the polymer backbone to twist, which would lead to ineffective π-conjugation along the polymer backbone (the thiophene-thiophene dihedral angle is at least 87°).[69] Secondly, for **Polymer B**, the twist between the two benzene rings in the octafluorobiphenyl unit would reduce the effective conjugation length even more.[70] If the extended conjugation as the polymer grew was indeed detrimental to the selectivity of the CDC reaction, higher % alt in **Polymer B** than in **Polymer A** should have been observed, and % alt should have decreased with the increasing chain length. However, as summarized in Table 2.2, the % alt remain similar for both polymerizations and does not change significantly as the polymerization proceeds.

Table 2.2 M_n, DP, and % alt of **Polymer A** and **Polymer B** at different time points during polymerizations. The Đ values of both polymers were determined to be 1.2 according to size-exclusion chromatography (SEC).

Timepoint (h)	M_n of Polymer A (kg/mol)	DP of Polymer A	% Alt for Polymer A	M_n of Polymer B (kg/mol)	DP of Polymer A	% Alt for Polymer B
24	4.1	15	71	5.6	17	67
48	4.8	18	73	6.7	20	71
96	4.8	18	72	7.5	22	68
120	4.9	18	72	7.9	24	69
144	4.9	18	76	8.7	26	70
168	4.5	16	67	8.1	25	69
192	5.1	18	69	9.4	28	69

2.2.2 *Cross-Coupling Mechanism Studies*

In order to understand the source of selectivity loss in polymerization, the mechanism of the polymerization was explored further. No reaction was observed when control polymerizations were performed in the absence of Ag and Au showing that the decline in selectivity is not due to oxidative homo-coupling of the bithiophene caused by PBX. We proposed that there were two possible mechanisms for this CDC reaction based on previous work: (i) where Au(I) is responsible for activating the electron-poor species, and Au(III) is activating the electron-rich species as shown in Scheme 2.1;[61] or (ii) where Ag was mainly responsible for the C-H activation of the electron-poor arene, and Au(III) activated the electron-rich arene, which was suggested as a possibility previously but not experimentally confirmed.[61] To this end, a series of experiments were carried out using slightly altered conditions to Scheme

2.2 (Table 2.3) in an attempt to elucidate the role of silver salts in this CDC reaction. Silver salts have been the subject of increased studies in recent reports in in Pd-catalyzed C-H activation.[66–68] It has been proposed that the silver salt could act as an oxidant, as a ligand source, halide scavengers and/or a C-H activating agent.[66] Similarly, for this gold-catalyzed method, AgOPiv could be playing multiple roles. From Table 2.3 and previous work,[61] it is clear that AgOPiv was not simply a ligand or base source, or a halide scavenger as the reaction still required the presence of Ag to proceed no matter whether PPh_3AuOAc or PPh_3AuCl was used (Table 2.3, entries 3, 4, 8, and 9) and even when a stoichiometric amount of pivalate was added in the absence of Ag (Table 2.3, entry 13). It was also shown that the AgOPiv was not a sufficient oxidant, as the reaction did not proceed without PBX, even in the presence of excess AgOPiv (Table 2.3, entries 5 and 10). There was also an observed decrease in yield with the reduction of the **B** to **A** ratio (Table 2.3, Entries 1, 2, 6, and 7). In combination with the observation that the yield of **C** increased as the AgOPiv loading increased (Table 2.3, Entries 7, 9, 11, and 12), it was speculated that both AgOPiv and **B** might be involved in the rate-determining step of the reaction. However, more detailed kinetic studies are required to confirm this.

Table 2.3 Control experiments for CDC reaction. Reactions were run on 0.1 mmol scale of **A** (1 eq) for 20 h using 5 mol % Au-catalyst. Reported yields are averages of 3 runs per reaction. The yields were determined by ^{1}H NMR using 4-nitrotoluene as an internal standard.

Entry	Eq. of B	L	Eq. of PBX	Additive (eq)	% Yield of C	% Yield of homo-coupled product of A
1	5	Cl	1.5	AgOPiv (0.35)	36±7	2.3±1.5
2	5	OAc	1.5	AgOPiv (0.35)	59±5	3.0±1.0
3	5	Cl	1.5	None	<1	<1
4	5	OAc	1.5	None	<1	<1
5	5	OAc	0	AgOPiv (0.7)	<1	<1

6	1	Cl	1.5	AgOPiv (0.35)	27±8	2.3±0.6
7	1	OAc	1.5	AgOPiv (0.35)	20±7	3.7±1.2
8	1	Cl	1.5	None	<1	<1
9	1	OAc	1.5	None	1.1±0.6	<1
10	1	OAc	0	AgOPiv (0.7)	<1	<1
11	1	OAc	1.5	AgOPiv (0.7)	41±9	6.7±1.5
12	1	OAc	1.5	AgOPiv (1)	66±12	13.0±1.0
13	1	OAc	1.5	NaOPiv (1)	<1	4.7±0.8

To determine which metal species was responsible for the C-H bonds activation of the electron-rich and electron-poor species, deuterium studies were performed. By reacting each of the starting materials (i.e., **A** and **B**) separately with different combinations of additives in the presence of deuterium oxide, the degree of deuteration was quantified (Tables 2.4 and 2.5). For both **A** and **B**, NaOPiv yielded no deuterated product confirming that pivalate on its own could not deprotonate the starting arenes (Table 2.4, entry 2 and Table 2.5, entry 2). In the case of pentafluorobenzene **B**, results in Table 2.4 indicate that AgOPiv itself can act as a C-H bond activating reagent with a deuterium conversion of 23 % (Table 2.4, entry 3), whereas no deuterium conversion in the presence of $PPh_3Au(I)OAc$ or Au(III) chloride ($AuCl_3$) (Table 2.4, entries 4-7) was detected. In the case of 2-methylthiophene **A**, while some deuterium conversion was observed in the presence of AgOPiv or PPh_3AuOAc, 10 % and 4 % respectively (Table 2.5, entries 3 and 7), significantly higher conversion of 42 % was observed in the presence of $AuCl_3$ (Table 2.5, entry 4). Upon the addition of pivalic acid, there was an increase in deuterated product, 69 %, showing that the addition of a carboxylate ligand to the gold catalyst increases its ability to activate C-H bond of **A** (Table 2.5, entry 5). A surprising phenomenon was observed in

both deuteration reactions with **A** and **B** separately. The combination of $AuCl_3$ and AgOPiv resulted in reduced deuteration incorporation (Tables 2.4 and 2.5, entry 6). Furthermore, these reactions also exhibited the formation of silver mirrors on the reaction vessels, indicating a decomposition pathway resulting in the formation of elemental silver. Silver mirror formation was not observed in the overall cross-coupling reactions, in which the Au(III) species would have carboxylate anions in place of chloride anions. Therefore, we believe that such a decomposition pathway is unique to the highly halogenated Au(III) chloride and is not occurring in the CDC reaction. These deuterium studies show that Ag is capable of activating the C-H bonds of both the electron-poor and electron-rich arenes and that the activation of the electron-poor arene is more favorable (23 % vs. 10 %). It was also suggested that Au(III) has a high reactivity for the C-H bond activation of the electron-rich species (69 %) but low reactivity for the electron-poor species (0 %).

Table 2.4 Deuterium study results of pentafluorobenzene. Reactions were run on 0.1 mmol scale of **B**. Reported yields are averages of 3 runs per reaction. The yields were determined by using an internal standard of DMSO-d_6, using similar conditions as those previously reported by Sanford et al.[67]

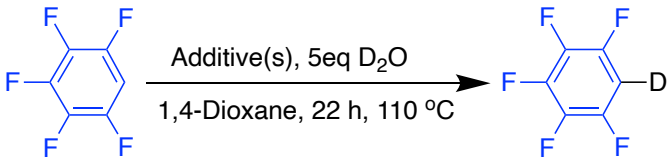

Entry	Additive(s)	Deuterium Incorporation (%)
1	None	0
2	0.35 eq. NaOPiv	0
3	0.35 eq. AgOPiv	23.1
4	0.05 eq. $AuCl_3$	0
5	0.05 eq. $AuCl_3$, 0.05 eq. PivOH	0

6	0.05 eq. $AuCl_3$, 0.35 eq AgOPiv	1.9
7	0.05 eq. PPh_3AuOAc	0
8	0.05 eq. PPh_3AuOAc, 0.35 eq. AgOPiv	17.7

Table 2.5 Deuterium study results of 2-methyl thiophene. Reactions were run on 0.1 mmol scale of **A**. Reported yields are averages of 3 runs per reaction. The yields were determined by using an internal standard of DMSO-d_6, using similar conditions as those previously reported by Sanford et al.[67]

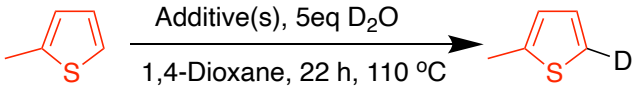

Entry	Additive(s)	Deuterium Incorporation (%)
1	None	0
2	0.35 eq. NaOPiv	0
3	0.35 eq. AgOPiv	10.0
4	0.05 eq. $AuCl_3$	41.8
5	0.05 eq. $AuCl_3$, 0.05 eq. PivOH	69.3
6	0.05 eq. $AuCl_3$, 0.35 eq. AgOPiv	0
7	0.05 eq. PPh_3AuOAc	4.4
8	0.05 eq. PPh_3AuOAc, 0.35 eq. AgOPiv	6.6

However, these studies cannot definitively show that Au(I) does not participate in the C-H bond activation. Specifically, if the Au(I)-C_6F_5 complex is stable under the reaction conditions, then the deuterium studies would provide an inaccurate representation of the degree of C-H bond activation. Indeed, when the Au(I)-C_6F_5 complex was synthesized independently and subjected to deuteration reaction conditions in presence of D_2O without additives, the formation of C_6F_5D was not observed by NMR suggesting that the reason for the lack of

deuterium incorporation shown in Tables 2.4 and 2.5, entry 7 could be a result of the high stability of the Au(I)-arene complexes rather than the inability of Au(I) to perform C-H bond activation under the cross-coupling reaction conditions. To overcome this issue, we chose to directly monitor the formation of the Au(I)- C_6F_5 complex (Figure 2.2) by ^{1}H NMR using similar conditions used for the cross-coupling reaction but in the absence of PBX, AgOPiv, and the electron-rich cross-coupling partner, while using a stoichiometric amount of PPh_3AuOAc. The formation of Au(I)- C_6F_5 complex was not observed unless a strong base, such as sodium tert-butoxide (Figure 2.2) was added, which has been shown previously.[71] This suggests that Au(I) cannot activate the C-H bond under the cross-coupling reaction conditions used, leading us to conclude that AgOPiv likely activates the C-H bond of the electron-poor arene, while the C-H bond of electron-rich species is activated by Au(III).

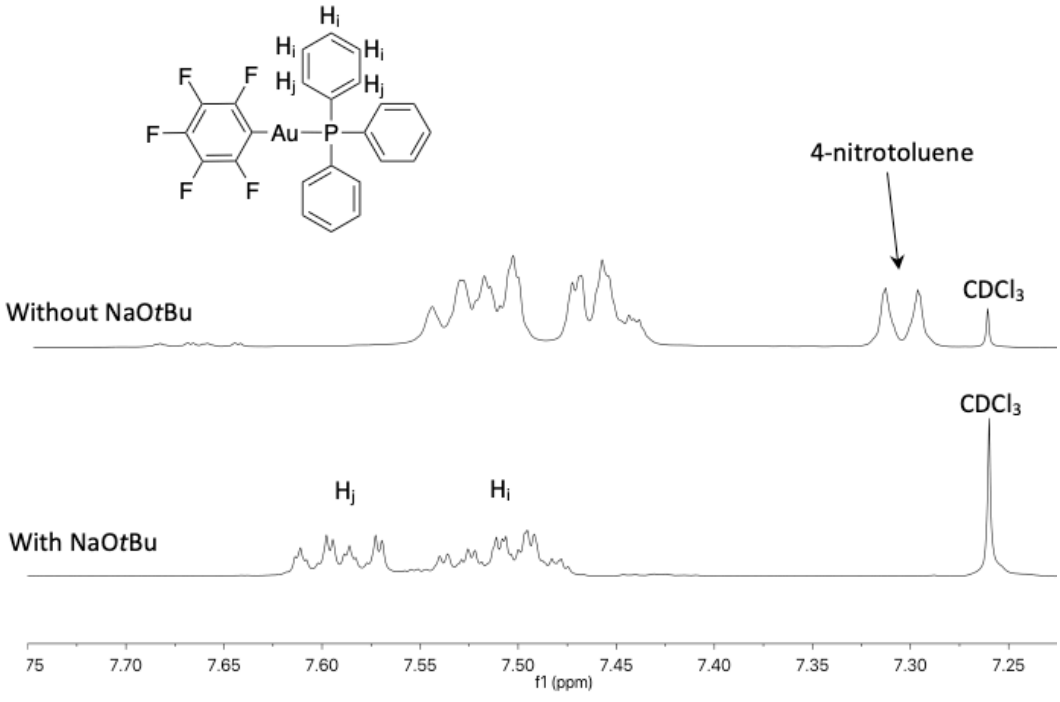

Figure 2.2 ^{1}H NMR spectra for synthesis of $PPh_3Au(I)$-C_6F_5 with and without NaO*t*Bu.

Based on the results from the above studies, we proposed that the cross-coupling mechanism consists of two overlapping cyclic pathways (Scheme 2.4). We also hypothesized that transmetalation is likely to occurs between Ag and Au(I) rather than between Ag and Au(III). The latter requirs Au(I) to be oxidized to Au(III) first. This hypothesis is based on the observed low yields of homo-coupled product of the thiophene species **A** (Table 2.3). In all entries in Table 2.3, the yields of the homo-coupled product of **A** were only up to 13 %. Additionally, from the deuterium studies, we learned that the Au(III) is very reactive in activating C-H bonds of the thiophene species **A**. If the Au(I) catalyst, $PPh_3Au(I)OAc$, without an aryl ligand is able to be oxidized to Au(III) by PBX, a high yield of homo-coupled product of **A** should have been observed, since the $PPh_3Au(I)OAc$ catalyst would have been oxidized by PBX to Au(III) species immediately, and Au(III) species would have activated the C-H bonds of two **A** molecules efficiently to generate a high yield of homo-coupled product of **A**. Therefore, we speculated that PBX cannot oxidize Au(I) species unless in the presence of an aryl ligand on the Au(I) species, and the transmetalation step is most likely to occurs between Ag and Au(I). Based on the discussion above, the homo-coupling product could arise via two possible pathways: (i) activation of C-H bonds on two thiophene molecules by Ag followed by transmetalation with Au catalyst; (ii) pathway shown in Scheme 2.4 but where pentafluorobenzene is replaced by 2-methyl thiophene. We believe that pathway (i) is not a dominant pathway because the homo-coupling of pentafluorobenzene **B** is never observed. Since the yield for homo-coupling of thiophene increases with silver loading (Table 2.3, entries 7,11, and 12), we believe that the pathway (ii) is the dominant formation pathway for the homo-coupled product of **A**. It should be noted that we see a similar trend in homo-coupling defect content in the polymerization as well, where a % alt of 77 % was achieved when 1 eq of AgOPiv

was used instead of 2 eq of AgOPiv, although M_n decreased significantly because of overall lowered monomer conversion.

Scheme 2.4 Simplified proposed mechanism of gold- and silver-catalyzed dehydrogenative cross-coupling

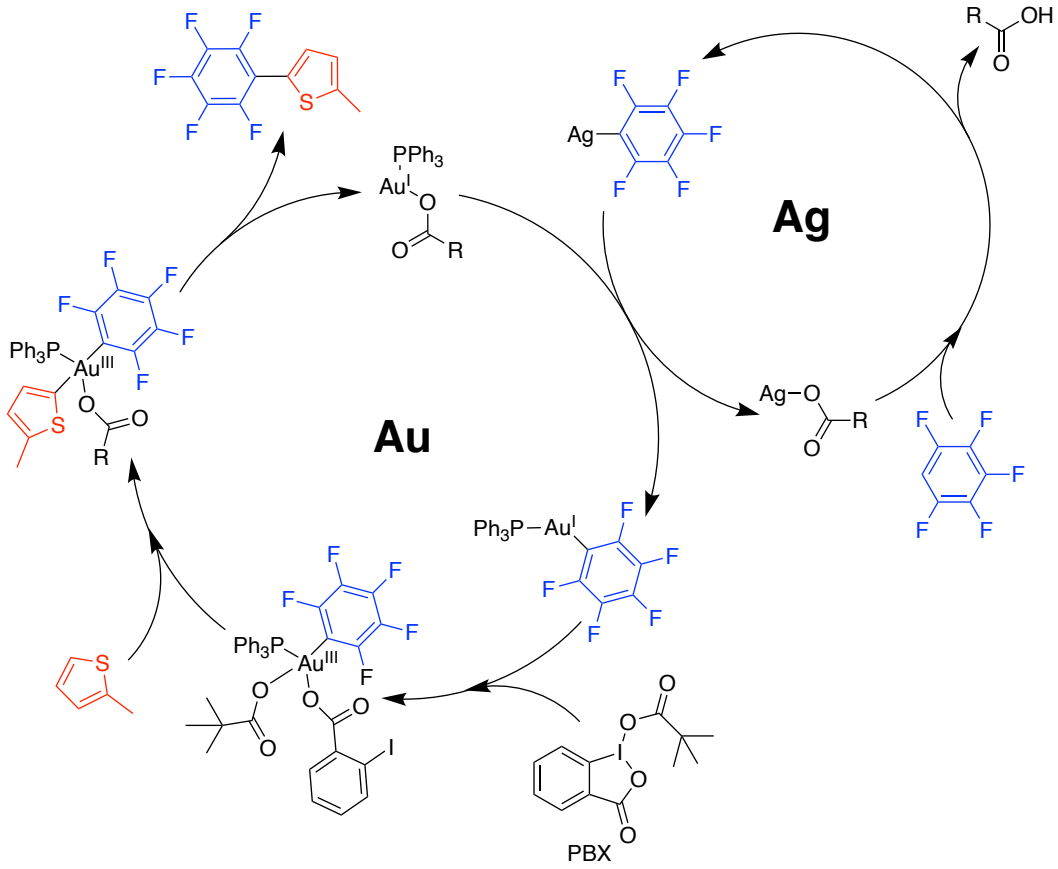

2.2.3 *Transition from Small Molecule Reactions to Polymer Synthesis*

The newly proposed mechanism presents a challenge for transitioning the Au/Ag cocatalyzed CDC method from a small molecule reaction to a polymer synthesis, as observed by the increase in amount of homo-coupling occurring in the polymerization compared to the small molecule coupling reactions. Polymer chain growth in a perfectly alternating manner in a dual cyclic mechanism would require both cycles to turn over in synchrony or for one of the intermediates to be a persistent intermediate, while also ensuring that each metal can only

selectively activate one monomer over the other.[60] The deuterium exchange studies indicated that Ag could activate the C-H bonds of both the electron-rich and electron-poor species with modest selectivity (23 % vs. 10 %). Our polymerizations indicated that the selectivity was even worse in the polymerization. We hypothesized that this was because once a thiophene coupled with an electron-poor fluorinated benzene species, the thiophene end could show increased reactivity towards Ag because of the electron-withdrawing effect from the fluorinated benzene, and/or that the generated M-bithiophene-fluorinated benzene complex, where M = Au or Ag, was more reactive than the M-bithiophene complex.

To test this hypothesis, we performed a CDC reaction of 3,3'-dihexyl-2,2'-bithiophene with **B** using similar reaction conditions to Scheme 2.2 and measured the mol % of the different products in the reaction mixture (Scheme 2.5). A 1:1 ratio of 3,3'-dihexyl-2,2'-bithiophene to **B** was used to mimic the polymerization conditions, while preventing a polymerization from taking place by using pentafluorobenzene. We observed the formation of four products by GC-MS, and the conversion of 3,3'-dihexyl-2,2'-bithiophene in this reaction was 67 % as observed by ^{1}H NMR (Figure 2.3). While the primary product was the cross-coupled dimer product **D**, the fact that mol % of product **G** was as high as that of product **F** supported our hypothesis that **D** or M-**D** complex is more reactive than the bithiophene or M-bithiophene complex and showed similar reactivity as **B** of M-**B** complex, thereby increasing the amount of homo-coupling in the polymerization. We believe that the electron-withdrawing effect from the fluorinated benzene is limited to two bithiophene units because of the twist in the monomer units, thus allowing one to maintain % alt of ~70 % throughout the polymerization. This new understanding of the selectivity in D-A semiconducting polymer synthesis via CDC provides us with a potential for controlling the incorporation ratio of donor vs. acceptor monomers. For example, choosing and

designing monomers with larger differences in their electronic properties could enhance the selectivity of Ag. Also, since we had observed that increased loading of electron-poor species resulted in higher yields of the cross-coupled product for the small molecule reactions, using different feed ratios of the two monomers would be another way to adjust % alt of the polymers leading to the development of synthetic methodologies to achieve sequence-specific polymers.

Scheme 2.5 CDC reaction between 3,3'-dihexyl-2,2'-bithiophene and B (1:1)

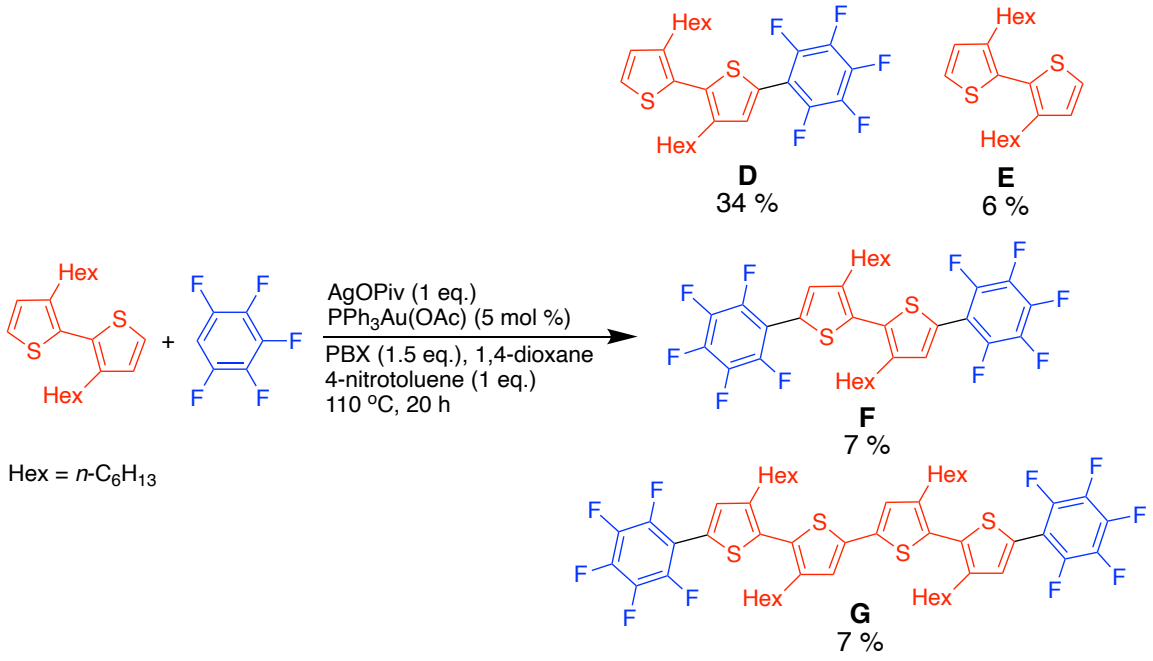

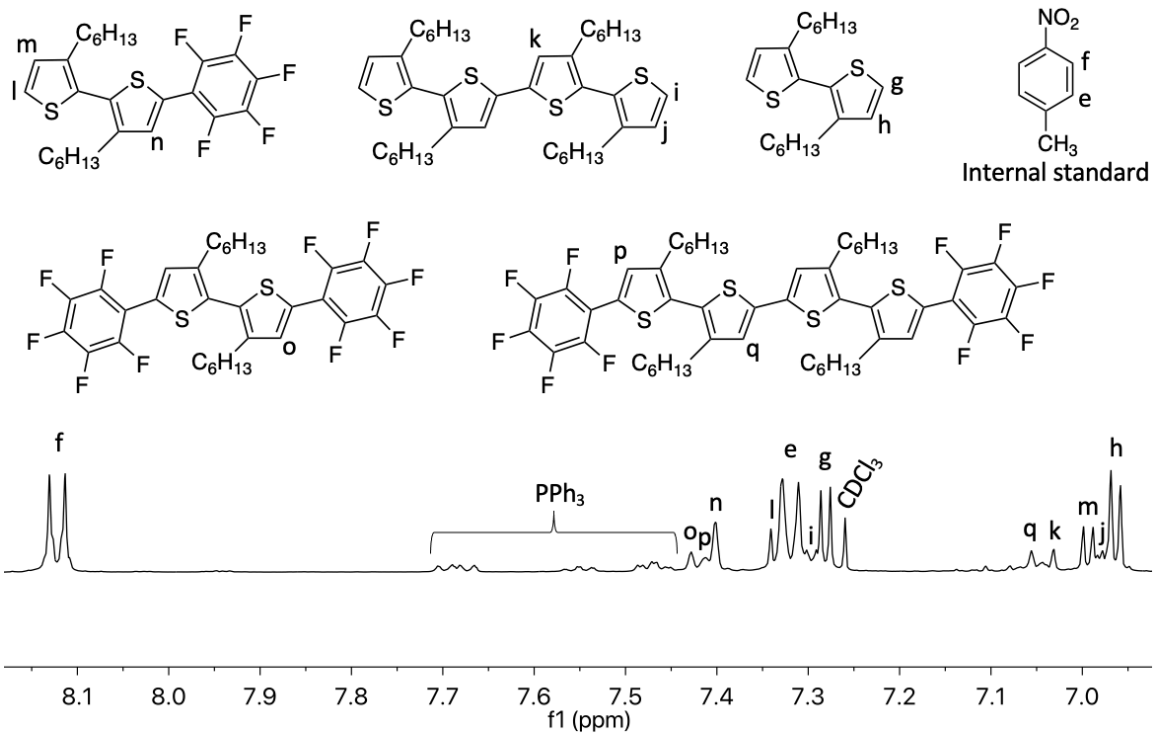

Figure 2.3 The aromatic region of ^{1}H NMR spectrum of the reaction shown in Scheme 2.5.

The low molecular weight of the resultant polymers is attributed to that the short oligomers (dimer, trimer, tetramer, etc.) formed at the early stage of the polymerization become less reactive than monomers as the polymerization proceeds, based on what we observed in Scheme 2.6. Scheme 2.6 shows a series of small molecule model reactions for the Au/Ag cocatalyzed CDC polymerization. Scheme 2.6a represents a model reaction of the 1st cross-coupling of the CDC polymerization. The cross-coupling yield in the 1st cross-coupling was as high as 88% and the homo-coupling yield was low (3%). The small molecule model reactions shown in Schemes 2.6b and 2.6c represent the chain extension in the CDC polymerization, in which the CDC occurs between the cross-coupled dimers (**3a** and **3b**) and monomers. This 2nd cross-coupling generated the cross-coupled trimers **5** and **6** in low yield, and unreacted starting materials **3a** (74 %) and **3b** (45 %) remained. Schemes 2.6d and 2.6e show the small molecule model reactions that model the overall CDC polymerization. In these reactions, the yields of **3a**

and **3b** were much higher than those of the trimer products **5** and **6**, confirming that the 2nd cross-coupling reaction is less effective than the 1st cross-coupling reaction. We can see that the CDC reactions with the cross-coupled dimers **3a** and **3b** proceeded less efficiently compared to ones with only monomers. Combined with the mechanistic studies of Au/Ag cocatalyzed CDC performed by Hong et al.,[45] where it was discovered that the Au/Ag catalyzed CDC is driven by C-H acidity of the electron-poor species and nucleophilicity of the electron-rich species, it is speculated that the difficulty for the polymers to grow is also a result of substrate-driven electronic effect. The acidity of the C-H bond on fluorobenzene of **3a** decreased upon the addition of a thiophene to the tetrafluorobenzene, and the nucleophilicity of the thiophene moiety of **3b** is also lowered due to the addition of a fluorinated benzene to the thiophene.

Scheme 2.6 Small molecule model reactions for Au/Ag cocatalyzed CDC polymerization

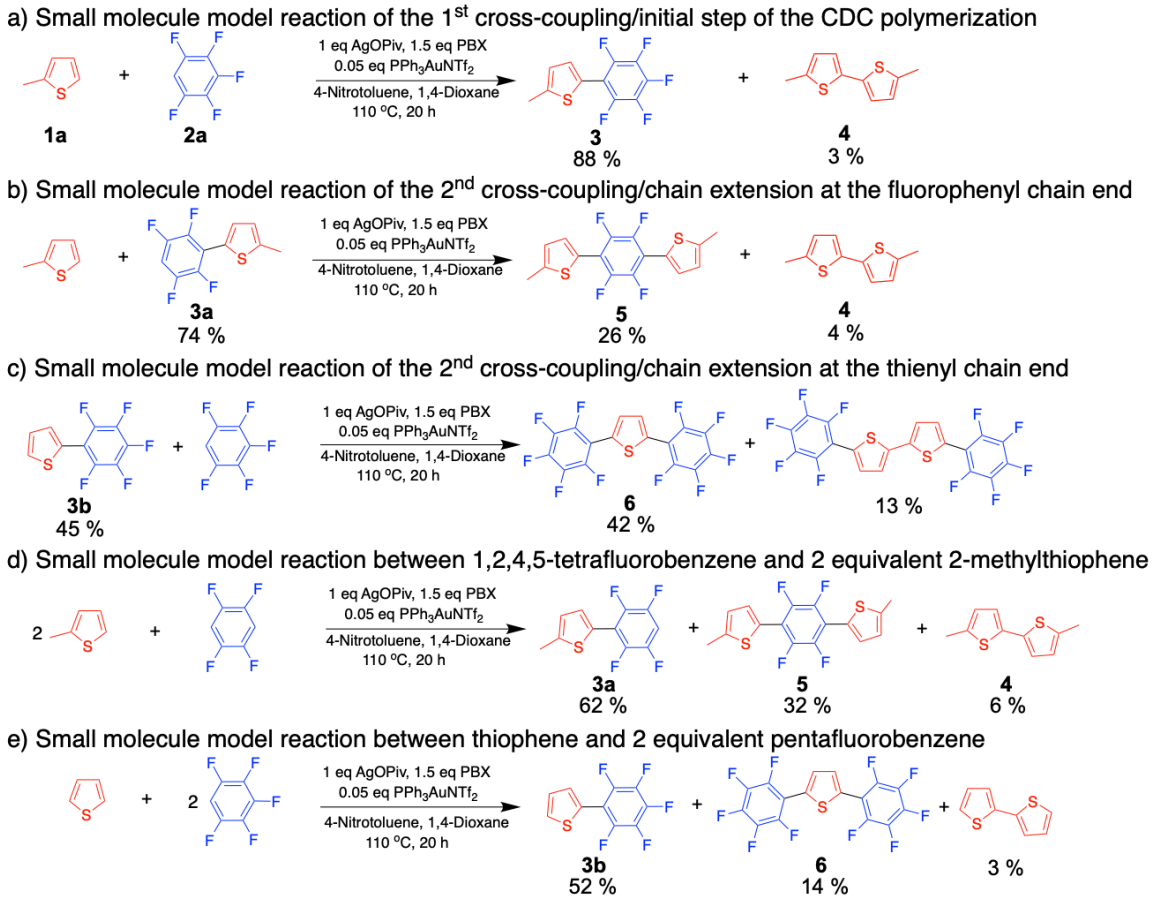

2.3 Conclusions

In conclusion, we applied the Au/Ag cocatalyzed CDC method to D-A semiconducting polymer synthesis which, to the best of our knowledge, was the first example where a dual-catalytic system being applied to the synthesis of D-A semiconducting polymers via CDC method. Through small molecule model studies, the roles of the various reagents in the reaction were elucidated. Specifically, we provide further experimental support to the suggestion that Ag is playing a role in the C-H bond activation. Our control experiments also suggest that the Ag-mediated C-H bond activation of the electron-poor species may be the rate-determining step, but detailed kinetic studies need to be carried out to confirm this. By performing the CDC reaction between 3,3'-dihexyl-2,2'-bithiophene and pentafluorobenzene, it was suggested that the chemo-selectivity loss when applying this reaction to polymer synthesis is primarily due to the increased reactivity of the bithiophene-fluorobenzene species compared to the bithiophene monomer toward Ag catalyst. In addition, this Au/Ag cocatalyzed CDC polymerization defies the Carothers equation, because the functional groups (C-H bonds) appear to be less reactive as the small oligomers form, which violates the equal reactivity assumption of the Carothers equation. Therefore, the actual molecular weights of the resultant polymers were lower than predicted by the Carothers equation and the small molecule model reaction. The originally proposed mono-metallic Au(I)/Au(III)-catalyzed mechanism may have appeared ideal for an $(\text{-AB-})_n$ alternating copolymer synthesis, but ultimately these studies show that the multi-metallic nature of the mechanism may provide a new and better tool for the facile synthesis of sequence-controlled polymers.

2.4 Supplementary Information

2.4.1 *General Information*

All manipulation of air- and/or moisture-sensitive compounds were carried out using standard Schlenk and glovebox techniques under a dry nitrogen atmosphere unless otherwise noted. NMR spectra were recorded on Bruker AV-300 and AV-500 spectrometers operating at 300 and 500 MHz, respectively. NMR chemical shifts (δ) are reported in parts per million (ppm) downfield of tetramethylsilane and are referenced relative to the residual solvent signal for ^{1}H NMR ($CDCl_3$ (7.26 ppm)). The integrals in ^{1}H NMR spectra were measured with 4-nitrotoluene as an internal standard. Anhydrous 1,4-dioxane, chloro(triphenylphosphine)gold(I), deuterium oxide, 3,3'-dihexyl-2,2'-bithiophene, gold(III) chloride, 2-methylthiophene, 4-nitrotoluene, 2,2',3,3',5,5',6,6'-octafluorobiphenyl, pentafluorobenzene, pivalic acid, sodium trimethylacetate hydrate, and 1,2,4,5-tetrafluorobenzene were used as purchased. Deuterated solvents were stored over 4 Å molecular sieves. Pivaloyloxy-1,2-benziodoxol-3(1H)-one (PBX),[61] silver pivalate (AgOPiv),[72] and acetate(triphenylphosphine)gold(I) (PPh_3AuOAc)[73] were synthesized using previously reported methods. Dispersity values were measured using a Waters Breeze GPC system in chloroform with 0.1 % triethylamine by volume, against a polyethylene glycol/oxide (PEG/PEO) standard, at a flowrate of 1 mg/mL at 30 °C.

2.4.2 *Cross-Coupling Studies*

A 4 mL amber vial and an acid-washed stir bar were oven dried overnight. PPh_3AuOAc (2.59 mg, 5.00 μmol), silver pivalate (14.6 mg, 70.0 μmol), 4-nitrotoluene (13.7 mg, 100 μmol), and PBX (52.2 mg, 150 μmol) were added to the previously mentioned vial and sealed with a septa cap. Vial was evacuated and refilled with nitrogen

three times. Under nitrogen pressure, anhydrous 1,4-dioxane (0.5 mL), pentafluorobenzene (16.8 mg, 100 µmol), and 2-methylthiophene (9.82 mg, 100 µmol) were injected into the reaction flasks in succession. The reactions were heated at 110 °C overnight. The resulting mixtures were passed through a celite plug using hexanes, washed with 1 M HCl, followed by 1 M NaOH aqueous solution, and then the organic layer was dried using anhydrous Na_2SO_4. The remaining solvent was removed under reduced pressure. The resulting mixtures were analyzed by NMR.

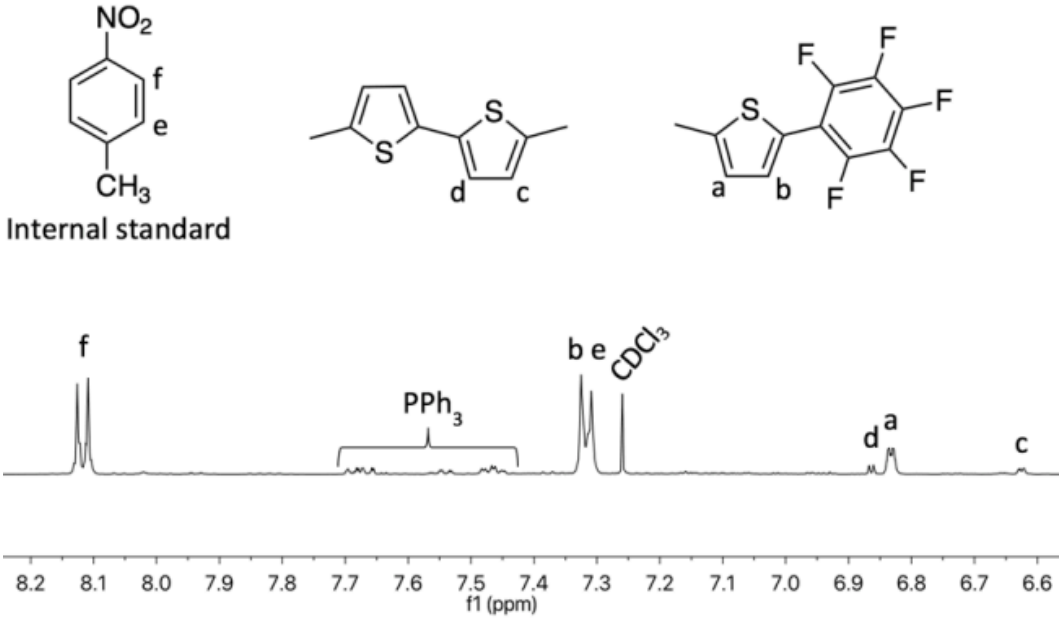

Figure 2.4 The aromatic region of a representative ^{1}H NMR spectrum of small molecule studies

2.4.3 *CDC Polymerizations*

A 20 mL amber vial and an acid-washed stir bar were oven dried overnight. PPh_3AuOAc (25.9 mg, 50.0 µmol), silver pivalate (418 mg, 2.00 mmol), 4-nitrotoluene (137 mg, 1.00 mmol), and PBX (696 mg, 2.00 mmol) were added to the previously mentioned vial and sealed with a septa cap. Vial was evacuated and refilled with nitrogen

three times. Under nitrogen pressure, anhydrous 1,4-dioxane (5 mL), 2,2',3,3',5,5',6,6'-octafluorobiphenyl (298 mg, 1.00 mmol) or 1,2,4,5-tetrafluorobenzene (150 mg, 1.00 mmol), and 3,3'-dihexyl-2,2'-bithiophene (334 mg, 1.00 mmol) were injected into the reaction flasks in succession. The reactions were heated at 110 °C. The reaction was quenched with 1 M HCl. The resulting mixture was washed with saturated EDTA solution, and then precipitated into excess MeOH. Then the resulting polymer was Soxhlet extracted with MeOH, then collected in chloroform. The remaining solvent was removed under reduced pressure. The resulting mixtures were analyzed by NMR, GPC.

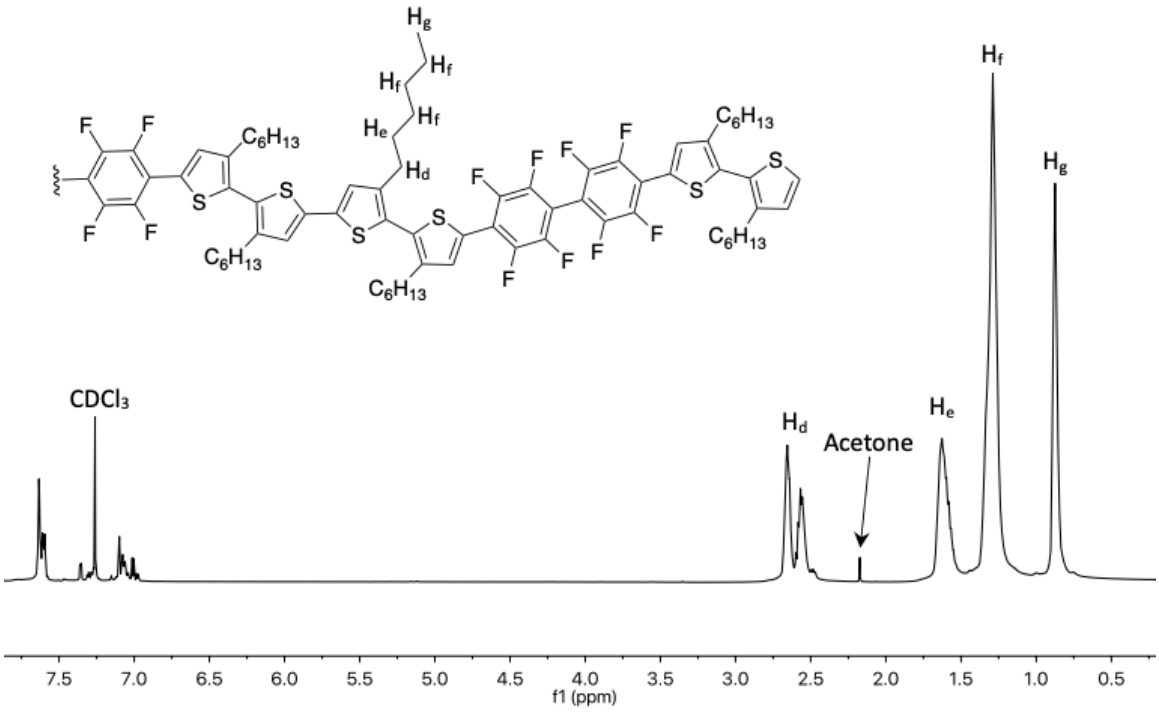

Figure 2.5 Example ^{1}H NMR (500 MHz, CDCl3) of **Polymer B** at 168 h time point.

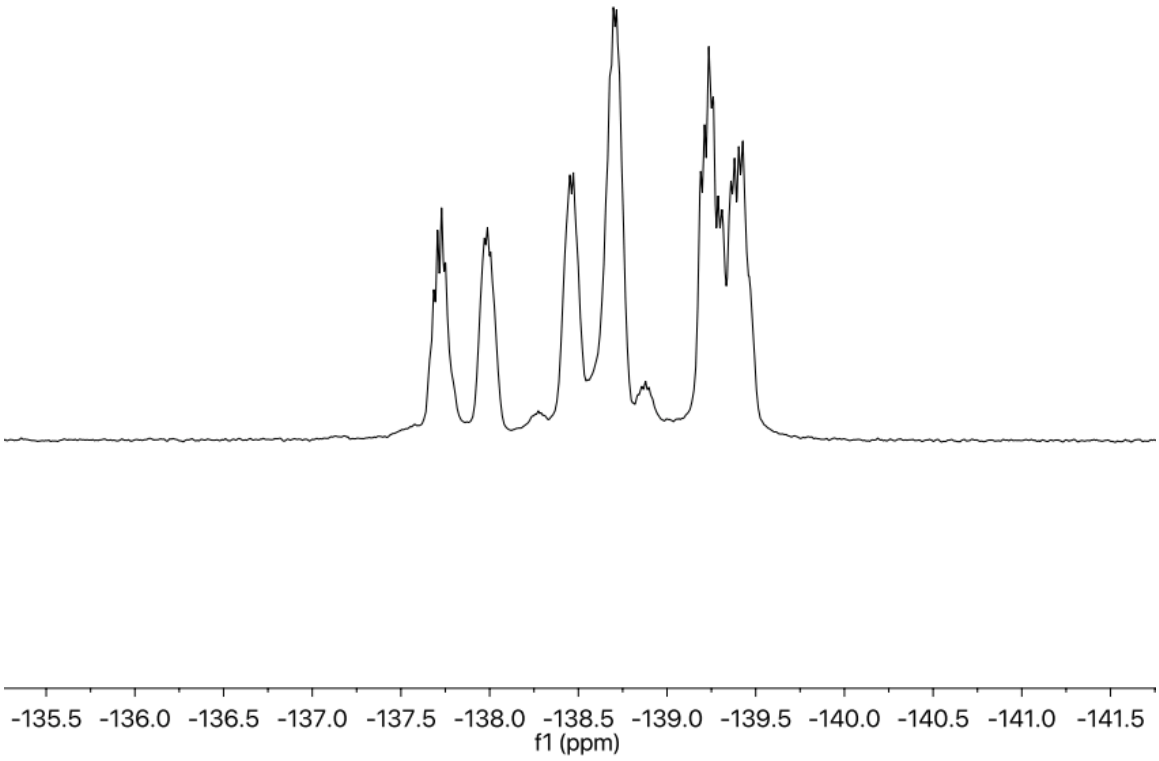

Figure 2.6 Example ^{19}F NMR (470 MHz, CDCl3) of **Polymer B** at 168 h time point.

2.4.4 *Deuterium Studies*

A 4 mL amber vial and an acid-washed stir bar were oven dried overnight. Varied combinations of additives were added and then the vial was evacuated and refilled with nitrogen three times. Under nitrogen pressure, anhydrous 1,4-dioxane (0.5 mL), 2-methylthiophene (9.82 mg, 100 μmol) or pentafluorobenzene (16.8 mg, 100 μmol), and deuterium oxide (10.0 mg, 500 μmol) were injected into the reaction flasks in succession. The reactions were heated at 110 °C overnight. DMSO-d_6 (10.0 μL, 141 μmol) were added. The reaction mixtures were passed through a celite plug. The mixture was analyzed using ^{2}H NMR, by comparing the deuterated aryl peak against the DMSO-d_6 peak.

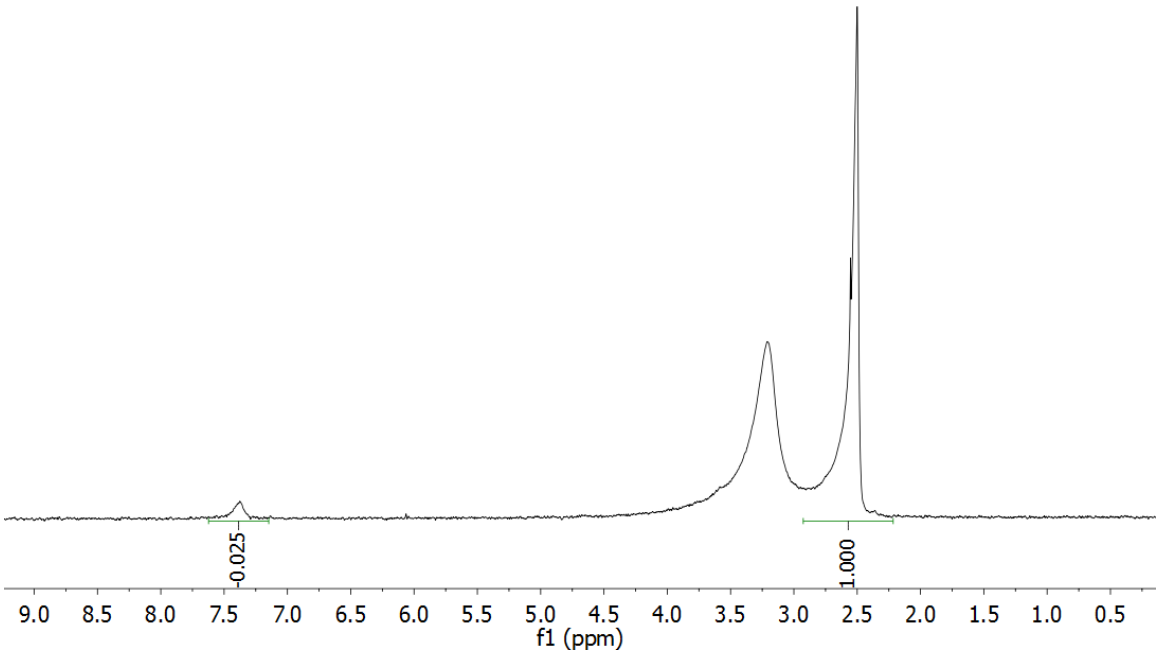

Figure 2.7 Example ^{2}H NMR of deuterated product of pentafluorobenzene reacted with AgOPiv and AuOAcPPh$_3$.

Equation 2.1. Deuterium incorporation calculation

$$\text{Deuterium incorporation \%} = \frac{I_P}{I_D} \times \frac{0.141\ \text{mmol} \times 6}{0.1\ \text{mmol}} \times 100\ \%$$

2.4.5 *Calculations of % Alt, M_n, and DP Using ^{1}H NMR*

% Alt, M_n, and DP were calculated using the integration of end groups (I_a, I_b, $I_{a'}$, and $I_{b'}$) and aromatic protons (I_h and I_c) on the chain backbone.

Equation 2.2 DP calculation, using end-group analysis

$$\text{DP} = \frac{2I_c}{I_a + I_b'} + \frac{I_h}{I_a + I_b'}$$

Equation 2.3 M_n calculation, using end-group analysis

$$M_n = \frac{I_c}{I_a + I_{b'}}(MW_D + MW_A) + \frac{I_h}{I_a + I_{b'}} MW_D + MW_D$$

Equation 2.4 % Alt calculation

$$\%\ \text{alt} = \frac{I_c}{I_c + I_h} * 100\ \%$$

Note that $I_a = I_b$ and $I_{a'} = I_{b'}$, and that I_a and $I_{b'}$ were chosen because they appear as clean non-overlapping doublets in the NMR spectra.

Chapter 3. Pd/Ag dual catalytic cross dehydrogenative coupling for donor-acceptor semiconducting polymer synthesis

*The work in Chapter 3 is adapted from a previously published article: Reprinted with permission from *J. Am. Chem. Soc.* **2022***, 144,* 2311–2322; DOI: 10.1021/jacs.1c12599.

3.1 Introduction

Here, we present another CDC polymerization that defies the Carothers equation, a Pd/Ag cocatalyzed CDC polymerization reported by Kanbara et al. in 2018.[47] The mechanistic sequence of this Pd/Ag cocatalytic CDC cycle was also reported by Kanbara et al. in 2020,[49] where the C-H bond of the electron-poor monomer is activated by Ag and the C-H bond of the electron-rich monomer being activated by Pd. Unlike the Au/Ag cocatalyzed CDC polymerization reported in Chapter 2, this Pd/Ag cocatalyzed CDC results in high molecular weight polymers (53.4 kg/mol within 48 h) with low homo-coupling defects content (4 %) despite the small molecule coupling reaction proceeding inefficiently (Scheme 3.1a). In the Pd/Ag cocatalyzed system, we find that the functional groups (C-H bonds) become more reactive after the 1st cross-coupling step. Specifically, in the 1st cross-coupling reaction, Pd-mediated C-H bond activation is the rate-determining step, whereas in the proceeding chain extending cross-coupling reaction (2nd cross-coupling), the energy barrier to break the C-H bond is reduced due to the presence of the thiophene substituent on the fluorinated benzene. While these findings have important implications in polymerizations leading to unexpectedly high molecular weight polymers and reduced homo-coupling defects, they could also affect the design of substrates in late-stage C-H functionalization.

3.2 Results and Discussion

3.2.1 *Small Molecule Model Reactions for the Pd/Ag Cocatalytic System*

The results of the small molecule model reactions for the Pd/Ag cocatalyzed CDC polymerization are shown in Scheme 3.1. Scheme 3.1a shows the small molecule model reaction for the initial step (1st cross-coupling) of the CDC polymerization. There is almost no chemo-selectivity, and the product yields are low. In Scheme 3.1b, the chain extension step (2nd cross-coupling), the trimerization of cross-coupled dimer **3a** displayed an exceptional reactivity and cross chemo-selectivity (the yield of cross-coupled trimer **5** was close to 100%). In Scheme 3.1d the yield of the trimer **5** (88%) is much higher than that of the dimer **3a** (12%). We speculated that in Scheme 3.1d, once **3a** was formed, it immediately reacted with another monomer **1a** to produce the cross-coupled trimer **5**, which drove the reaction forward. For Schemes 3.1c and 3.1e, no desired product was detected by NMR spectroscopy because both C-H bonds at the α- and β-positions of the thiophene moiety that is attached to an electron-withdrawing group (**3b**) can be activated during the reaction, leading to the formation of insoluble polymeric materials.[74] Generally, Scheme 3.1 shows that the chain extension CDC proceeded more readily than the 1st CDC reaction, which is opposite to what was observed in the Au/Ag system in Scheme 2.6. We can see that the Pd/Ag cocatalyzed CDC polymerization also defies the Carothers equation because the functional groups (C-H bonds) appear to be more reactive as the polymerization proceeds. In this chapter, we focus on the mechanistic investigation of the Pd/Ag catalyzed chain extension CDC (Scheme 3.1b) to elucidate the factors that contribute to the high molecular weight polymer with minimal homo-coupling defects using both experimental and computational methods.

Scheme 3.1 Small molecule model reactions for Pd/Ag cocatalyzed CDC polymerization

a) Small molecule model reaction of the 1st cross-coupling/initial step of the CDC polymerization

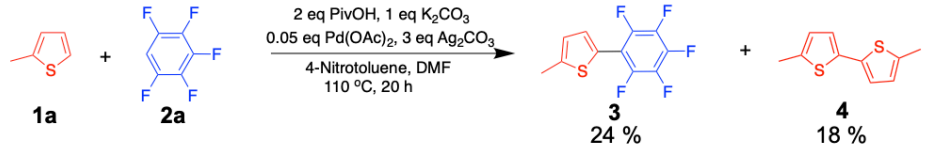

b) Small molecule model reaction of the 2nd cross-coupling/chain extension at the fluorophenyl chain end

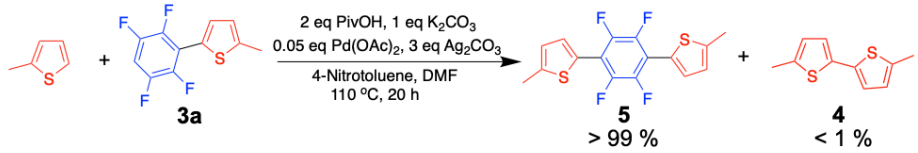

c) Small molecule model reaction of the 2nd cross-coupling/chain extension at the thienyl chain end

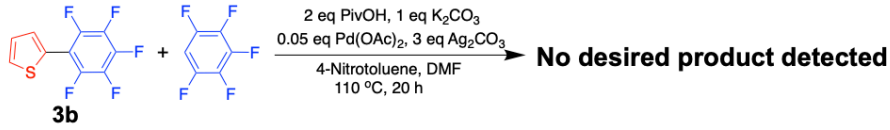

d) Small molecule model reaction between 1,2,4,5-tetrafluorobenzene and 2 equivalent 2-methylthiophene

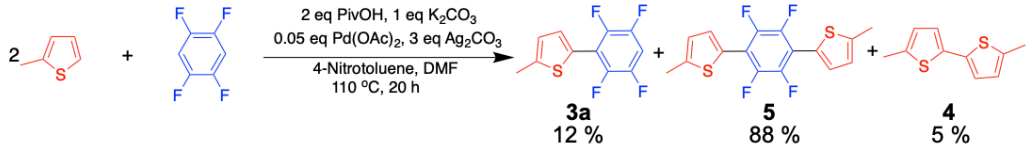

e) Small molecule model reaction between thiophene and 2 equivalent pentafluorobenzene

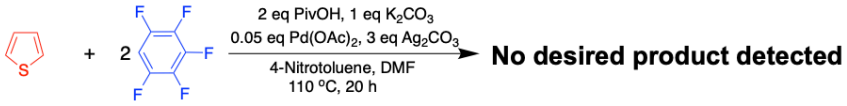

3.2.2 *Stepwise CDC Sampling Experiments*

Our mechanistic studies for the chain extension CDC started with the stepwise CDC sampling experiment (Scheme 3.2). The yield of each species was tracked using ^{19}F NMR and is shown in Table 3.1. In this sampling experiment, **3a** and Ag_2CO_3 and other additives were first mixed and heated at 100 °C for one hour. Then, the first aliquot (sampling 1) was taken. Next, $Pd(OAc)_2$ was added and the reaction continued for another hour and the second aliquot (sampling 2) was taken. Finally, **1a** was added, and after 15 min the third aliquot (sampling 3) was taken. The ^{19}F NMR spectrum of each sampling is shown in Figure 3.1. In sampling 1, we

observed the formation of Ag-**3a**, which indicated that the Ag-mediated C-H bond activation on **3a** occurred (Figure 3.1, bottom). After adding $Pd(OAc)_2$ and heating the reaction for one hour (sampling 2), the peaks corresponding to Ag-**3a** disappeared, and the peaks corresponding to Pd complexes (Pd-**3a** and Pd-(**3a**)$_2$) appeared up (Figure 3.1, middle spectrum), which suggested that transmetalation between Ag-**3a** and Pd(II) occurred in this step. Sampling 2 also showed that the bifluoroaryl palladium, Pd-(**3a**)$_2$, was more prevalent than the monofluoroaryl palladium, Pd-**3a**. In sampling 3, the cross-coupled trimer product **5** was detected, which implied a C-C bond formation between **3a** and **1a** (Figure 3.1, top). Based on the results above, we conjectured that the mechanistic sequence of the Pd/Ag cocatalyzed chain extension CDC is: 1) Ag-mediated C-H bond activation on electron-poor **3a**; 2) Transmetalation between Ag-**3a** and Pd(II) to form Pd-**3a** and Pd-(**3a**)$_2$; 3) Pd-mediated C-H bond activation of the electron-rich **1a**; 4) Reductive elimination to form the cross-coupled product **5**; and then 5) Oxidation of Pd(0) by Ag(I) to reactivate the Pd catalyst. This is consistent with the mechanistic sequence of the 1st cross-coupling reaction uncovered by the Kanbara group.[49]

Scheme 3.2 Stepwise CDC sampling experiments to determine the mechanistic sequence of the Pd/Ag catalyzed chain extension CDC

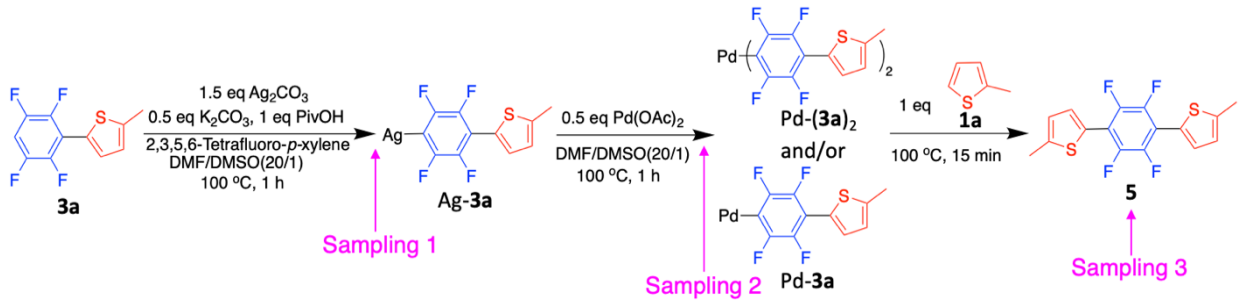

Table 3.1 Yield of each species in the stepwise CDC sampling experiment shown in Scheme 3.2

Sampling	**3a** (%)	Ag-**3a** (%)	Pd-**3a** (%)	Pd-(**3a**)$_2$ (%)	**5** (%)
1	90	10	-	-	-
2	9	Not detected	11	60	-
3	14	Not detected	Not detected	12	64

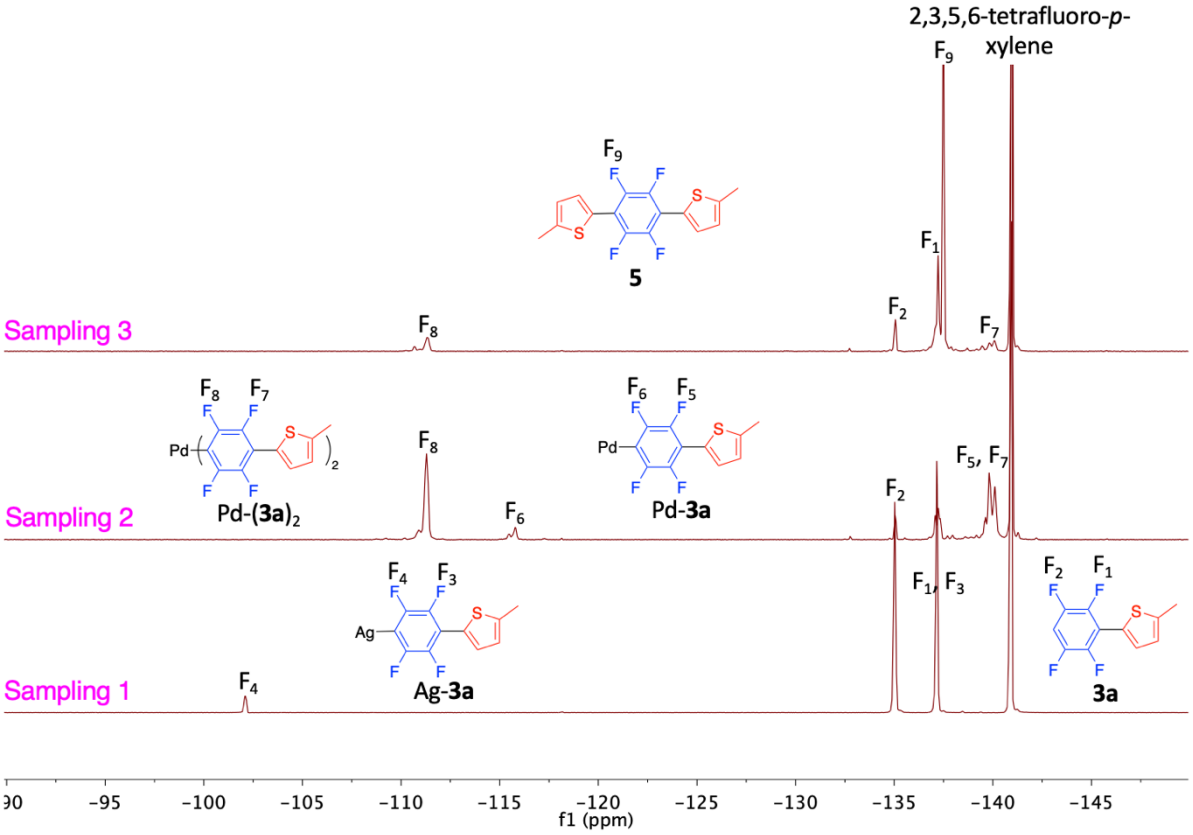

Figure 3.1 ^{19}F NMR spectrum of each sampling in the stepwise CDC sampling experiment shown in Scheme 3.2 with 2,3,5,6-tetrafluoro-*p*-xylene (-140.95 ppm in DMSO-d_6) as an internal standard.

To confirm this proposed mechanistic sequence of the chain extension step, controlled stepwise CDC sampling experiments were conducted (Scheme 3.3). The yield of each species is

summarized in Tables 3.6, 3.7, and 3.8 in Section 3.4.5, and the NMR spectrum of each sampling is shown in Figures 3.4, 3.5, and 3.6 in in Section 3.4.5. When the sequence of adding **1a** and **2a** was reversed (Scheme 3.3a), no cross-coupled product **3** was observed in sampling 3 according to ^{1}H NMR, which means the mechanistic sequence shown in Scheme 3.3a can be ruled out. It is worth noting that no homo-coupled thiophene dimer **4** was present in any sampling in Scheme 3.3a, which will be explained later. When the sequence of adding Ag_2CO_3 and $Pd(OAc)_2$ was reversed (Scheme 3.3b), 72% of **5** was formed in sampling 3, and no Ag-**3a** was observed in any sampling according to ^{19}F NMR. The generation of Pd-**3a** and Pd-(**3a**)$_2$ in sampling 1 indicates that Pd-**3a** and Pd-(**3a**)$_2$ can form in the absence of the Ag additive. After adding Ag_2CO_3, the yield of Pd-(**3a**)$_2$ increased slightly, and Pd-**3a** dis-appeared (sampling 2). Compared to the experiment where Ag_2CO_3 was added first, and $Pd(OAc)_2$ was added second (Scheme 3.2), the yields of Pd-**3a** and Pd-(**3a**)$_2$ were much lower (11% and 60% vs. 3% and 28%), which suggests that the presence of Ag additive can promote the formation of fluoroaryl Pd intermediates by activating the C-H bonds of fluoroarenes. Therefore, based on the results in Scheme 3.3b, the proposed mechanistic sequence of the chain extension CDC still stands. In the sampling experiment shown in Scheme 3.3c, where the addition of Ag_2CO_3 was skipped, only 11% cross-coupled trimer **5** was produced in sampling 2, and the yield of Pd-(**3a**)$_2$ decreased only a little. The results in Schemes 3.3b and 3.3c indicate that the Ag additive is required for this CDC to proceed mainly because the active intermediate Pd-**3a**, which is responsible for C-H bond activation of **1a**, cannot be generated from the inactive intermediate Pd-(**3a**)$_2$ in the absence of [Ag]. This was also observed in the mechanistic study of the 1st cross-coupling performed by the Kanbara group.[49] Overall, the controlled stepwise CDC sampling experiments (Scheme 3.3) supported the proposed mechanistic sequence of the chain extension step shown in Scheme 3.2.

Scheme 3.3 Controlled stepwise CDC sampling experiments to verify the proposed mechanistic sequence of the chain extension step. a) The sequence of adding 1a and 2a was reversed. b) the sequence of adding Ag_2CO_3 and $Pd(OAc)_2$ was reversed. c) The addition of Ag_2CO_3 was skipped

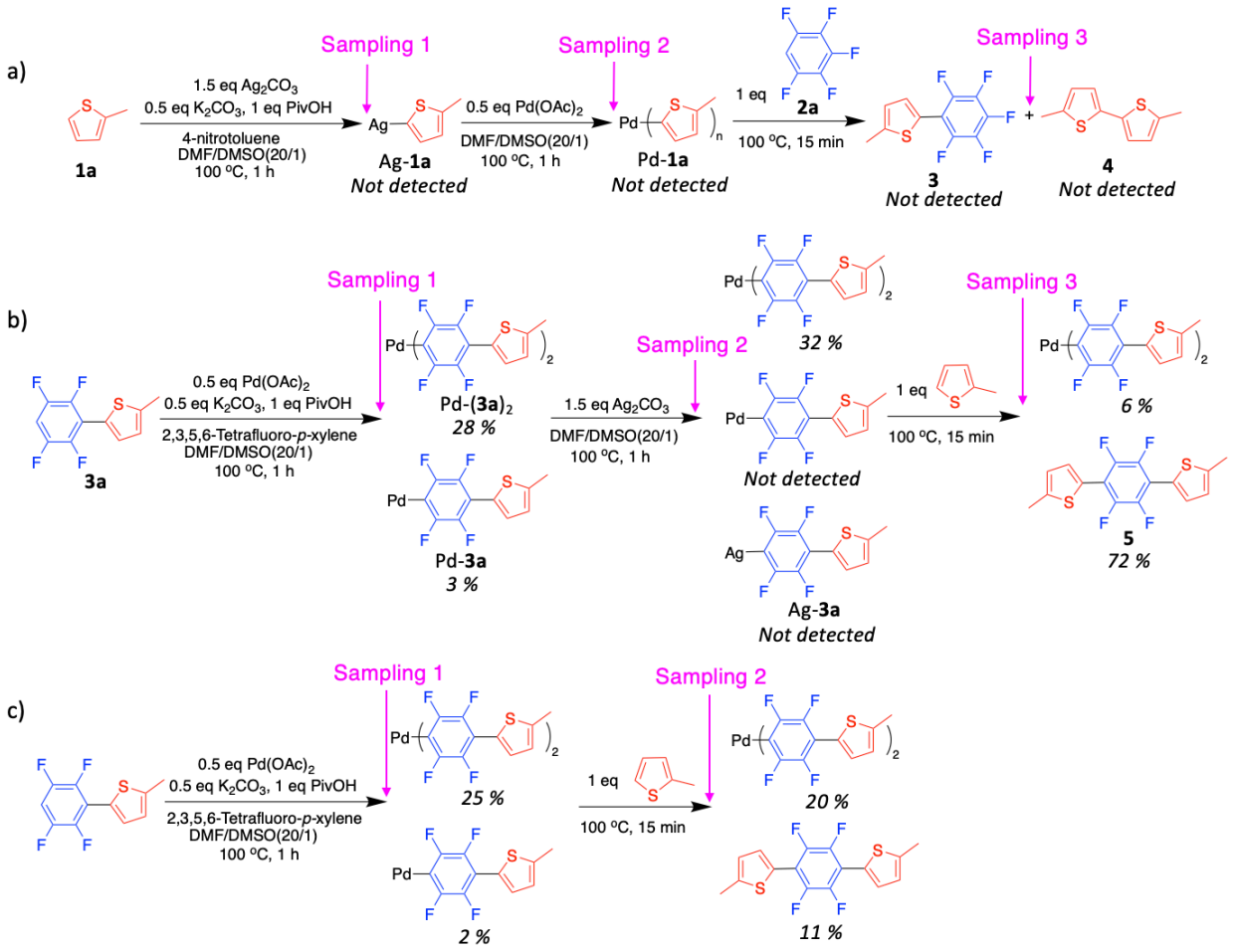

3.2.3 *Kinetic Analysis*

To obtain more information about the chain extension CDC, we performed kinetic analysis via reaction progress kinetic analysis (RPKA) and variable time normalization analysis (VTNA) based on the standard conditions shown in scheme 3.4.[75,76] The "same excess" experiment confirmed that there was no catalyst deterioration or product inhibition during the reaction (Figure 3.2a). The rate dependence of the important reagents was determined via VTNA. The order of zero was obtained for both **1a** and **3a**, which indicated that neither **1a** nor

3a was involved in the rate-determining step (RDS) (Figures 3.2b and 3.2c). 1st order in [Pd] was determined in Figure 3.2d. The 2nd order in [Ag] was obtained by measuring the initial reaction rates under different AgOPiv loadings due to the poor solubility of Ag_2CO_3 in the reaction system (Figure 3.2e). The 1st order in [Pd] and the 2nd order in [Ag] implied that both Pd and Ag catalysts were involved in the RDS. The 2nd order in AgOPiv indicated that 2 equivalents of AgOPiv were participating in the RDS.

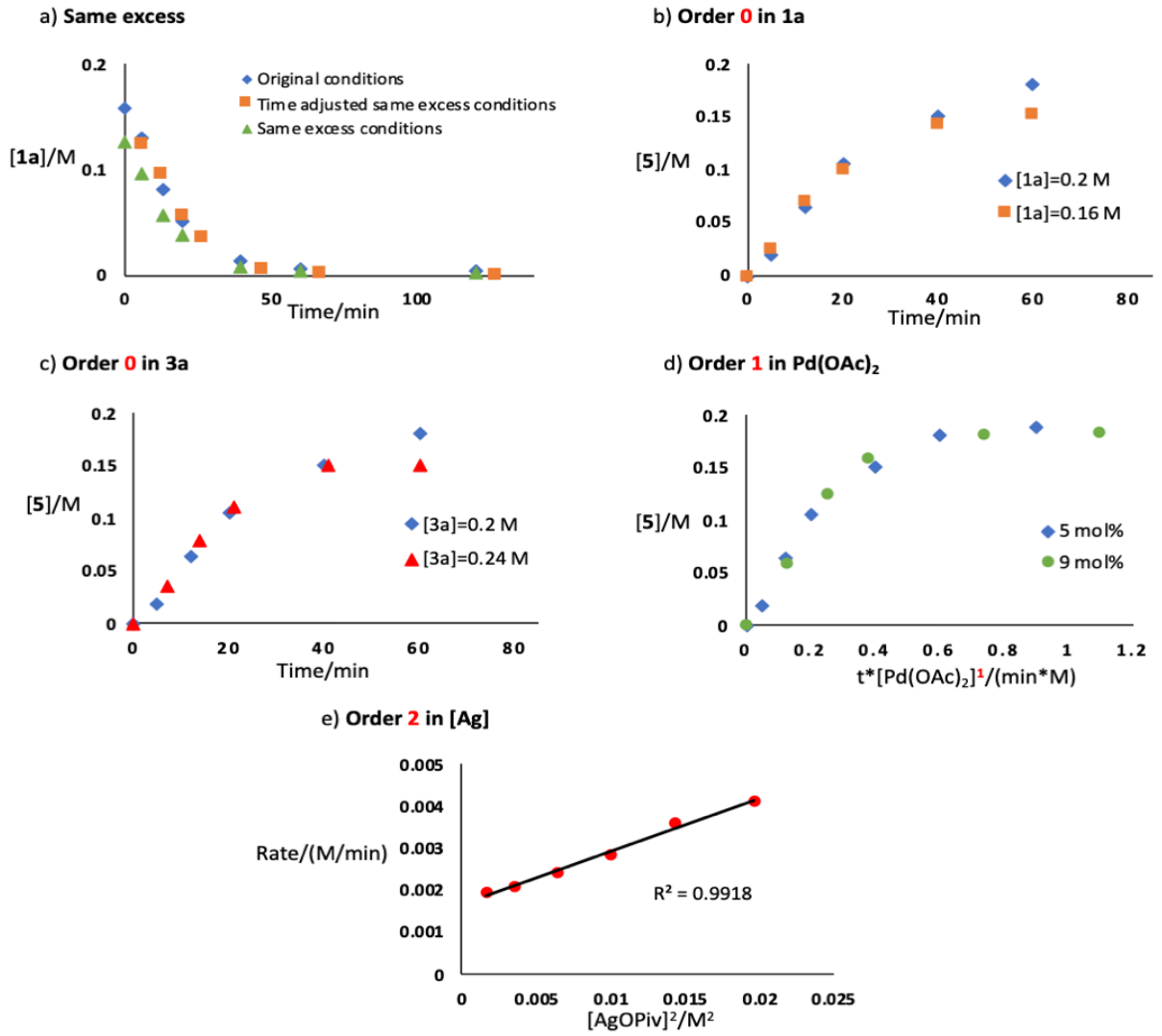

Figure 3.2 a) Same excess experiment and determination of the order in b) **1a**, c) **3a**, d) $Pd(OAc)_2$, and e) [Ag] (due to the poor solubility of Ag_2CO_3 in DMF, a soluble Ag salt, AgOPiv was used to determine the order in [Ag]).

Scheme 3.4 The chain extension step CDC under standard conditions for kinetic analysis

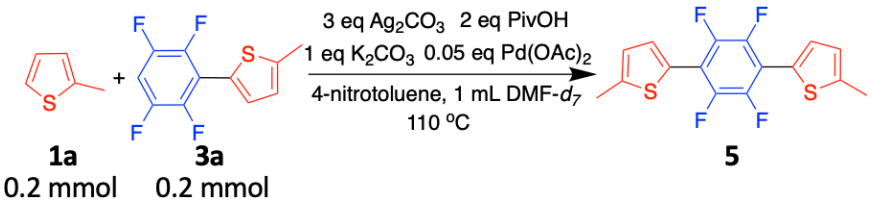

The kinetic isotope effect (KIE) studies were also carried out via VTNA. As shown in Scheme 3.5 (note that 2 eq K_2CO_3 was added to reach kinetic saturation), the KIE value for the CDC between **1a** and **3a/3a-*d*$_1$** (Scheme 3.5a) was measured to be 1.1. The KIE value for the CDC between **3a** and 2-hexylthiophene/2-hexylthiophene-*d*$_1$ (Scheme 3.5b) was measured to be 1.3. The use of 2-hexylthiophene instead of **1a** was chosen because of the difficulty in synthesizing and isolating the deuterated 2-methylthiophene (**1a-*d*$_1$**). The results of the KIE studies verified that the RDS was not the C-H bond activation of either **1a** or **3a**.

Scheme 3.5 KIE studies: a) the reaction between 1a and 3a/3a-*d*$_1$ and b) the reaction between 3a and 2-hexylthiophene/2-hexylthiophene-*d*$_1$

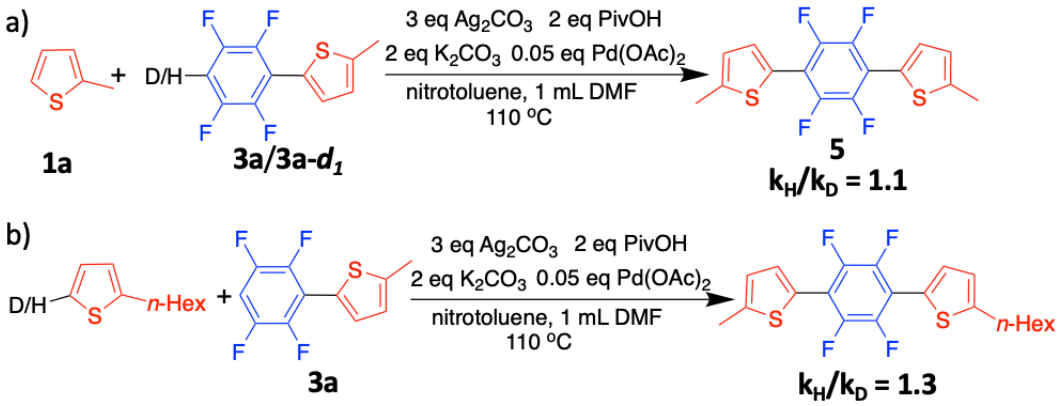

3.2.4 *Origins of the High Molecular Weight/Efficient Chain Extension CDC*

The fact that neither **1a** nor **3a** was involved in the RDS, but the Ag and Pd catalysts were both involved in RDS led us to the possibility that the oxidation of Pd(0) by Ag(I) was the RDS in the chain extension CDC. It is worth noting that in the kinetic profile of the 1st CDC reaction

reported by the Kanbara group,[49] the Pd-mediated C-H bond activation of the electron-rich thiophene species was determined to be the RDS, and that the homo-bifluoroaryl Pd complex (Pd−$(Ar^{pf})_2$, [Ar^{pf} = perfluoroarene]), was demonstrated to be a stable resting state. However, in the chain extension CDC, we found that the oxidation of Pd(0) by Ag(I) was likely the RDS. Under the same reaction conditions, the rate of oxidation is expected to remain the same in both the initial and chain extension steps. Therefore, it was surmised that the thienyl substituent on fluorobenzene (**3a**) may have accelerated the Pd-mediated C-H bond activation on the electron-rich thiophene species in the chain extension CDC, leading to the change of RDS. This also implies that the overall rate of the chain extension CDC is faster than that of the initial step CDC. In addition, the corresponding homo-bifluoroaryl Pd complex (Pd-(**3a**)$_2$) may no longer be the resting state in the chain extension CDC since the concentration of fluorobenzene does not exhibit a negative rate dependence. Therefore, the chain extension CDC proceeds more efficiently than the initial step CDC, which results in high molecular weights of the D-A semiconducting polymers synthesized via Pd/Ag cocatalyzed CDC. Based on our findings so far, we proposed a Pd/Ag cocatalytic cycle for the mechanism of chain extension CDC as well as the background homo-coupling cycle of thiophene species (Scheme 3.6). The mechanism of the homo-coupling side reaction of thiophene species was putatively proposed based on previous reports, where the Ag additive was determined to be the C-H bond activation reagent for thiophene species.[49,65,67]

Scheme 3.6 Proposed mechanisms of Pd/Ag cocatalyzed chain extension step CDC as well as the background homo-coupling of thiophene species

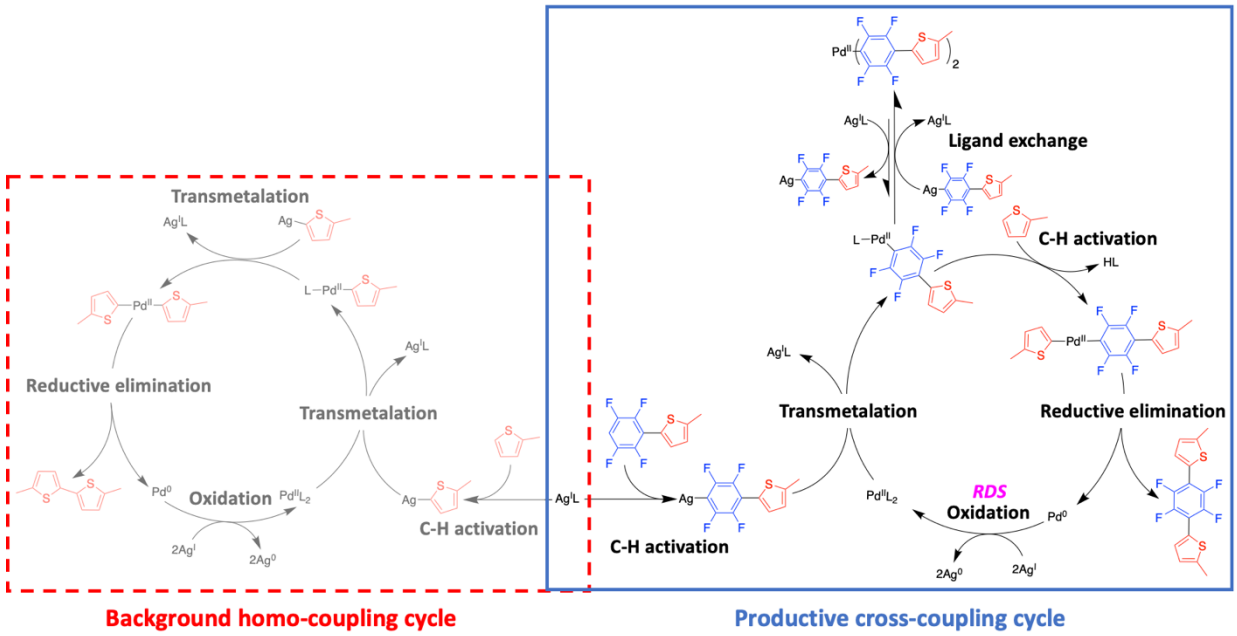

3.2.5 *Origins of the Minimal Homo-Coupling Defects/High Cross Chemo-Selectivity*

To understand of the origins of the extraordinary cross chemo-selectivity in the chain extension CDC, we conducted two additional stepwise CDC sampling experiments (Scheme 3.7). We mixed Ag_2CO_3, **3a** or **2a**, 2-(2-fluoroethyl)thiophene (**2-FET**), and other additives together at the beginning of the sampling experiments and tracked the yield of each species using ^{1}H NMR in DMSO-d_6 (^{1}H NMR spectra are shown in Figures 3.7 and 3.8 in Section 3.4.5). We chose to use 2-(2-fluoroethyl)thiophene (**2-FET**) over 2-methylthiophene here, as the use of **2-FET** allows all species to be monitored with ^{19}F NMR spectroscopy. The yields of all the species in each sampling are summarized in Tables 3.2 and 3.3. Looking at the sampling 2 in Tables 3.2 and 3.3, it was noticeable that only the fluoroaryl Ag intermediates (Ag-**2a** and Ag-**3a**) were observed. This observation was unexpected because according to our deuterium studies shown in

Tables 3.4 and 3.5 and Schemes 3.8a and 3.8c in Section 3.4.3, Ag_2CO_3 was able to cleave the C-H bonds of both thiophene and fluorobenzene arenes. Therefore, we speculated that the absence of Ag-**2-FET** is related to the relative thermodynamic stability of aryl Ag intermediates.[67] The fact that the yield of **2-FET** was still ~100% in sampling 2 in both Tables 3.2 and 3.3 suggests that during the one hour between sampling 1 and sampling 2, Ag-**2-FET** was formed after C-H bond activation, but it immediately reacted with a proton source in the reaction mixture (most likely PivOH) to regenerate **2-FET**. After the addition of $Pd(OAc)_2$ (sampling 3 in Tables 3.2 and 3.3), only cross-coupled products, some leftover fluoroarenes (**2a** and **3a**), and homo-bifluoroaryl Pd complexes (Pd-(**3a**)$_2$ and Pd-(**2a**)$_2$) were detected. No homo-coupled **2-FET** dimerization product in all the samplings in Tables 3.2 and 3.3 implied that the formation of the homo-coupled thiophene dimer requires the initial Ag-mediated C-H bond activation of the thiophene species, followed by immediate transmetalation with Pd(II) catalyst to generate the thienyl Pd intermediate. This supported the homo-coupling catalytic cycle proposed in Scheme 3.6. The above observations and discussion also explained the absence of homo-coupled product in Scheme 3.3a. The absence of Pd-**2-FET** in sampling 3 in both Tables 3.2 and 3.3 was probably the consequence of the instability of the thienyl Pd intermediate under the reaction conditions because Pd (II) was known to be capable of activating the C-H bonds of thiophene species.[65,77,78] The absence of **2-FET** in sampling 3 in Tables 3.2 and 3.3 suggests that the disappearance of Pd-**2-FET** did not regenerate the **2-FET**, and that deterioration was likely to happen to Pd-**2-FET**.

Scheme 3.7 Stepwise CDC sampling experiments for the mixture of 2-FET and a) 3a or b) 2a as the starting material

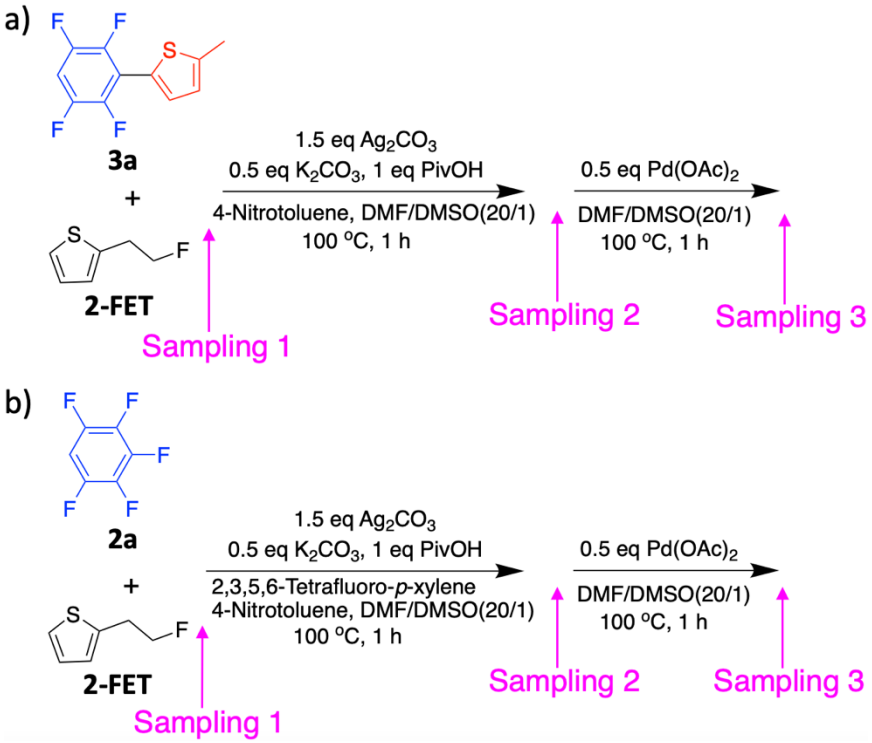

Table 3.2 Yield of each species in the stepwise CDC sampling experiment shown in Scheme 3.7a

Sampling	**3a** (%)	**2-FET** (%)	Ag-**2-FET** (%)	Ag-**3a** (%)	Pd-**2-FET** (%)	Pd-**3a** (%)	Pd-(**3a**)$_2$[a] (%)	Cross-coupled product **(3a-2-FET)** (%)	**2-FET** dimerization product (%)
1	100	100	Not detected	Not detected	-	-	-	Not detected	Not detected
2	91	100	Not detected	9	-	-	-	Not detected	Not detected
3	19	Not detected	Not detected	Not detected	Not detected	Not detected	12	48	Not detected

[a]The yield was obtained via ^{19}F NMR using the same NMR sample.

Table 3.3 Yield of each species in the stepwise CDC sampling experiment shown in Scheme 3.7b

Sampling	**2a**[a] (%)	**2-FET** (%)	Ag-**2-FET** (%)	Ag-**2a**[a] (%)	Pd-**2-FET** (%)	Pd-**2a**[a] (%)	Pd-(**2a**)$_2$[a] (%)	Cross-coupled product **(2a-2-FET)** (%)	**2-FET** dimerization product (%)
1	100	100	Not detected	Not detected	-	-	-	Not detected	Not detected
2	69	98	Not detected	30	-	-	-	Not detected	Not detected
3	26	Not detected	Not detected	Not detected	Not detected	Not detected	38	25	Not detected

[a]The yield was obtained via ^{19}F NMR using the same NMR sample.

Based on the kinetic profiles of both the initial and chain extension CDCs and the discoveries about the homo-coupling mechanism, the reasons for the extremely high cross chemo-selectivity in the chain extension CDC as well as the nearly unnoticeable chemo-selectivity in the initial step CDC can be deduced. At the beginning of either the initial or the chain extension CDC reaction, both thienyl Ag and fluoroaryl Ag intermediates can be formed via Ag-mediated C-H bond activation. In the chain extension CDC, the thienyl substituent of **3a** accelerates the rate of the whole cross-coupling cycle, which makes the cross-coupling cycle much more efficient than the background dimerization of **1a**. Consequently, the fluoroaryl Ag intermediate (Ag-**3a**) outcompetes the thienyl Ag intermediate (Ag-**1a**) in the subsequent transmetalation with the Pd catalyst (only 5 mol% in the reaction). The remaining unreacted Ag-**1a** will react with the proton source PivOH in the reaction to regenerate **1a**. This contrasts with the initial CDC where the cross-coupling cycle with **2a** progresses relatively slowly. This gives the Pd catalyst enough time to undergo transmetalation with Ag-**1a** and the homo-coupling cycle before Ag-**1a** is consumed by the proton source PivOH in the reaction. The extraordinary cross chemo-selectivity in the chain extension CDC leads to a minimal content of homo-coupling defects in the D-A semiconducting polymer product.

3.2.6 *Density Functional Theory (DFT) Calculations*

To further understand the origins of the substituent effect of thienyl group of **3a** on its Pd-mediated C-H bond activation, we next explored the free energy changes using density functional theory (DFT) calculations in collaboration with Houk and Hong et al.[79] Figure 3.3a shows the DFT-computed free energy changes of the sequential C-H bond activation and reductive elimination in the cross-coupling reaction with pentafluorobenzene **2a**. From the intermediate **Int6-A**, DMF first coordinates to generate the intermediate **Int7-A**, which allows the C-H bond activation of thiophene via **TS8-A**. This overall C-H bond activation requires a barrier of 25.2 kcal/mol as compared to **Int6-A**. Subsequently, a secondary DMF exchanges the coordination of HCO_3^-, leading to the biaryl Pd(II) intermediate **Int10-A**. This intermediate undergoes the aryl-aryl reductive elimination via **TS11-A** to produce the cross-coupling product-coordinated complex **Int12-A**. From **Int12-A**, the product liberation and oxidation of Pd(0) can occur to release the observed cross-coupled dimer product **3** and regenerate the active Pd(II) catalyst. Figure 3.3b shows the DFT-computed free energy changes of the same processes with the cross-coupled dimer coupling partner **3a**. Comparing with **Int6-A**, **Int6-B** has an extra thienyl substituent on the para-position of the fluorophenyl group. **Int6-B** undergoes the DMF exchange and subsequent C-H bond activation of thiophene via **TS8-B** to generate the biaryl Pd(II) intermediate **Int9-B**. This C-H bond activation process requires a barrier of 23.5 kcal/mol as compared to **Int6-B**. Subsequent aryl-aryl reductive elimination through **TS11-B** leads to the product-coordinated complex **Int12-B**, which further liberates the cross-coupled trimer product **5**.

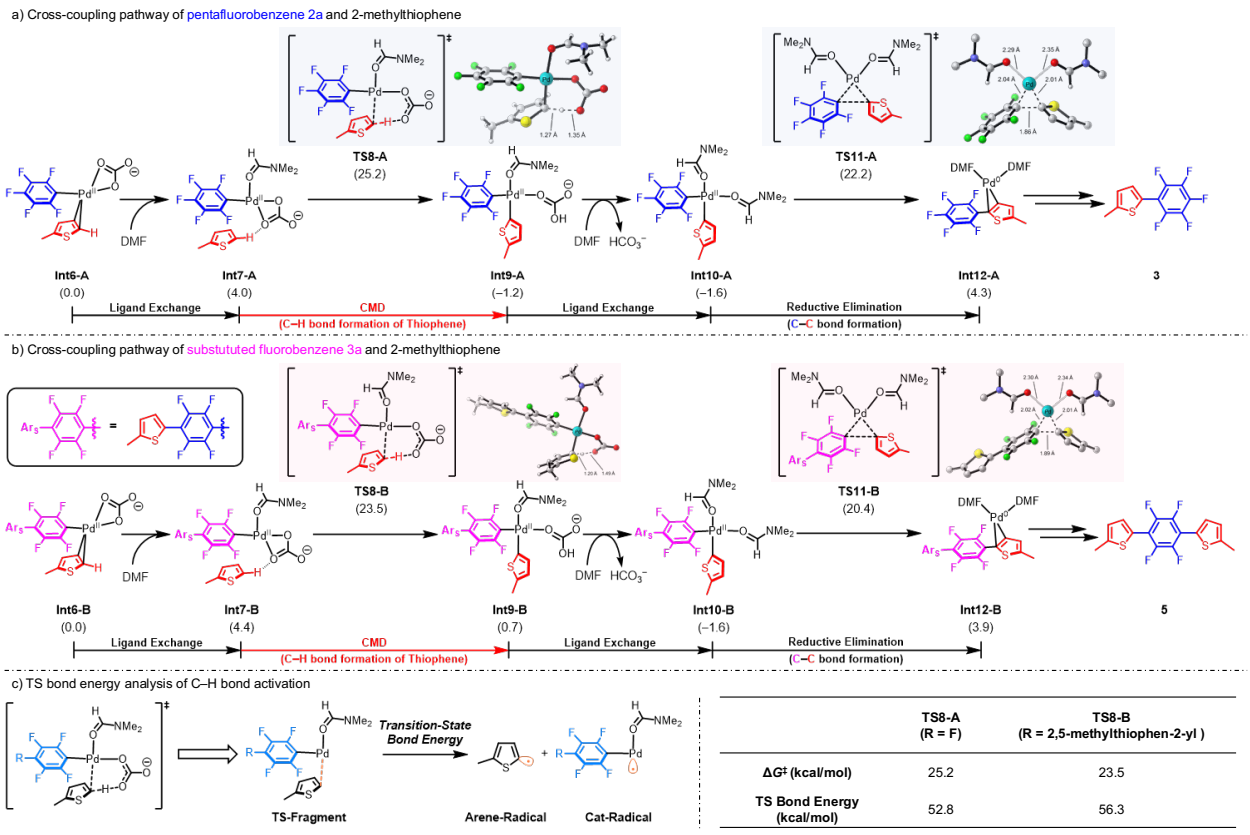

	TS8-A (R = F)	TS8-B (R = 2,5-methylthiophen-2-yl)
$\Delta G^{\ddagger}$ (kcal/mol)	25.2	23.5
TS Bond Energy (kcal/mol)	52.8	56.3

Figure 3.3 Computational studies of the substituent effect on the Pd-catalyzed C-H bond activation of thiophene.

Our computational results corroborated the above mechanistic proposal that the additional thienyl substituent in the CDC extension step accelerates the Pd-mediated C-H bond activation and promotes the chain growth of the polymerization. Without the thienyl substituent, the C-H bond activation via **TS8-A** requires a barrier of 25.2 kcal/mol as compared to the thiophene-coordinated intermediate **Int6-A**. With the additional thienyl substituent, the Pd-mediated C-H bond activation in the CDC extension step now requires a barrier of 23.5 kcal/mol (from **Int6-B** to **TS8-B**), which corresponds to about one order of magnitude rate acceleration. We also verified this barrier change with calculations using additional functionals (Table 3.9 in Section 3.4.7). We believe that the additional thienyl substituent promotes the Pd-thiophene interaction

in the C-H bond activation transition state **TS8-B**, which leads to the rate acceleration. This rationale is supported by the TS bond energy analysis of **TS8-A** and **TS8-B** (Figure 3.3c). TS bond energy analysis, developed by Ess and co-workers,[80] calculates the bond energy between the thiophene and Pd complex fragments in the C-H bond activation transition state, which provides a straightforward analysis of the strength of interaction in the transition state and has been successfully applied in the analysis of other C-H bond activation transition states. In **TS8-A**, the TS bond energy of the Pd-thiophene bond is 52.8 kcal/mol, while the same bond in **TS8-B** has a 56.3 kcal/mol interaction energy (Figure 3.3c). Therefore, the additional thienyl substituent in the CDC extension process strengthens the Pd-thiophene interaction in the transition state of C-H bond activation of 2-methylthiophene (**1a**). This rate acceleration of the C-H bond activation makes the chain growth faster than the initial step of the polymerization and suppresses the homo-coupling side reactions, eventually resulting in the excellent polymerization performance.

3.3 Conclusions

In summary, this study shows that the Pd/Ag cocatalyzed CDC system exceeds the expectations of the Carothers equation because the reactivity of C-H bond is enhanced in the cross-coupled dimer due to the presence of the thienyl substituent. The stepwise CDC sampling experiments revealed a Pd/Ag cocatalytic cycle of the chain extension CDC, where Ag catalyst activates the C−H bond of the electron-poor fluoroaryl species, Pd catalyst activates the C−H bond of the electron-rich thiophene species, and homo-bifluoroaryl Pd complex is formed during the reaction as an inactive intermediate. This sequence is the same as the reaction pathway of the 1st CDC which was uncovered by the Kanbara group.[49] However, delving into the kinetics of the Pd/Ag cocatalyzed CDC system, we discovered the accelerated Pd-mediated C-H bond

activation during the 2nd cross-coupling, which results in the faster chain extension CDC than the initial CDC. This explains the high molecular weight of the produced D-A semiconducting polymer. It was also demonstrated that the homo-coupling pathway requires the initial Ag-mediated C-H bond activation of thiophene species, followed by immediate transmetalation with Pd catalyst. From all the findings above, it is deduced that the high cross chemo-selectivity in the chain extension CDC, which leads to a perfectly alternating D-A semiconducting polymer, is caused by the cross-coupling cycle in the chain extension CDC being more efficient than the thiophene homo-coupling cycle, so that in the chain extension step the cross-coupling cycle outcompetes the homo-coupling cycle. Finally, free energy changes calculated by DFT revealed that the accelerated Pd-mediated C-H bond activation in the chain extension CDC is a result of the lowered energy barrier required for the Pd-mediated C-H bond activation of the thiophene coupling partner (25.2 without the thienyl substituent, 23.5 kcal/mol with the thienyl substituent). The lowered energy barrier is attributed to the stronger Pd-thiophene interaction in the C-H bond activation transition state in the presence of additional thienyl substituent on the fluoroaryl coupling partner. The work provides valuable insight for future studies in obtaining high molecular weight D-A semiconducting polymers. More broadly speaking, this work has implications in small molecule synthesis — introduction of the thiophene has a significant effect on the chemo-selectivity in the CDC reaction offering a method to engineer the substrate structure to enhance the utility of C-H activation.

3.4 Supplementary Information

3.4.1 *General Information*

All manipulation of air- and/or moisture-sensitive compounds were carried out using standard Schlenk and glovebox techniques under a dry nitrogen atmosphere unless otherwise noted. NMR spectra were recorded on Bruker AV-300 and AV-500 spectrometers operating at 300 and 500 MHz, respectively. NMR chemical shifts (δ) are reported in parts per million (ppm) downfield of tetramethylsilane and are referenced relative to the residual solvent signal for ^{1}H NMR ($CDCl_3$ (7.26 ppm)). The integrals in ^{1}H NMR spectra were measured with 4-nitrotoluene as an internal standard. ^{19}F NMR spectra were collected on a Bruker Avance DRX series instrument operating at 470 MHz. The integrals in ^{19}F NMR spectra were measured with 2,3,5,6-tetrafluoro-*p*-xylene (-140.95 ppm in DMSO-d_6) as an internal standard. Anhydrous solvents such as dichloromethane (DCM), 1,4-dioxane, dimethyl sulfoxide (DMSO), N,N-dimethylformamide (DMF), and tetrahydrofuran (THF) were used as purchased from Sigma Aldrich. [Bis(trifluoromethanesulfonyl)imidate](triphenylphosphine)gold(I) (2:1) toluene adduct, deuterium oxide, diethylaminosulfur trifluoride (DAST), 2-methylthiophene, 4-nitrotoluene, n-BuLi (2.5 M in hexanes), 2,2',3,3',5,5',6,6'-octafluorobiphenyl, palladium acetate ($Pd(OAc)_2$), potassium carbonate (K_2CO_3), pentafluorobenzene, pivalic acid (PivOH), silver carbonate (Ag_2CO_3), 1,2,4,5-tetrafluorobenzene, 2,3,5,6-tetrafluoro-*p*-xylene, and other chemicals were used as purchased from commercial suppliers. Deuterated solvents were stored over 4 Å molecular sieves. Column chromatography was performed using VWR Common Silica Gel 60 Å.

3.4.2 *General Methods of Pd/Ag Cocatalytic CDC Reactions*

A 4 mL amber vial and an acid-washed stir bar were oven dried overnight. Palladium acetate (1.12 mg, 5.00 μmol), silver carbonate (82.7 mg, 300 μmol), 4-nitrotoluene (13.7 mg, 100 μmol), K_2CO_3 (13.8 mg, 100 μmol), and PivOH (20.4 mg, 200 μmol) were added to the previously mentioned vial and sealed with a septa cap. The vial was evacuated and refilled with

nitrogen three times. Under nitrogen pressure, anhydrous DMF (0.5 mL), pentafluorobenzene (16.8 mg, 100 µmol), and 2-methylthiophene (9.82 mg, 100 µmol) were injected into the reaction flasks in succession. The reactions were heated at 110 °C for 20 h. The resulting mixtures were passed through a celite plug using chloroform, washed with 1 M HCl, followed by 1 M NaOH aqueous solution, and then the organic layer was dried using anhydrous Na_2SO_4. The remaining solvent was removed under reduced pressure. The resulting mixtures were analyzed by ^{1}H NMR. The formula might change accordingly as needed.

3.4.3 *Deuterium Studies*

The results of deuterium studies are shown in Table 3.4 and Table 3.5. By reacting each of the coupling partner separately with different combinations of additives in the presence of deuterium oxide, we could roughly evaluate the ability of a catalyst to perform C-H activation by looking at the deuteration incorporations.[46] From Table 3.4 and Table 3.5, we can see that both PivOH and K_2CO_3 are essential to obtain quantitative C-H bond activation.

Table 3.4 Deuterium study results of pentafluorobenzene **2a**. Reactions were run on 0.1 mmol scale of **2a**. Reported yields are averages of 3 runs per reaction. The yields were determined by using an internal standard of DMSO-d_6, using similar conditions as those previously reported by Sanford et al.[67]

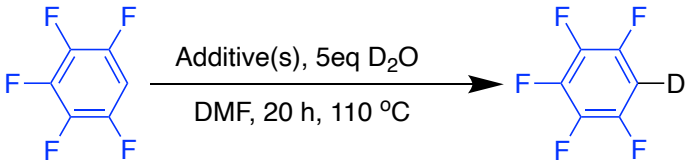

Entry	$Pd(OAc)_2$ (0.05 eq) or/and Ag_2CO_3 (0.3 eq)	Additives	Deuteration incorporation (%)
1	$Pd(OAc)_2$	None	5.1
2	$Pd(OAc)_2$	0.2 eq PivOH	12
3	$Pd(OAc)_2$	0.1 eq K_2CO_3	24

4	$Pd(OAc)_2$	0.2 eq PivOH 0.1 eq K_2CO_3	25
5	Ag_2CO_3	None	10
6	Ag_2CO_3	0.2 eq PivOH	34
7	Ag_2CO_3	0.1 eq K_2CO_3	31
8	Ag_2CO_3	0.2 eq PivOH 0.1 eq K_2CO_3	36

Table 3.5 Deuterium study results of 2-methylthiophene **1a**. Reactions were run on 0.1 mmol scale of **1a**. Reported yields are averages of 3 runs per reaction. The yields were determined by using an internal standard of DMSO-d_6, using similar conditions as those previously reported by Sanford et al.[67]

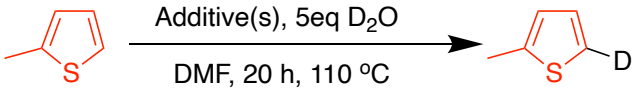

Entry	**$Pd(OAc)_2$ (0.05 eq) or/and Ag_2CO_3 (0.3 eq)**	**Additives**	**Deuteration incorporation (%)**
1	$Pd(OAc)_2$	None	2.3
2	$Pd(OAc)_2$	0.2 eq PivOH	1.4
3	$Pd(OAc)_2$	0.1 eq K_2CO_3	13
4	$Pd(OAc)_2$	0.2 eq PivOH 0.1 eq K_2CO_3	11
5	Ag_2CO_3	None	0
6	Ag_2CO_3	0.2 eq PivOH	9.8
7	Ag_2CO_3	0.1 eq K_2CO_3	15
8	Ag_2CO_3	0.2 eq PivOH 0.1 eq K_2CO_3	32

Scheme 3.8 a) Deuteration reaction of the mixture of 1a and 2a catalyzed by Ag_2CO_3. b) Deuteration reaction of the mixture of 1a and 2a catalyzed by $Pd(OAc)_2$. c) Deuteration reaction of the mixture of 1a and the cross-coupled dimer 3a catalyzed by Ag_2CO_3

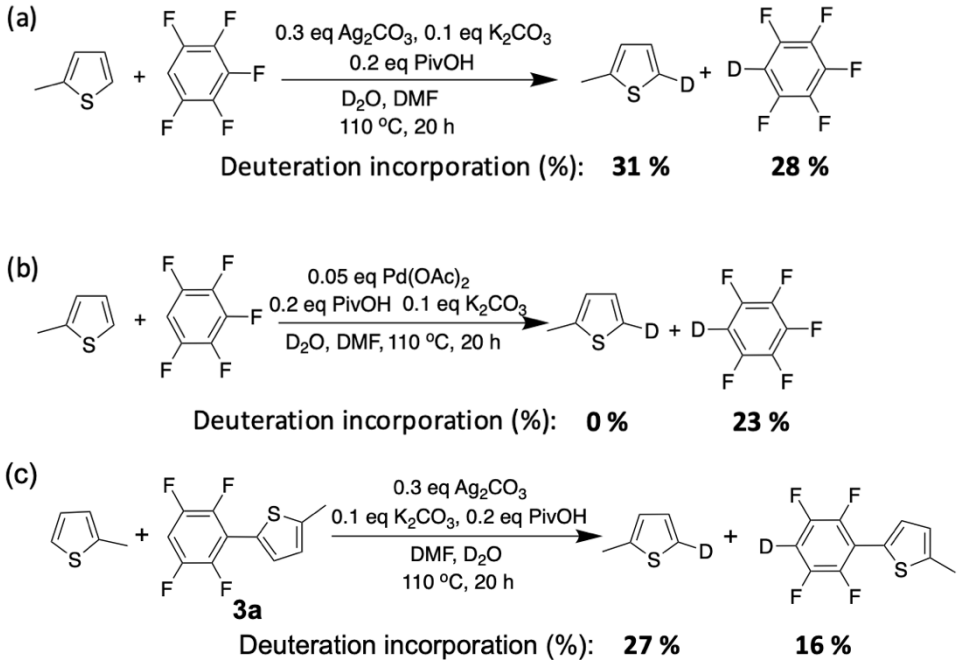

3.4.4 *Synthesis of the Cross-Coupled Dimer **3a***

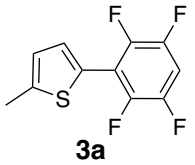

A 20 mL amber vial and an acid-washed stir bar were oven dried overnight. [Bis(trifluoromethanesulfonyl)imidate](triphenylphosphine)gold(I) (2:1) toluene adduct (118 mg, 0.0750 mmol), silver pivalate (313 mg, 1.50 mmol), and PBX (627 mg, 1.80 mmol) were added to the previously mentioned vial and sealed with a septa cap. The vial was evacuated and refilled with nitrogen three times. Under nitrogen pressure, anhydrous 1,4-dioxane (5 mL), 1,2,4,5-tetrafluorobenzene (788 mg, 5.25 mmol), and 2-methylthiophene (147 mg, 1.50 mmol) were injected into the reaction flasks in succession. The reactions were heated at 110 °C overnight. The resulting mixtures were passed through a celite plug using hexanes, washed with 1 M HCl, followed by 1 M NaOH aqueous solution, and then the organic layer was dried using anhydrous Na_2SO_4. The organic layer was concentrated under reduced pressure. The cross-coupled dimer

3a was isolated by column chromatography in *n*-hexane. A white solid was collected (212 mg, 57 % yield). ^{1}H NMR (300 MHz, 298 K, chloroform-*d*): δ 7.41 (d, *J* = 3.7 Hz, 1H), 6.96 (dtt, *J* = 30.3, 9.6, 7.3 Hz, 1H), 6.84 (dq, *J* = 3.7, 1.1 Hz, 1H), 2.56 (d, *J* = 1.1 Hz, 3H). ^{19}F NMR (470 MHz, 298 K, DMSO-d_6): δ -135.03 (dd, *J* = 21.4, 12.1 Hz, 2F), -137.16 (dd, *J* = 22.5, 11.2 Hz, 2F).

3.4.5 *Stepwise CDC Sampling Experiments*

A 4 mL amber vial and an acid-washed stir bar were oven dried overnight. Silver carbonate (51.7 mg, 188 μmol), K_2CO_3 (8.64 mg, 62.5 μmol), PivOH (12.8 mg, 125 μmol), and the cross-coupled dimer **3a** (30.8 mg, 125 μmol) were added to the previously mentioned vial and sealed with a septa cap. The vial was evacuated and refilled with nitrogen three times. Under nitrogen pressure, a stock solution (1 mL) of 2,3,5,6-tetrafluoro-*p*-xylene (22.3 mg, 0.125 mmol) in anhydrous DMF as well as anhydrous DMSO (50 μL) were injected into the reaction flask in succession. The reactions were heated at 100 °C. After 1 h, a 50 μL aliquot was taken out and filtrated with a celite plug with DMSO-d_6 directly into an NMR tube (sampling 1), and palladium acetate (14.0 mg, 62.5 μmol) was added to the reaction flask, and the reaction was allowed to continue for 1 h. Then a 50 μL aliquot was taken out again and filtrated with a celite plug with DMSO-d_6 directly into an NMR tube (sampling 2). At the same time, 2-methylthiophene (12.3 mg, 125 μmol) was injected to the reaction flask, and the reaction was allowed to continue for 15 min. Then a 50 μL aliquot was taken out again and filtrated with a celite plug with DMSO-d_6 directly into an NMR tube (sampling 3). The aliquots were analyzed by ^{19}F NMR. These samples were stored in a freezer until just before the NMR measurement. This procedure was also applied to all other sampling experiments unless otherwise noted.

Table 3.6 Yield of each species in the controlled stepwise CDC sampling experiment shown in Scheme 3.3a (measured by ^{1}H NMR)

Sampling	1a (%)	Ag-1a (%)	Pd-1a (%)	2a (%)	3 (%)	4 (%)
1	82	Not detected	-	-	-	Not detected
2	32	Not detected	Not detected	-	-	Not detected
3	32	Not detected	Not detected	Detected	Not detected	Not detected

Table 3.7 Yield of each species in the controlled stepwise CDC sampling experiment shown in Scheme 3.3b (measured by ^{19}F NMR)

Sampling	3a (%)	Pd-3a (%)	Pd-$(3a)_2$ (%)	Ag-3a (%)	5 (%)
1	38	3	28	-	-
2	29	Not detected	32	Not detected	-
3	11	Not detected	6	Not detected	72

Table 3.8 Yield of each species in the controlled stepwise CDC sampling experiment shown in Scheme 3.3c (measured by ^{19}F NMR)

Sampling	3a (%)	Pd-3a (%)	Pd-$(3a)_2$ (%)	5 (%)
1	41	2	25	-
2	48	Not detected	20	11

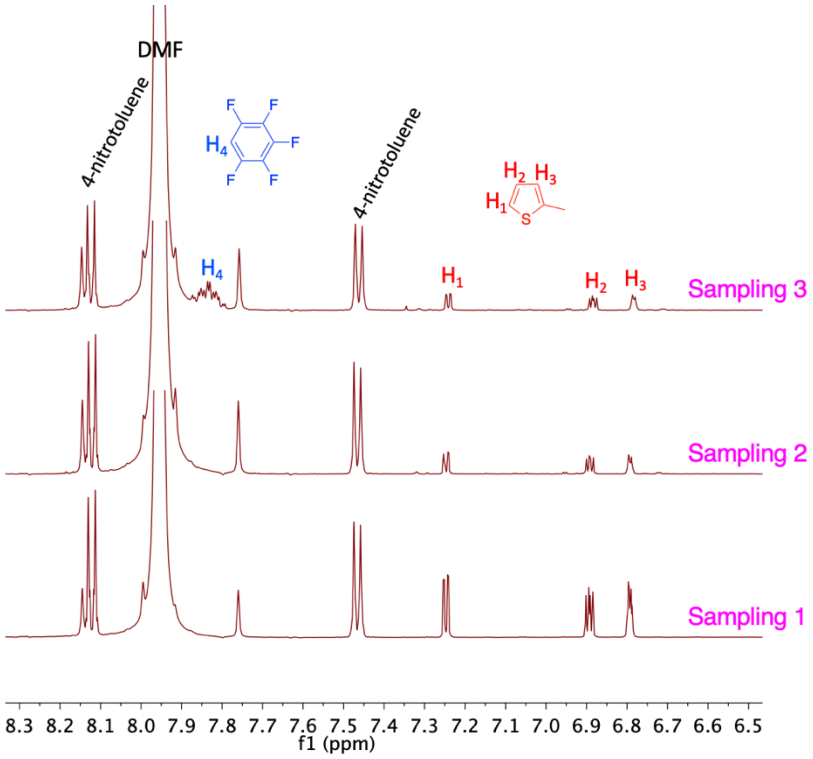

Figure 3.4 [1]H NMR spectra of the controlled stepwise CDC sampling experiments in Scheme 3.3a with 4-nitrotoluene (in DMSO-d_6) as an internal standard.

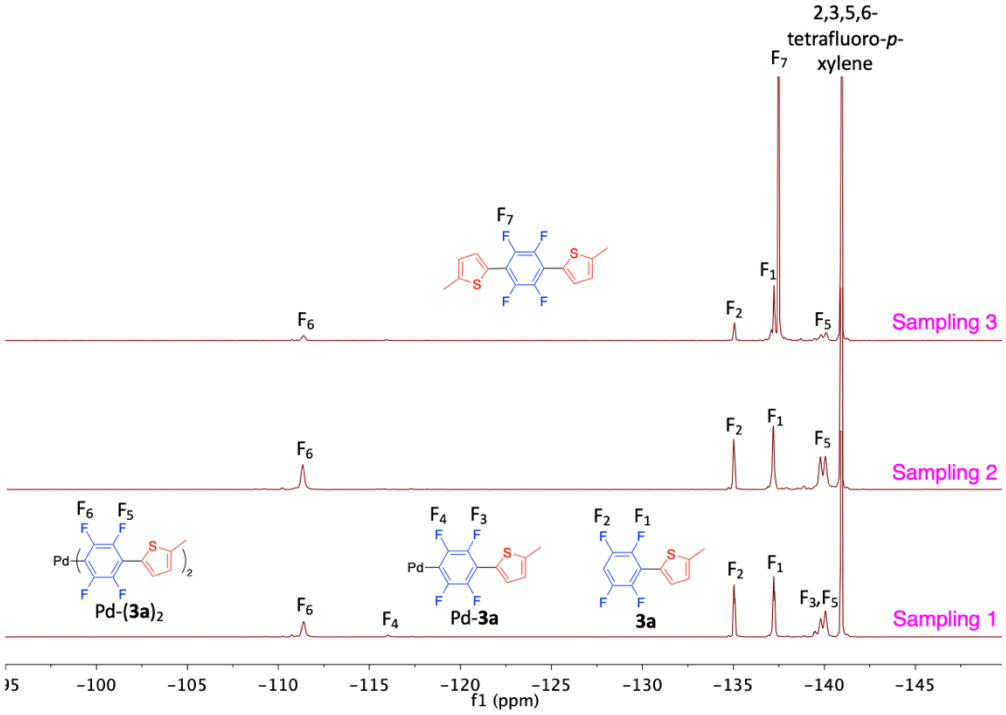

Figure 3.5 [19]F NMR spectra of the controlled stepwise CDC sampling experiments in Scheme 3.3b with 2,3,5,6-tetrafluoro-*p*-xylene (-140.95 ppm in DMSO-d_6) as an internal standard.

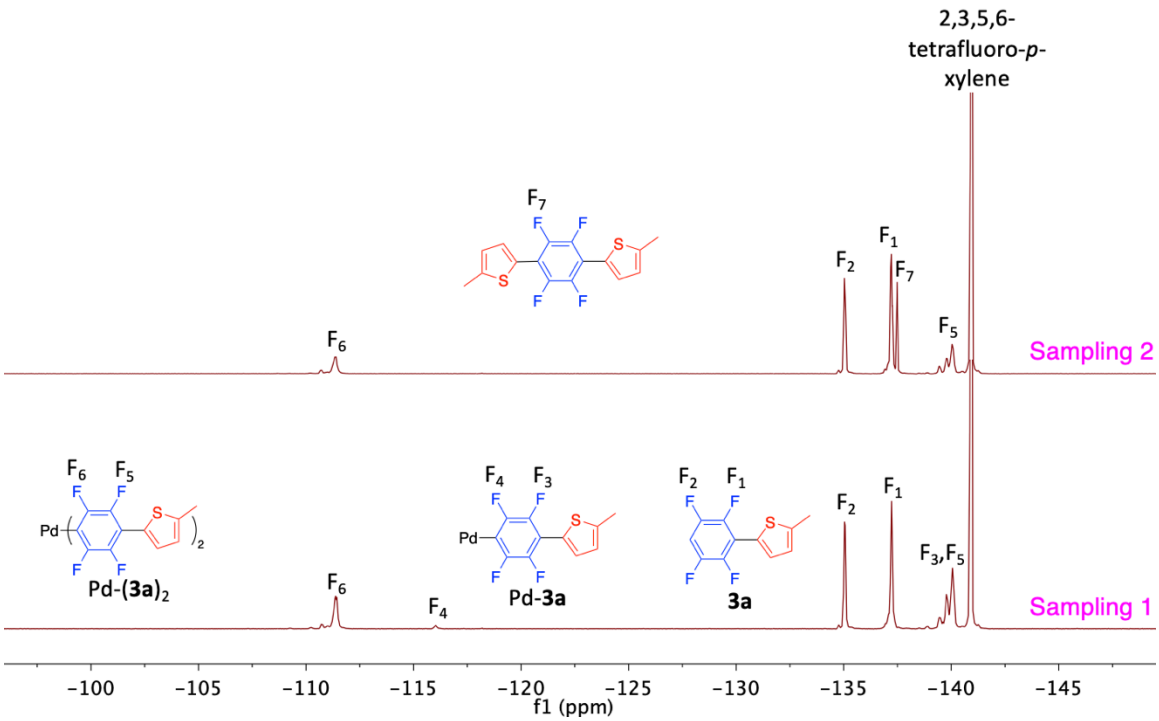

Figure 3.6 ^{19}F NMR spectra of the controlled stepwise CDC sampling experiments in Scheme 3.3c with 2,3,5,6-tetrafluoro-*p*-xylene (-140.95 ppm in DMSO-d_6) as an internal standard.

Scheme 3.9 Synthesis of 2-(2-fluoroethyl)thiophene (2-FET)

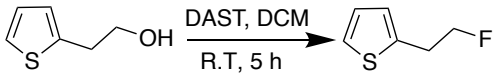

A 50 mL round bottom flask equipped with an acid-washed stir bar was oven dried overnight. The round bottom flask was evacuated and refilled with nitrogen three times. Then anhydrous DCM (10 mL) was injected to the round bottom flask under nitrogen. The DCM was cooled to -78 °C, and trifluoride (DAST) (1.61 g, 10.0 mmol) and 2-thiopheneethanol (1.28 g, 10.0 mmol) were added dropwise to the DCM while stirring under nitrogen in succession. The reaction was allowed to slowly warm up to room temperature and was stirred at room temperature for 5 h. The reaction was quenched by carefully adding saturated aqueous Na_2CO_3 solution until the bubbling stopped. Extraction was performed with DI water for three times and with brine once. The organic layer was dried using anhydrous Na_2SO_4 and condensed under

reduced pressure. Column chromatography was conducted with the mixture of *n*-hexane and chloroform (4:1) as the eluent to isolate 2-(2-fluoroethyl)thiophene (**2-FET**). A colorless oil (602 mg, 46 % yield) was obtained. ^{1}H NMR (500 MHz, 298 K, chloroform-*d*): δ 7.18 (dd, *J* = 5.1, 1.1 Hz, 1H), 6.96 (dd, *J* = 5.1, 3.5 Hz, 1H), 6.89 (dt, *J* = 3.3, 1.0 Hz, 1H), 4.68 (td, *J* = 6.4, 0.7 Hz, 1H, CH_2CH_2F), 4.59 (td, *J* = 6.4, 0.7 Hz, 1H, CH_2CH_2F), 3.26 (td, *J* = 6.4, 0.9 Hz, 1H, CH_2CH_2F), 3.21 (td, *J* = 6.4, 0.9 Hz, 1H, CH_2CH_2F).^{19}F NMR (500 MHz, 298 K, DMSO-d_6): δ -210.14 (s, 1F).

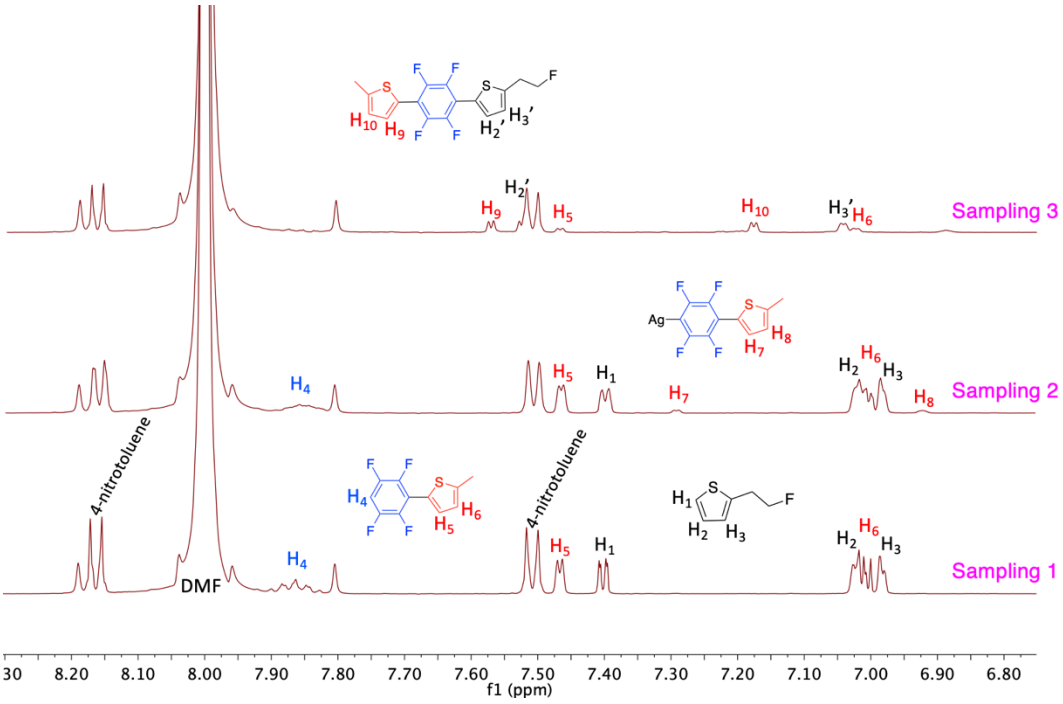

Figure 3.7 ^{1}H NMR spectra of stepwise CDC sampling experiments in Scheme 3.7a.

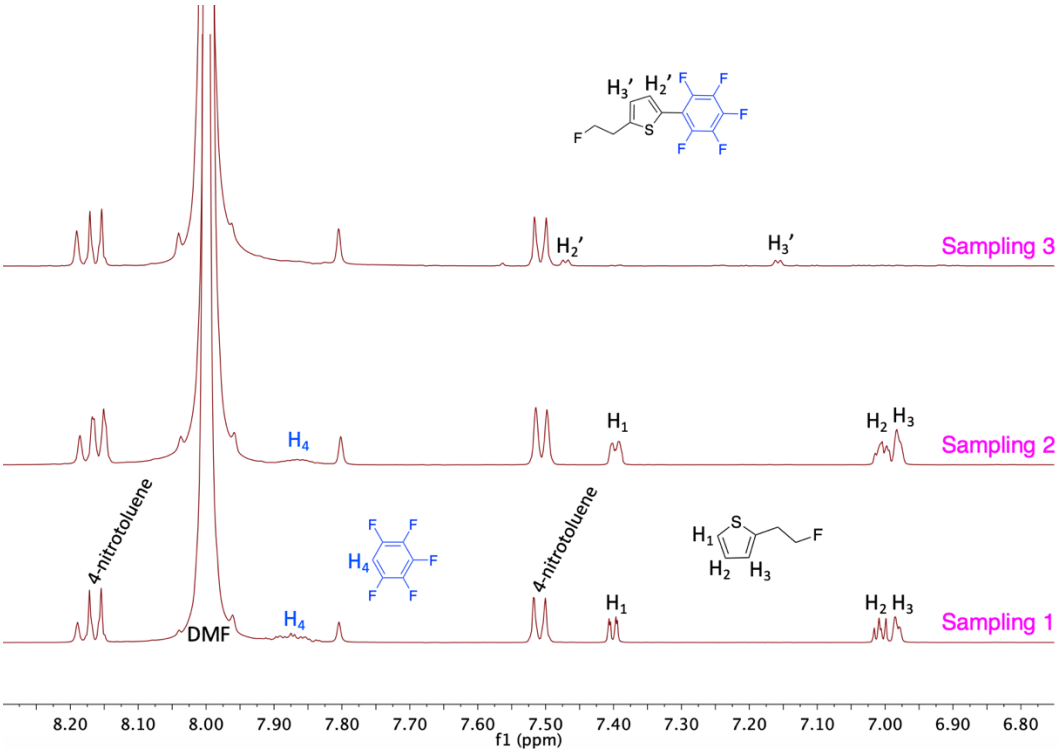

Figure 3.8 ^{1}H NMR spectra of stepwise CDC sampling experiments in Scheme 3.7b.

3.4.6 *Kinetic Analysis*

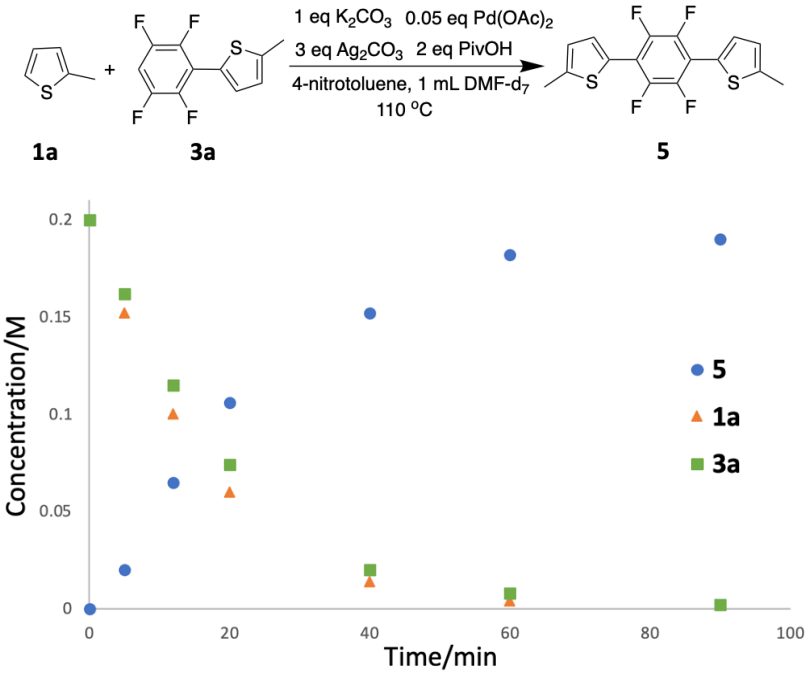

Figure 3.9 Temporal reaction profiles for **5**, **1a** and **3a**.

A 4 mL amber vial and an acid-washed stir bar were oven dried overnight. Palladium acetate (2.25 mg, 10.0 μmol), silver carbonate (165 mg, 600 μmol), 4-nitrotoluene (27.4 mg, 200 μmol), K_2CO_3 (27.7 mg, 200 μmol), PivOH (40.9 mg, 400 μmol), and the cross-coupled dimer **3a** (49.2 mg, 200 μmol) were added to the previously mentioned vial and sealed with a septa cap. The vial was evacuated and refilled with nitrogen three times. Under nitrogen pressure, DMF-d_6 (1.0 mL), and 2-methylthiophene (19.6 mg, 200 μmol) were injected into the reaction flasks in succession. The reactions were heated at 110 °C. 50 μL Aliquots were taken out during the reaction at various time points and filtered with celite plugs with chloroform-*d* directly to NMR tubes. The aliquots were analyzed by ^{1}H NMR. This procedure was also applied to obtain all the kinetic data unless otherwise noted.

The cross-coupled dimer **5**: ^{1}H NMR (500 MHz, 298 K, chloroform-*d*): δ 7.45 (d, J = 3.7 Hz, 2H), 6.84 (d, J = 3.7 Hz, 2H), 2.56 (d, J = 1.1 Hz, 6H). ^{19}F NMR (470 MHz, 298 K, DMSO-d_6): δ -137.49 (s, 4F).

Figure 3.10 shows that a significant overlap between the curves was observed when the order in **1a** was equal to 0, which suggests that the order in **1a** is 0, and that **1a** is not involved in the rate-determining step.

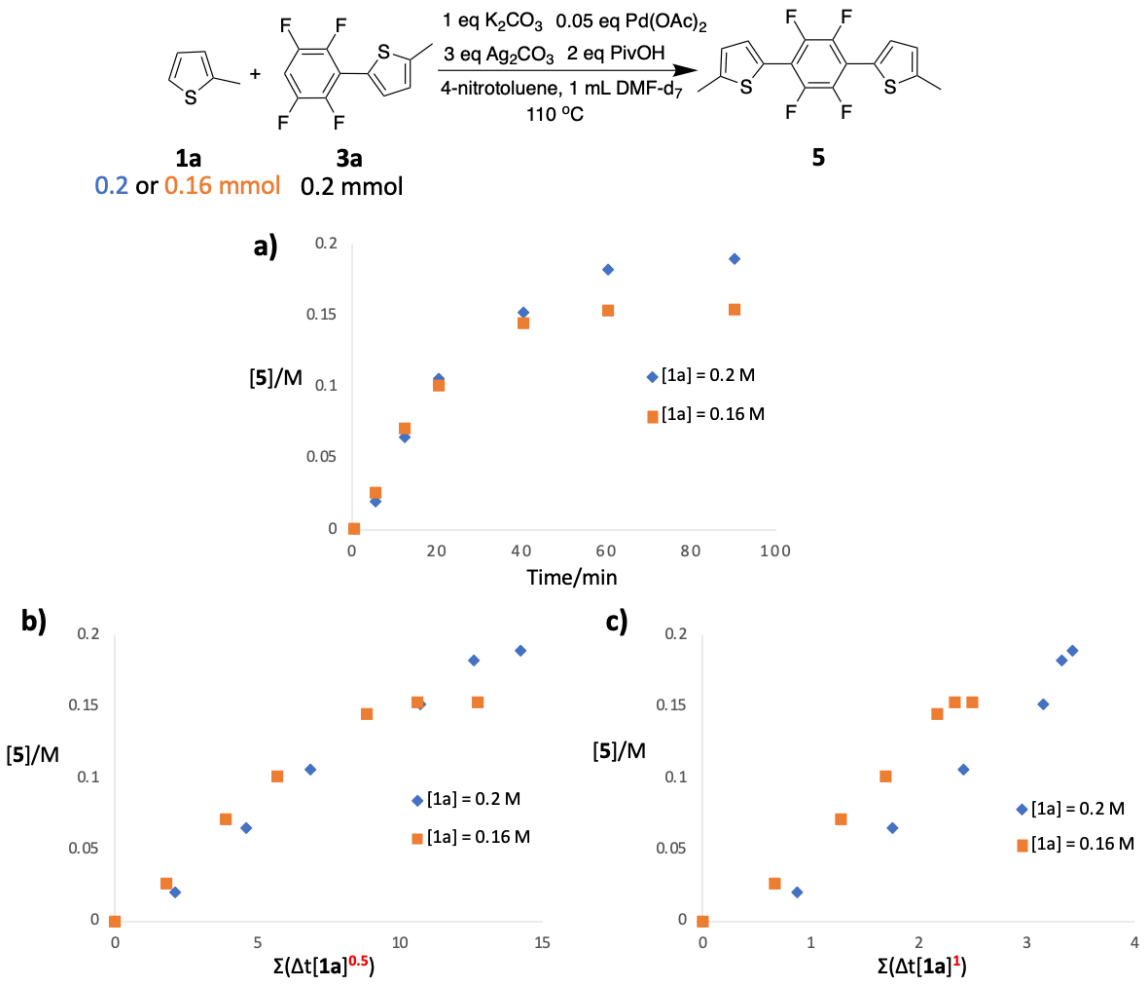

Figure 3.10 Determination of order in **1a.** a) Temporal reaction profiles with different concentrations of **1a**. b) Normalized time scale profiles for order 0.5 in **1a**. c) Normalized time scale profiles for order 1 in **1a**.

Figure 3.11 shows that a significant overlap between the curves was observed when the order in **3a** was equal to 0, which suggests that the order in **3a** is 0, and that **3a** is also not involved in the rate-determining step.

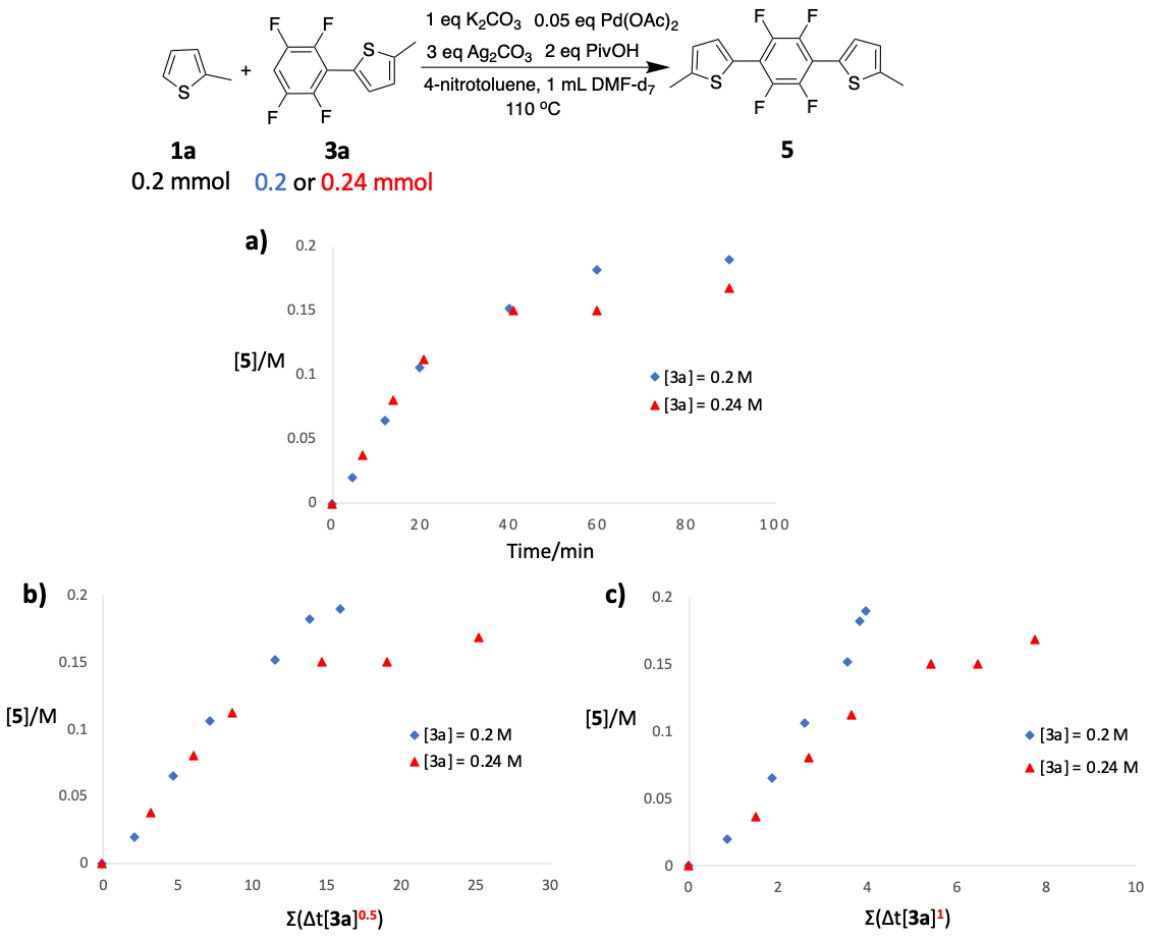

Figure 3.11 Determination of order in **3a.** a) Temporal reaction profiles with different concentrations of **3a**. b) Normalized time scale profiles for order 0.5 in **3a**. c) Normalized time scale profiles for order 1 in **3a**.

Figure 3.12 shows that a significant overlap between the curves was observed when the order in $Pd(OAc)_2$ was equal to 1, which suggests that the order in $Pd(OAc)_2$ is 1, and that $Pd(OAc)_2$ was involved in the rate-determining step.

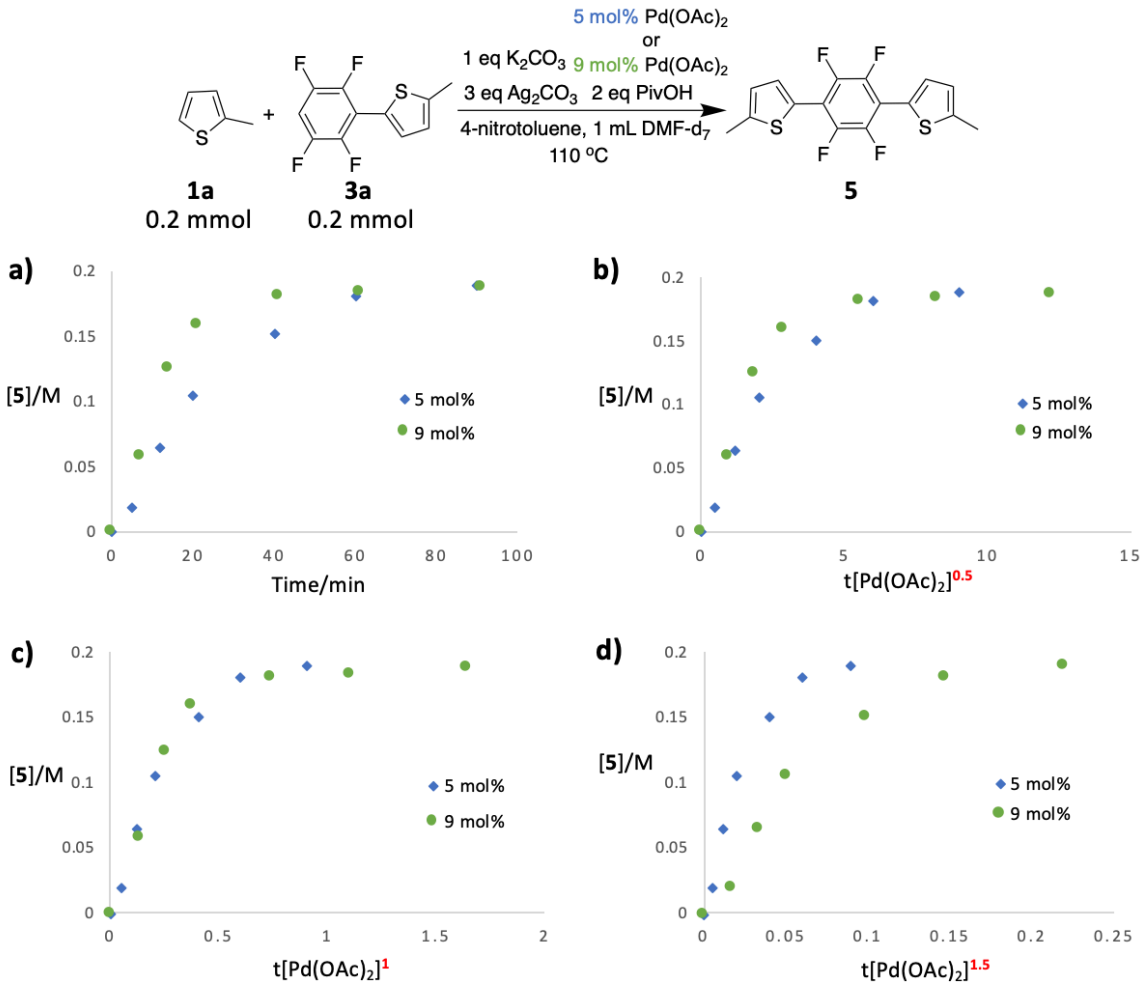

Figure 3.12 Determination of order in $Pd(OAc)_2$. a) Temporal reaction profiles with different loadings of $Pd(OAc)_2$. b) Normalized time scale profiles for order 0.5 in $Pd(OAc)_2$. c) Normalized time scale profiles for order 1 in $Pd(OAc)_2$. d) Normalized time scale profiles for order 1.5 in $Pd(OAc)_2$.

Figure 3.13 shows that the reaction rate profile with respect to [Ag] is parabolic, and the reaction rate profile with respect to $[Ag]^2$ is linear. This indicates that the order in [Ag] is 2, and that 2 equivalents of Ag were participating in the rate-determining step.

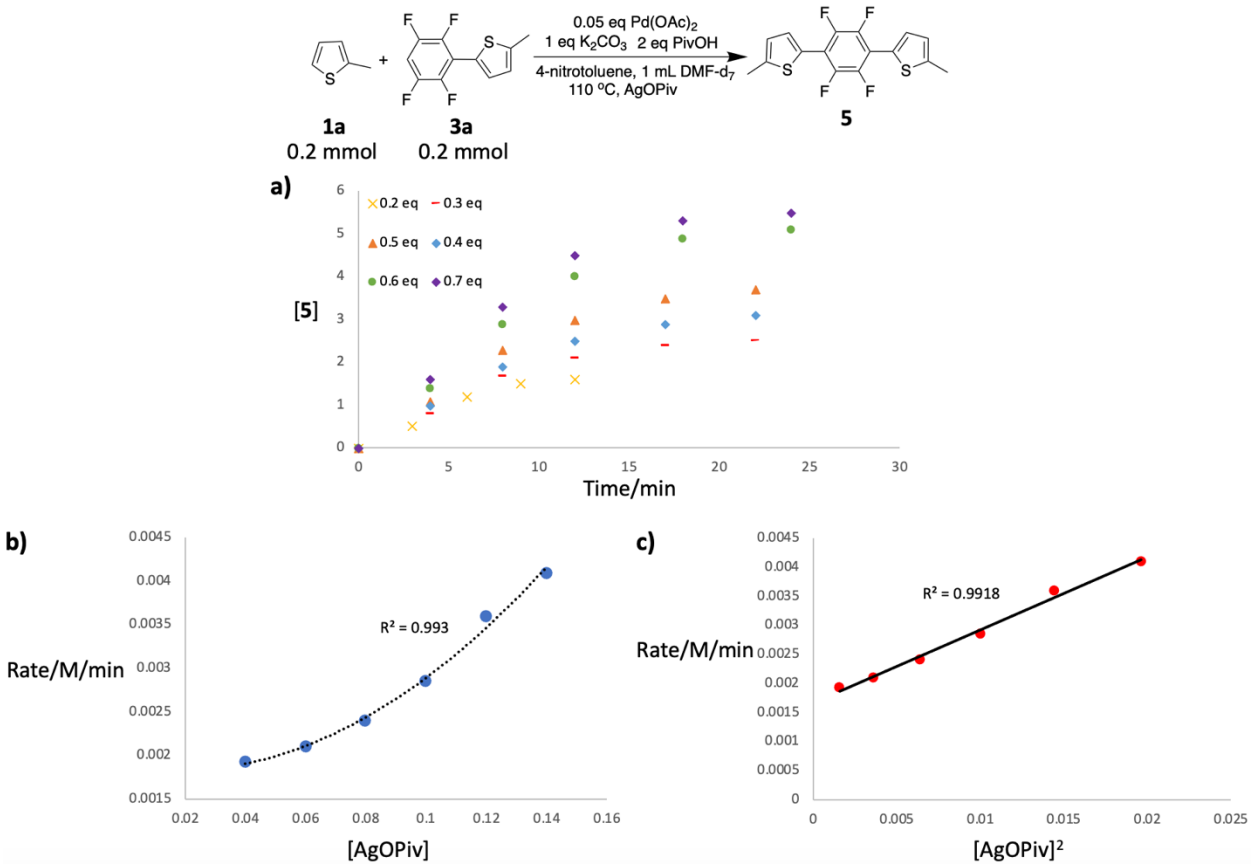

Figure 3.13 Determination of order in [Ag]. a) Temporal reaction profiles with different loadings of AgOPiv (Reaction rates were calculated based on the change in [5] within the first 10 min of the reactions). b) Reaction rate profile with respect to [AgOPiv]. c) Reaction rate profile with respect to $[AgOPiv]^2$.

Scheme 3.10 Synthesis of deuterium cross-coupled dimer 3a-*d*$_1$

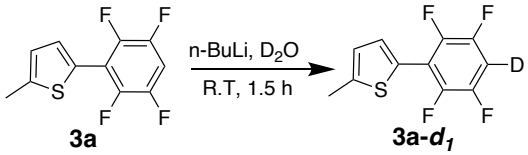

A 25 mL round bottom flask equipped with an acid-washed stir bar was oven dried overnight. The cross-coupled dimer **3a** (65.0 mg, 264 µmol) were added to the previously mentioned round bottom flask and sealed with a rubber septum. The round bottom flask was evacuated and refilled with nitrogen three times. Anhydrous THF (1.5 mL) was injected into the round bottom flask under nitrogen. The solution was cooled to -78 °C, and n-BuLi (2.5 M in

hexanes) (0.126 mL, 317 µmol) was added to the solution while stirring under nitrogen drop-wise over 1 min. The reaction was slowly warmed up to room temperature and was stirred at room temperature for 1.5 h. After 1.5 h, deuterium oxide (51 µL, 2.64 mmol) was added to the round bottom flask to quench the reaction. The mixture was stirred for another 30 min. 5 mL DI water was added, and extraction was done with diethyl ether for three times. All the organic layers were combined, dried using anhydrous Na_2SO_4, and concentrated under reduced pressure. Column chromatography was performed with n-hexane to isolate the **3a-*d*$_1$**. A white solid (25.2 mg, 39 % yield, deuteration incorporation: 96 %) was collected. ^{1}H NMR (500 MHz, 298 K, chloroform-*d*) δ 7.41 (d, *J* = 3.9 Hz, 1H), 6.84 (dq, *J* = 3.7, 1.1 Hz, 1H), 2.56 (d, *J* = 1.1 Hz, 3H).

Figure 3.14 shows that $k_H = 0.6422$, and $k_D = 0.584$. Therefore, KIE = 0.6422/0.584 = 1.1. This shows that the C-H activation on **3a** is not the rate-determining step.

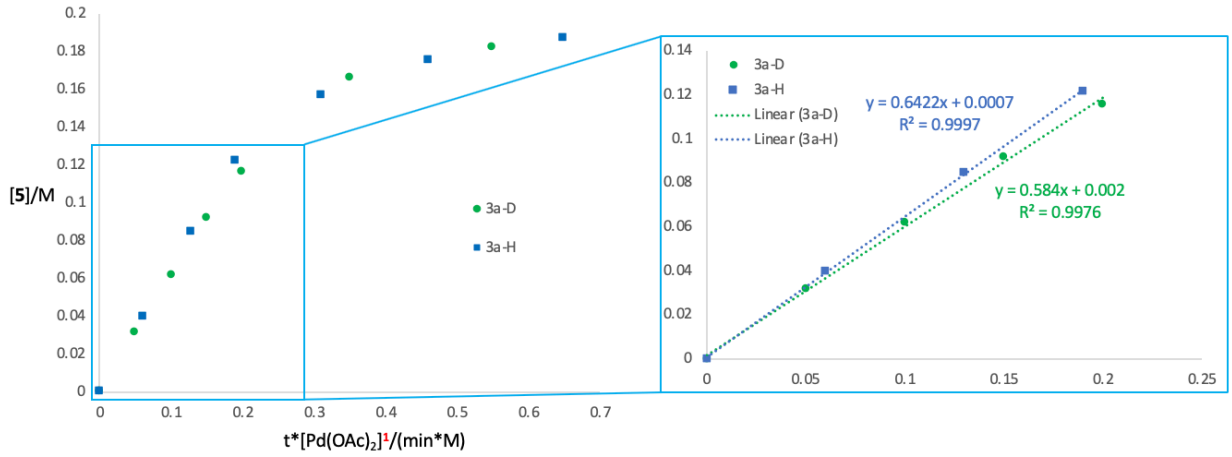

Figure 3.14 Reaction profiles with **3a** or **3a-*d*$_1$** with normalized time scales.

Scheme 3.11 Synthesis of deuterium 2-hexylthiophene (2-hexylthiophene-*d*$_1$)

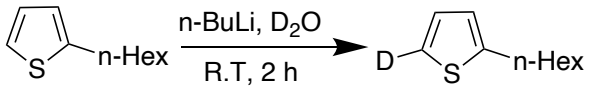

2-hexylthiophene **2-hexylthiophene-*d*$_1$**

A 50 mL round bottom flask equipped with an acid-washed stir bar was oven dried overnight. The round bottom flask was evacuated and refilled with nitrogen three times. Then 3-bromo-2-hexyl thiophene (247 mg, 1.00 mmol) and anhydrous THF (5 mL) were injected to the round bottom flask under nitrogen. The solution was cooled to -78 ^{o}C, and *n*-BuLi (2.5 M in hexanes) (0.480 mL, 1.20 mmol) was added to the solution while stirring under nitrogen drop-wise over 5 min. The reaction was slowly warmed up to room temperature and was stirred at room temperature for 2 h. After 2 h, deuterium oxide (181 µL, 10 mmol) was added to the round bottom flask to quench the reaction. The mixture was stirred for another 30 min. 10 mL DI water was added to the reaction mixture, and extraction was done with diethyl ether for three times. All the organic layers were combined, dried using anhydrous Na_2SO_4, and concentrated under reduced pressure. Column chromatography was performed with *n*-hexane to isolate the **2-hexylthiophene-*d*$_1$**. A colorless oil (135 mg, 80 % yield, deuteration incorporation: 92 %) was collected. ^{1}H NMR (500 MHz, 298 K, chloroform-*d*): δ 6.91 (d, *J* = 3.5 Hz, 1H), 6.77 (dt, *J* = 3.4, 1.0 Hz, 1H), 2.84 – 2.80 (m, 2H), 1.72 – 1.62 (m, 2H), 1.42 – 1.25 (m, 6H), 0.94 – 0.83 (m, 3H).

Figure 3.15 shows that $k_H = 0.575$, and $k_D = 0.45$. Therefore, KIE = 0.575/0.45 = 1.3. This shows that the C-H activation on thiophene species **1a** is not the rate-determining step.

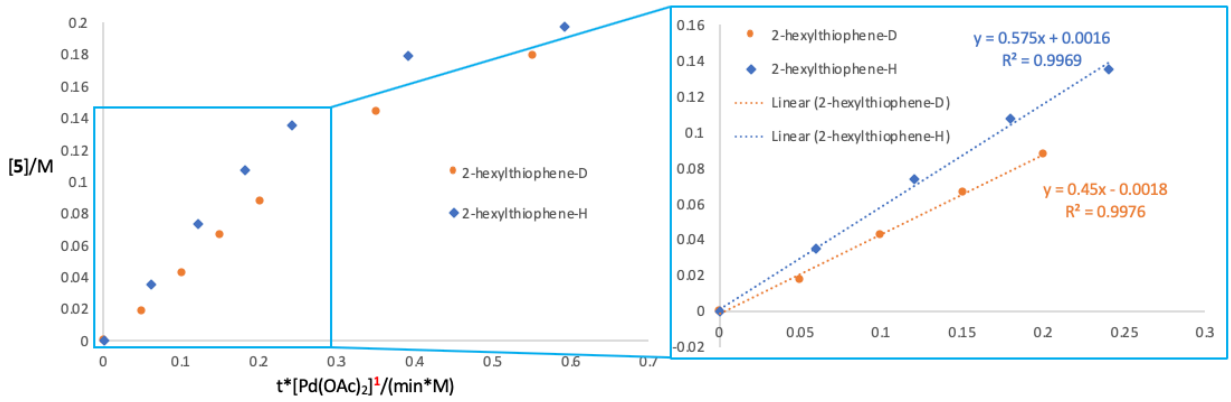

Figure 3.15 Reaction profiles with 2-hexylthiophene/2-hexylthiophene-d_1 with normalized time scales.

3.4.7 *DFT Calculations*

All density functional theory (DFT) calculations were performed using Gaussian 16 program.[81] Geometry optimizations were employed with B3LYP functional,[82,83] with the D3 version of Grimme's dispersion corrections[84] and Becke-Johnson damping.[85] LANL2DZ basis set[86–89] was applied for copper and 6-31G* basis set was used for all other atoms. Frequency analysis was also performed at the same level of theory as geometry optimization to confirm optimized stationary points were either local minimum or transition state, as well as to evaluate zero-point vibrational energies and thermal corrections for enthalpies and free energies at 298.15 K.

Single-point energies and solvent effects at N,N-dimethylformamide (DMF) were evaluated with B3LYP functional[82,83] with D3 version of Grimme's dispersion corrections[84] with Becke-Johnson damping.[85] SDD basis set[86,90–92] was used for copper and 6-311+G(d,p) basis set was used for all other atoms. The solvation energies were calculated with a self-consistent reaction field (SCRF) using the SMD implicit solvent model.[93]

To correct the Gibbs free energies under 1 atm to the standard state in solution (1 mol/L), a correction of $RT\ln(c_s/c_g)$ is added to energies of all species. c_s stands for the standard molar concentration in solution (1 mol/L), c_g stands for the standard molar concentration in gas phase (about 0.040876 mol/L), and R is the gas constant. For the DMF solvent when it is involved in studied reaction, the standard state of 12.9 mol/L (density: 0.9445 g/cm^3, molecular weight: 73.09) at 298.15 K was applied, leading to a 3.40 kcal/mol free energy correction. For other calculated intermediates at the standard state of 1 mol/L at 298.15 K, the correction value equaling to 1.89 kcal/mol was used.

The 3D diagrams of optimized structures shown in the main text and below here in supplementary information for computations were generated with CYLview software.[94]

Table 3.9. Verification of rate acceleration by various functionals

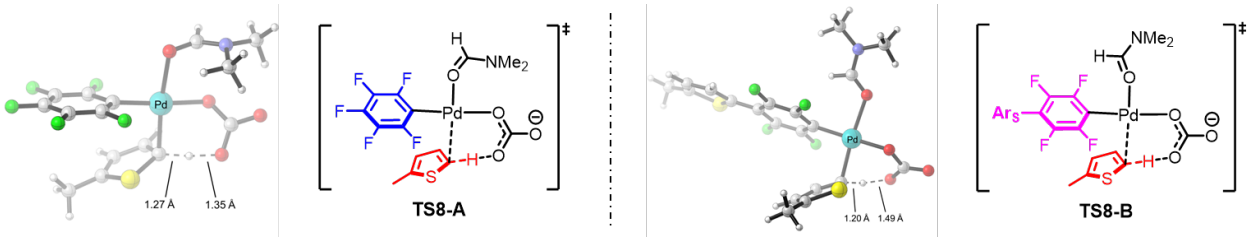

Method for Single Point Energy Calculation	$\Delta G^{\ddagger}$ (**TS8-A**)(kcal/mol)	$\Delta G^{\ddagger}$ (**TS8-B**)(kcal/mol)
B3LYP-D3(BJ)/6-311+G(d, p)-SDD	25.2	23.5
B3LYP-D3(BJ)/Def2-TZVP[95]	27.4	25.2
M06[96] **/6-311+G(d, p)-SDD**	28.5	27.2
PBE0-D3(BJ)[84,85,97] **/6-311+G(d, p)-SDD**	26.1	24.9
ωB97X-D[98] **/6-311+G(d, p)-SDD**	27.2	26.6

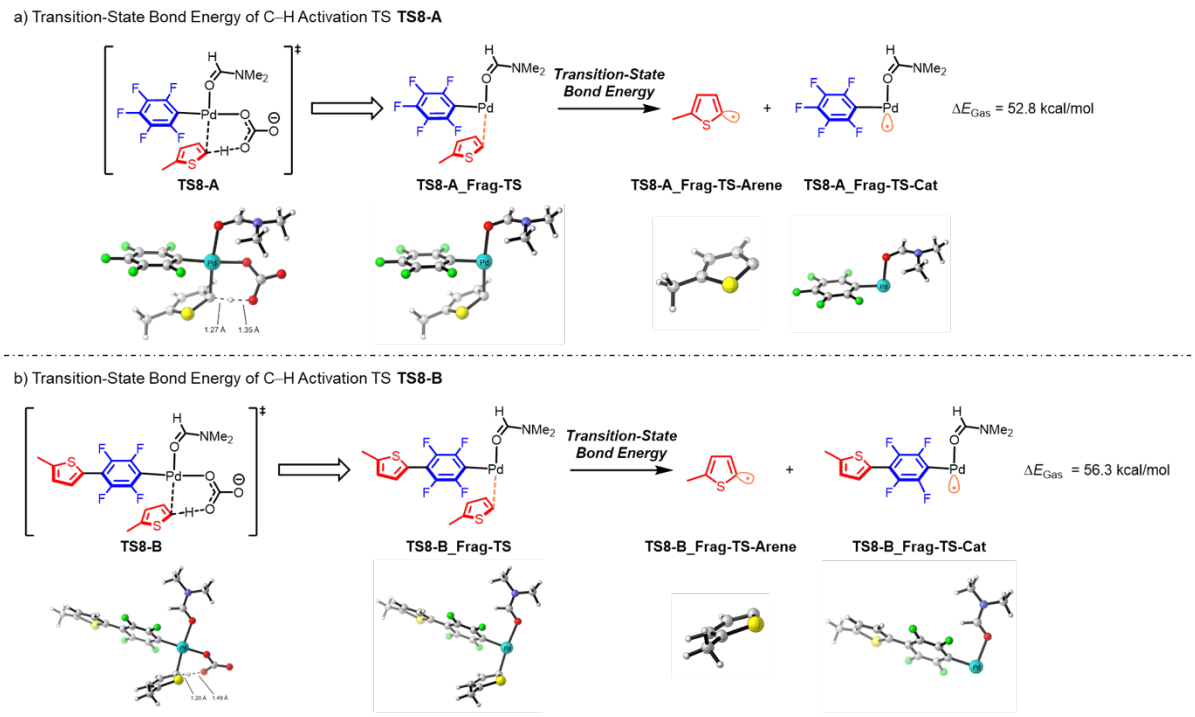

Figure 3.16 Details on calculations for transition state bond energy. a) Transition-state bond energy of C–H activation TS **TS8-A**. b) Transition-state bond energy of C–H activation TS **TS8-B**.

Chapter 4. Rate enhancement of the Pd/Ag dual catalytic cross dehydrogenative coupling polymerization

4.1 Introduction

In addition to atom economy, minimizing time and energy input in the synthetic process of D-A semiconducting polymers is an important part of improving the environmental friendliness and scalability of D-A semiconducting polymer production. As we can see in the Chapters 2 and 3, both Au/Ag and Pd/Ag cocatalytic CDC polymerizations took at least 48 hours to achieve high molecular weight polymers and are carried out at relatively elevated temperatures (~100 °C). Synthetic reactions that are highly efficient and undergo under mild conditions can lessen the energy consumption of D-A semiconducting polymer production.[99,100] However, highly efficient transformations, due to the need of high reactivity/reaction rate, often require high temperature, which cancels out the energy saved by the high efficiency of a transformation. Therefore, to reduce the environmental impact of D-A semiconducting polymer synthesis via the Pd/Ag cocatalytic CDC, it is desired to find a method to improve the reaction rate without increasing the reaction temperature.

From the Chapter 3, it was discovered that the CDC reaction between thiophene and fluorinated benzene with the thienyl substituent proceeded much more efficiently than that without the thienyl substituent (one order of magnitude faster). The energy barrier to break the C−H bond on the thiophene coupling partner is reduced due to the presence of the thienyl substituent on the fluorinated benzene.[79] This significant discovery presented a way to improve the reaction rate without increasing the reaction temperature by redesigning the monomer structure in the CDC polymerization. Herein, a new monomer was synthesized and applied in the

Pd/Ag cocatalytic CDC polymerization (Scheme 4.1) to improve the reaction rate. The 3,3′-dihexyl-2,2′-bithiophene and 1,2,4,5-tetrafluorobenzene were coupled together to form the new monomer which consists of three arenes (monomer **H**). By having the thienyl substituent on tetrafluorobenzene, the slow first coupling reaction between fluorobenzene and thiophene comonomers in the original polymerization is eliminated, and the high cross coupling rate can be achieved throughout the entire polymerization process.

Scheme 4.1 The synthetic route of AB type monomer H

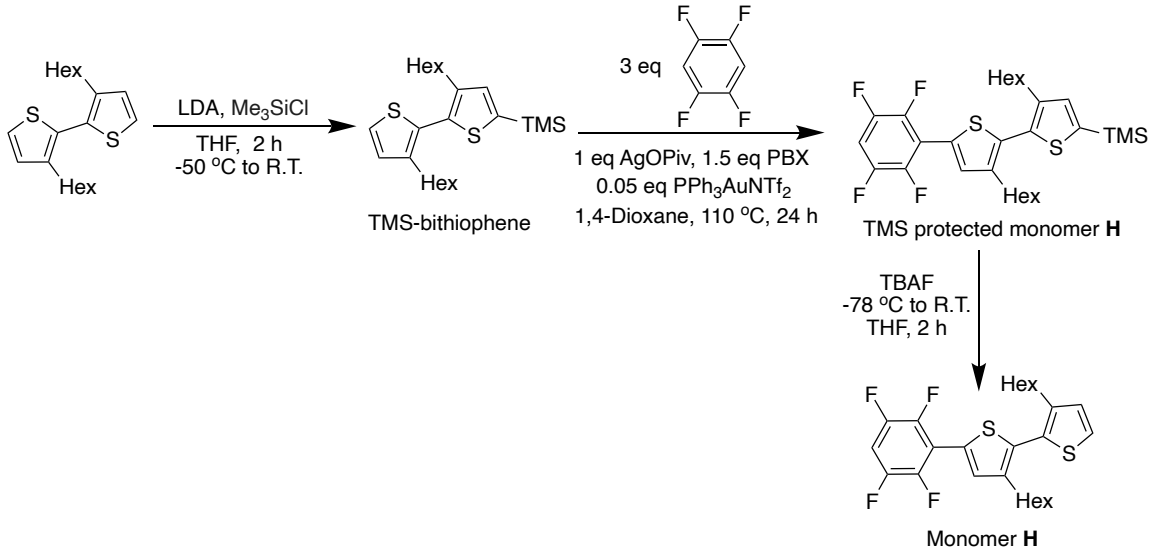

Besides the rate acceleration effect of bithiophene moiety on the new monomer **H**, there are other benefits to designing the monomer **H** this way. In general, there are two approaches to step-growth polymerizations: i) AA+BB approach, which involves two types of bifunctional monomers. One possesses the same two reacting functional groups, A, and the other possesses the same two reacting functional groups, B; ii) AB approach, which involves only one bifunctional monomer – an AB type monomer that has both A and B reacting functional groups.[53] In the case of CDC polymerizations, the reacting functional groups are C-H bonds with difference electronic characteristics. While AA and BB types of monomers are generally more

available and easier to synthesize than the AB type monomer, such as 3,3′-dihexyl-2,2′-bithiophene and 2,2′,3,3′,5,5′,6,6′-octafluorobiphenyl which are commercially available, the AA+BB type of polycondensations is notoriously sensitive to monomer purity even if impurities do not directly interfere with the polymerization. This is because the presence of impurities results in a stoichiometric imbalance, which limits the molecular weight of the product according to the Carothers equation.[54,101] AB type of polycondensations, however, is a lot less sensitive to the impurities of the monomer due to the stoichiometric ratio of the reacting functional groups is always 1. In addition, the AB type monomer **H** can inherently polymerize in a more controlled manner (lower homo-coupling defects and more explicit end group identity). Moreover, AB type monomers is more advantageous in achieving a chain-growth mechanism, which allows preparation of polymers with fewer batch-to-batch variations, well-defined chemical structures, controlled molecular weights, and narrow molecular weight distribution.[101,102]

4.2 Results and Discussion

The kinetic experiments on the Pd/Ag cocatalytic CDC polymerizations with 3,3′-dihexyl-2,2′-bithiophene and 2,2′,3,3′,5,5′,6,6′-octafluorobiphenyl and with the new AB type monomer **H** were performed, respectively. The polymerization conditions are shown in Schemes 4.2 and 4.3. Note that for AA+BB CDC polymerization, the homocoupling defects content is less than 3 %, and for AB CDC polymerization, the homocoupling defects content is 0 according to ^{1}H NMR. The DP versus monomer conversion (% conv.) plots for both polymerizations are shown in Figure 4.1. For the original AA+BB type polymerization (left plot), the increasing slope of the plot with % conv. (the conversion of 3,3′-dihexyl-2,2′-bithiophene) indicates a step-growth mechanism. Likewise, the polymerization with the AB type monomer also proceeds through a step-growth mechanism (right plot).

Scheme 4.2 Pd/Ag cocatalytic AA+BB type of CDC polymerization

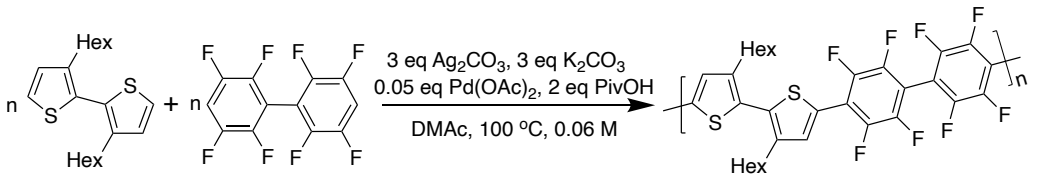

Scheme 4.3 Pd/Ag cocatalytic AB type of CDC polymerization

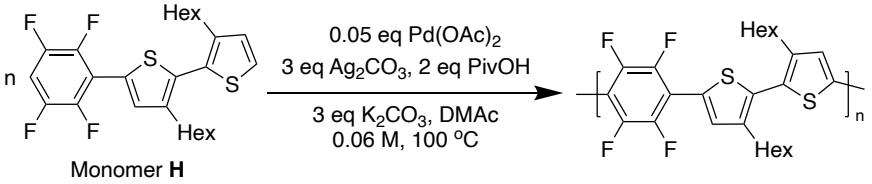

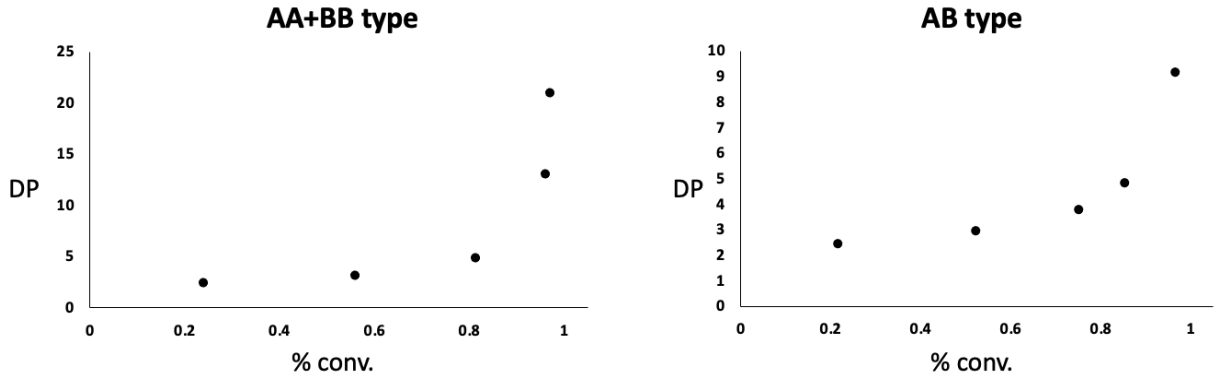

Figure 4.1 Number-average degree of polymerization (DP) versus monomer conversion (% conv.) plots for the AA+BB type CDC polymerization (left) and for the AB type CDC polymerization (right).

Comparison of the reaction rates of AA+BB and AB types of Pd/Ag cocatalytic CDC polycondensations shows that AB approach proceeds 5 times faster than the AA+BB approach under the same conditions (Figure 4.2). The reaction rate of AB type of polycondensation is 3×10^{-3} M/min, while the reaction rate of AA+BB type of polycondensation is 6×10^{-4} M/min. The comparison between the polymer growth rates of AA+BB and AB types of CDC polycondensations (Figure 4.3) indicates that the AB approach takes only approximately one third of the time that the AA+BB approach takes to reach the same DP. For instance, to obtain a

DP of 10, it only takes around 40 min for AB approach, while it takes about 120 min for AA+BB approach.

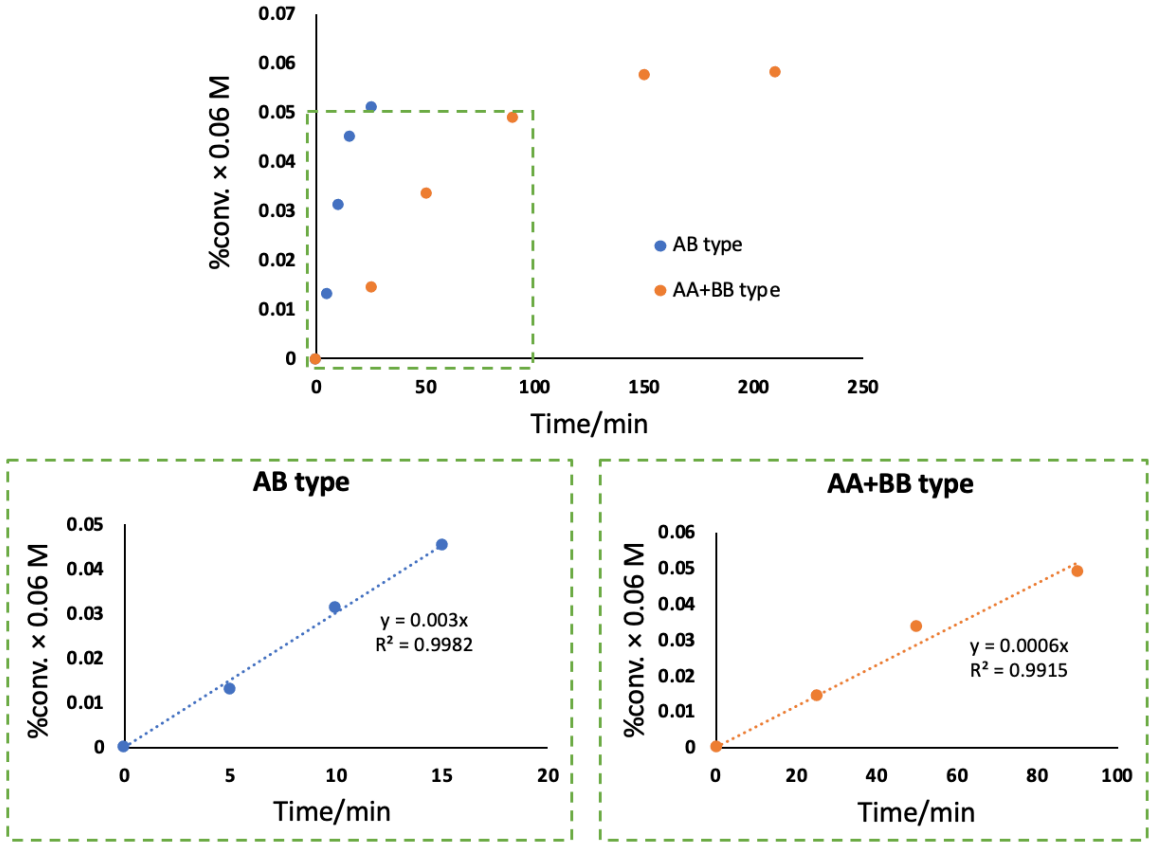

Figure 4.2 Comparison of the reaction rates (% conv. × 0.06 M versus time) of the AB versus AA+BB types of CDC polycondensations.

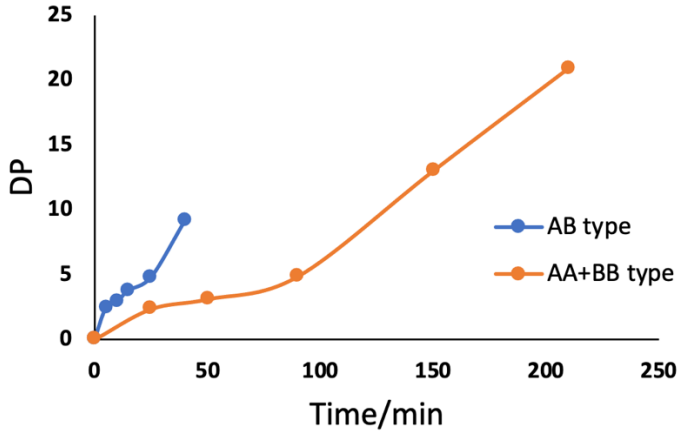

Figure 4.3 Comparison of the polymer growth rates (DP versus time) of the AB versus AA+BB types of CDC polycondensations.

4.3 Conclusions

In summary, by switching from AA+BB approach to AB approach, the CDC polymerization rate increased drastically (~5 folds) without raising the temperature. At the same time, the time required to obtain the same DP was shortened significantly (~3 folds). These accomplishments reduced the energy consumption of the D-A semiconducting polymer synthesis and improved the environmental friendliness of this chemical transformation.

4.4 Supplementary Information

4.4.1 *General Information*

All reactions were carried out under nitrogen atmosphere using standard Schlenk techniques unless otherwise noted. NMR spectra were recorded on Bruker AV-300 and AV-500 spectrometers operating at 300 and 500 MHz, respectively. NMR chemical shifts (δ) are reported in parts per million (ppm) downfield of tetramethylsilane and are referenced relative to the residual solvent signal for ^{1}H NMR ($CDCl_3$ (7.26 ppm)). The integrals in ^{1}H NMR spectra were measured with 4-nitrotoluene as an internal standard. Anhydrous solvents such as 1,4-dioxane, dimethyl sulfoxide (DMSO), N,N-dimethylacetamide (DMAc) and tetrahydrofuran (THF) were used as purchased from Sigma Aldrich. Deuterated solvents were stored over 4 Å molecular sieves. Pivaloyloxy-1,2-benziodoxol-3(1H)-one (PBX)[61] and silver pivalate (AgOPiv)[72] were synthesized using previously reported methods. All other reagents and chemicals were purchased from Sigma-Aldrich or Tokyo Chemical International and used without further purification. Column chromatography was performed using VWR Common Silica Gel 60 Å.

4.4.2 *Synthesis of the AB Type Monomer **H***

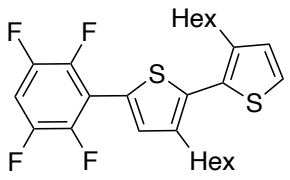

Monomer **H**

A 50 mL round bottom flask equipped with an acid-washed stir bar was oven dried overnight. The round bottom flask was sealed with a rubber septum and evacuated and refilled with nitrogen three times. 3,3′-Dihexyl-2,2′-bithiophene (669 mg, 2.00 mmol) and anhydrous THF (2 mL) were injected into the round bottom flask under nitrogen. The solution was cooled to -50 °C, and under nitrogen pressure, lithium diisopropylamide (LDA) (1.5 M in THF) (1.4 mL, 2.10 mmol) was injected into the reaction flasks dropwise. The mixture was stirred at -50 °C for 1 h, and trimethylsilyl chloride (760 mg, 7.00 mmol) was injected into the reaction mixture dropwise. After that, the reaction mixture was stirred at -50 °C for another hour. The reaction mixture was slowly warmed up to room temperature and stirred at room temperature for 1 h. The reaction was quenched with saturated NH_4Cl/H_2O solution (40 mL). The organic phase was extracted with diethyl ether for three times (3 × 30 mL). The organic layers were combined, dried using anhydrous $MgSO_4$, and concentrated under reduced pressure. The crude TMS-bithiophene was analyzed with ^{1}H NMR and stored in freezer before the next reaction. ^{1}H NMR (300 MHz, 298 K, chloroform-*d*): δ 7.27 (d, *J* = 5.2 Hz, 1H), 7.07 (s, 1H), 6.96 (d, *J* = 5.2, 1H), 2.49 (m, 4H), 1.54 (m, 4H), 1.24 (m, 12H), 0.85 (m, 6H), 0.32 (s, 9H).

A 20 mL amber vial equipped with an acid-washed stir bar were oven dried overnight. [Bis(trifluoromethanesulfonyl)imidate](triphenylphosphine)gold(I) (2:1) toluene adduct (157 mg, 100 μmol), silver pivalate (418 mg, 2.00 mmol), and PBX (836 mg, 2.40 mmol) were added to the previously mentioned vial and sealed with a septa cap. The vial was evacuated and refilled with nitrogen three times. Under nitrogen pressure, anhydrous 1,4-dioxane (8 mL), 1,2,4,5-

tetrafluorobenzene (1.05 g, 7.00 mmol), and the crude TMS-bithiophene were injected into the reaction flasks in succession. The reactions were heated at 110 °C for 24 h. The resulting mixtures were passed through a celite plug using hexanes, washed with 1 M HCl and 1 M NaOH aqueous solutions in succession, and then the organic layer was dried using anhydrous Na_2SO_4. The organic layer was concentrated under reduced pressure. The crude TMS protected monomer **H** was analyzed with NMR and stored in freezer before the next deprotection reaction. ^{1}H NMR (300 MHz, 298 K, chloroform-*d*): δ 7.48 (s, 1H), 7.09 (s, 1H), 6.98 (m, 1H), 2.55 (m, 4H), 1.58 (m, 4H), 1.27 (m, 12H), 0.86 (m, 6H), 0.33 (s, 9H). ^{19}F NMR (470 MHz, 298 K, chloroform-*d*): δ -139.29 (dd, J = 21.5, 11.8 Hz, 2F), -140.25 (dd, J = 21.6, 11.9 Hz, 2F).

A 50 mL round bottom flask equipped with an acid-washed stir bar was oven dried overnight. The round bottom flask was sealed with a rubber septum and evacuated and refilled with nitrogen three times. The crude TMS protected monomer **H** and anhydrous THF (5 mL) were injected into the round bottom flask under nitrogen. The solution was cooled to -78 °C, and under nitrogen pressure, tetrabutylammonium fluoride (TBAF) (1 M in THF) (2.1 mL, 2.10 mmol) was injected into the reaction flasks dropwise. After that, the reaction mixture was slowly warmed up to room temperature and stirred at room temperature for 2 h. The reaction was quenched with H_2O (10 mL). The organic phase was extracted with hexanes for three times (3 × 10 mL). The organic layers were combined, dried using anhydrous $MgSO_4$, and concentrated under reduced pressure. The monomer **H** was isolated by column chromatography in n-hexane. A light yellow liquid was collected (262 mg, 26 % yield). ^{1}H NMR (500 MHz, 298 K, chloroform-*d*): δ 7.48 (s, 1H), 7.33 (d, J = 5.2 Hz, 1H), 6.99 (d, J = 5.2 Hz, 1H), 6.99 (m, 1H), 2.55 (t, J = 7.8 Hz, 4H), 1.57 (m, 4H), 1.26 (m, 12H), 0.85 (m, 6H). ^{19}F NMR (470 MHz, 298 K, chloroform-*d*): δ -139.24 (dd, J = 21.5, 11.8 Hz, 2F), -140.26 (dd, J = 21.5, 11.9 Hz, 2F).

4.4.3 *General Methods of Kinetic Experiments on Polymerizations*

Five 4 mL amber vials equipped with acid-washed stir bar were oven dried overnight. Palladium acetate (0.337 mg, 1.50 μmol), silver carbonate (24.8 mg, 90.0 μmol), 4-nitrotoluene (4.11 mg, 30.0 μmol), K_2CO_3 (12.4 mg, 90.0 μmol), and PivOH (6.14 mg, 60.0 μmol) were added to each of the previously mentioned vials, and the vials were each sealed with a septa cap (2,2′,3,3′,5,5′,6,6′-octafluorobiphenyl (8.94 mg, 30.0 μmol) was also added to each vial along with the solids above for the AA+BB polycondensation). The vials were then evacuated and refilled with nitrogen three times. Under nitrogen pressure, anhydrous DMAc (0.5 mL) and 3,3′-dihexyl-2,2′-bithiophene (10.0 mg, 30.0 μmol) for AA+BB polycondensation or monomer **H** (15.3 mg, 30.0 μmol) for AB polycondensation were injected into each vial. The reactions were heated to 100 °C together at the same time. Heating was stopped for each vial at different time points. For each reaction, the resulting mixtures were passed through a celite plug using chloroform, washed with 1 M HCl and 1 M NaOH aqueous solutions in succession, and then the organic layer was dried using anhydrous Na_2SO_4. The remaining solvent was removed under reduced pressure. The resulting mixtures were analyzed by ^{1}H NMR and ^{19}F NMR. The formula might change accordingly as needed. For AA+BB polycondensation, the % conv., DP, and %alt were calculated using ^{1}H NMR assuming that both chain ends are bithiophene. For AB polycondensation, the % conv. and DP were calculated using ^{19}F NMR, and %alt were calculated using ^{1}H NMR. The formula might change accordingly as needed.

4.4.4 *Calculations of DP and % Conv. of the AB Type Polycondensation Using ^{19}F NMR*

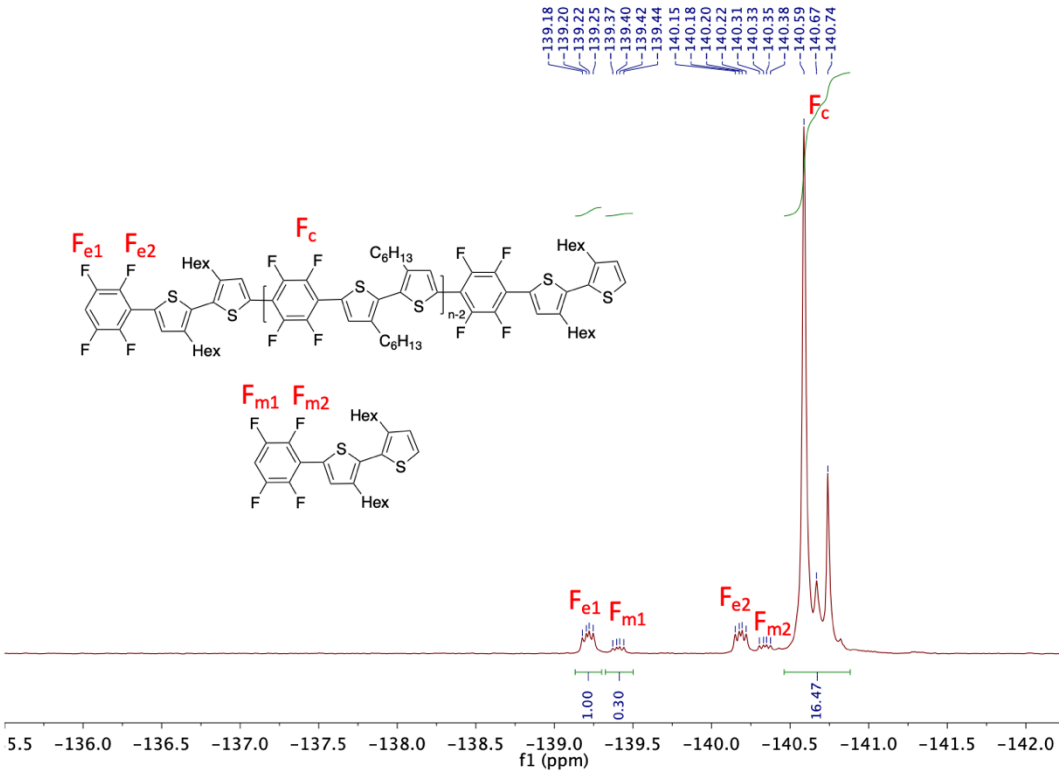

Figure 4.4 The aromatic region ^{19}F NMR (bottom) of AB type D-A polymer at 40 min.

DP was calculated using the integral of the fluorine (I_{e1}) on the end group and the fluorine (I_c) on the chain backbone.

$$DP = \frac{I_c}{2I_{e1}} + 1$$

% Conv. was calculated using the DP and the integral of fluorine (I_{m1}) on the unreacted monomer.

$$\% \text{ conv.} = \frac{DP}{DP + I_{m1}}$$

4.4.5 *^{1}H NMR and ^{19}F NMR Spectra*

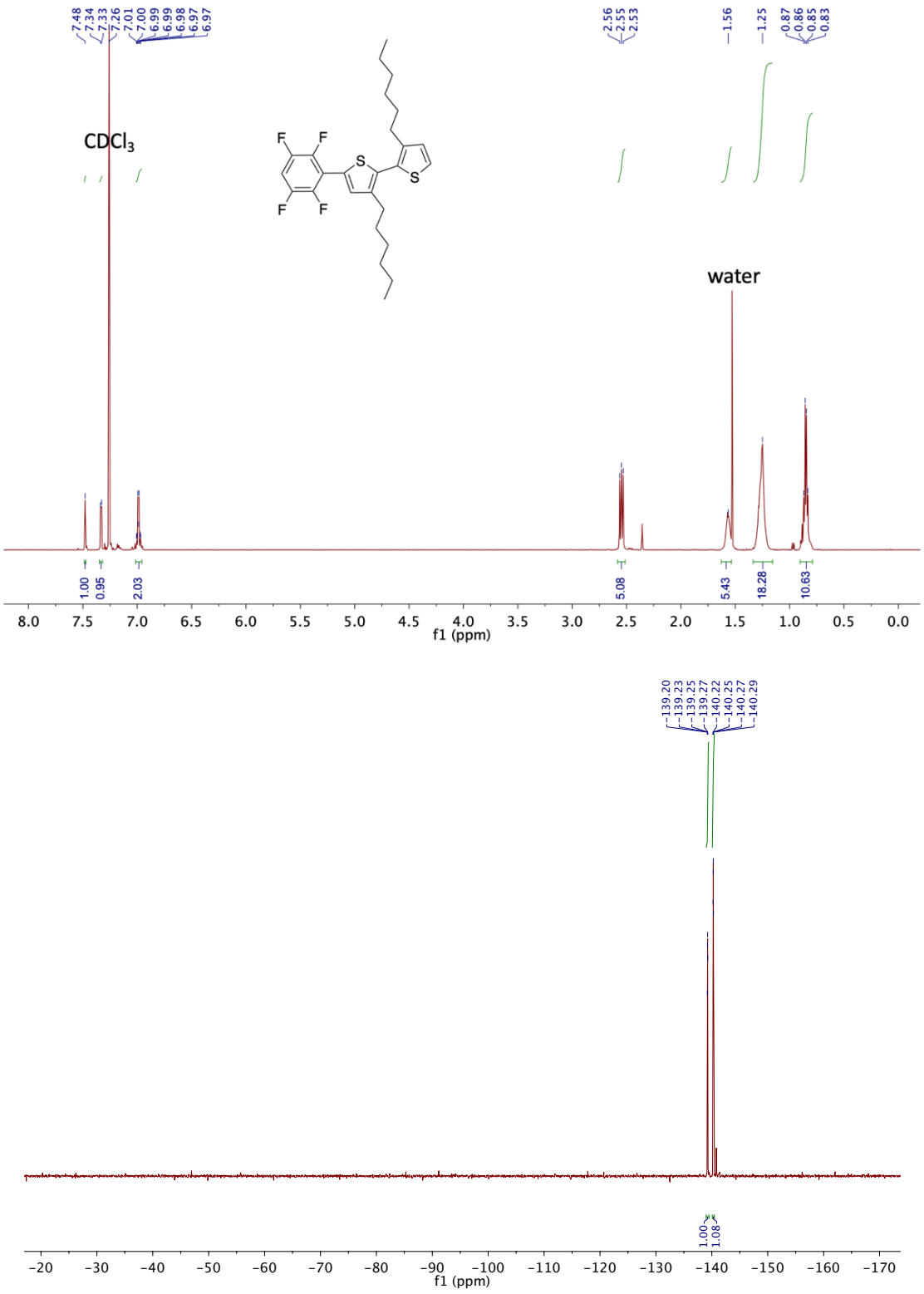

^{1}H NMR (top) and ^{19}F NMR (bottom) of monomer **H**.

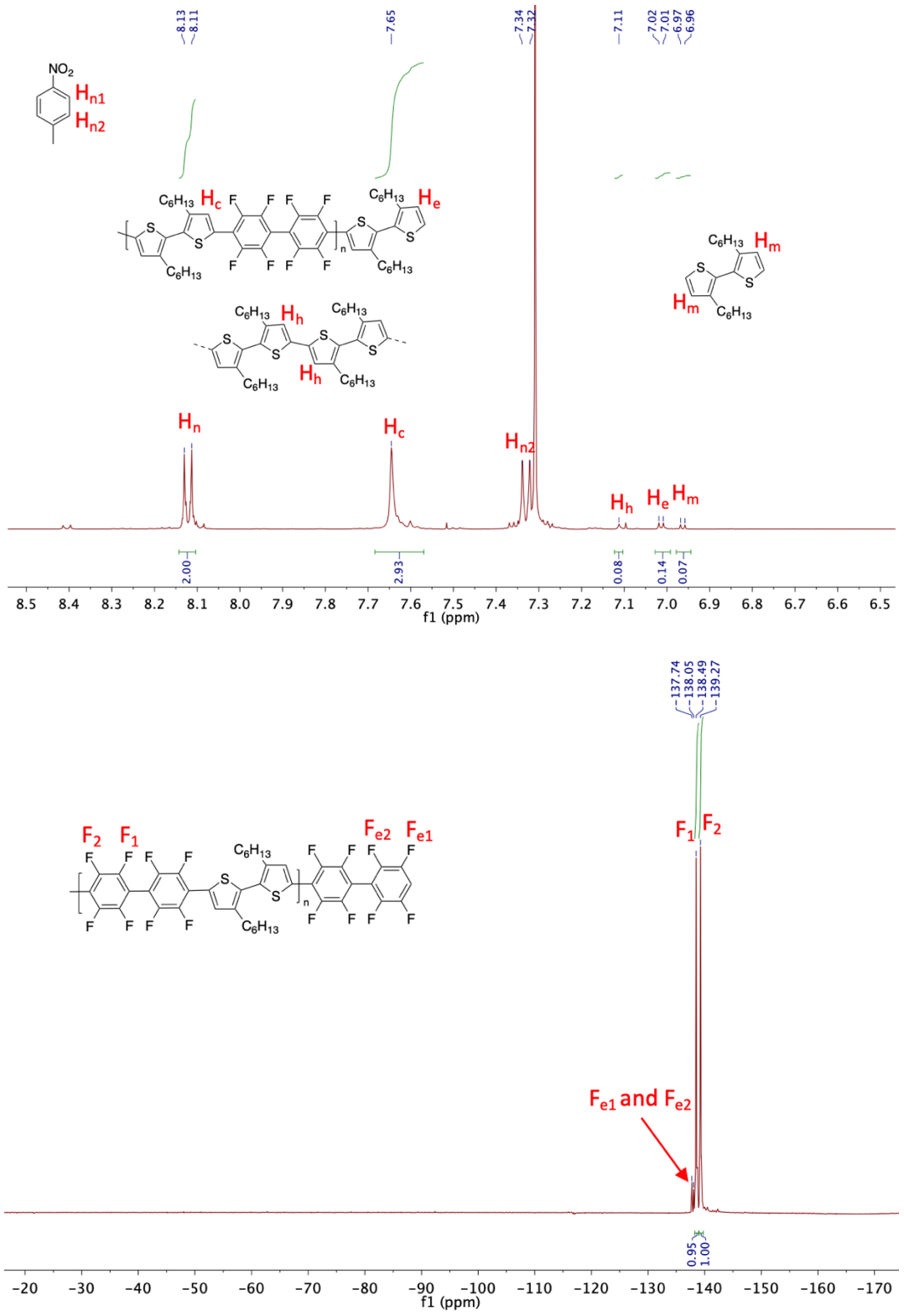

^{1}H NMR (aromatic region) (top) and ^{19}F NMR (bottom) of AA+BB type polymer at 210 min.

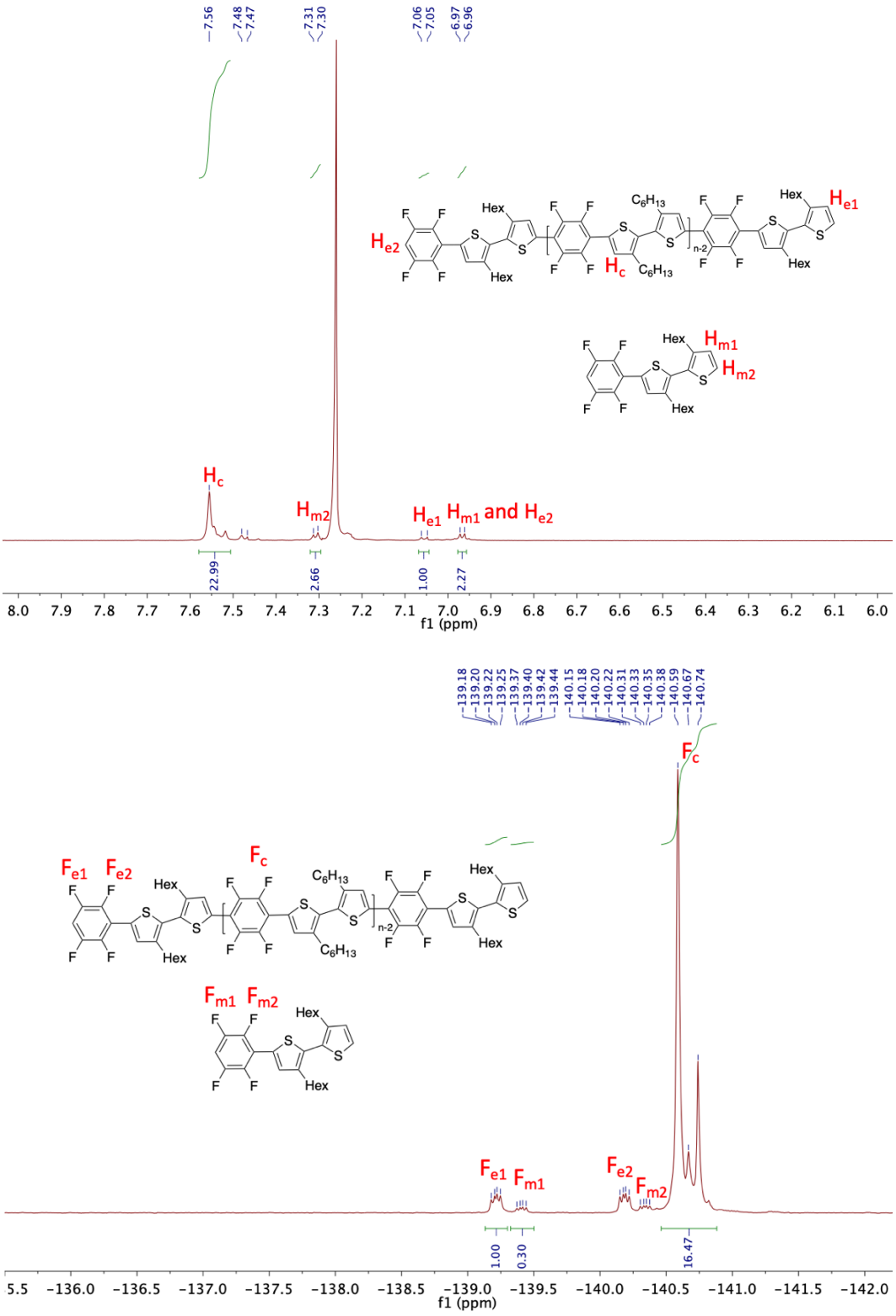

The aromatic regions of ^{1}H NMR (top) and ^{19}F NMR (bottom) of AB type D-A polymer at 40 min.

Chapter 5. Development of pre-catalysts for the Pd/Ag dual catalytic cross dehydrogenative coupling polymerization in the pursuit of chain-growth mechanism

5.1 Introduction

In general, there are two main categories of polymerizations based on their polymer extending mechanisms, step- and chain-growth polymerizations. In step-growth polymerizations, bifunctional monomers react with each other to form dimers, trimers, then longer oligomers, and eventually long polymer chains. During the step-growth polymerizations, reactions between molecules of all degrees of polymerization would occur. Whereas in the chain-growth polymerization, an initiator is normally required, and the monomers add onto the reactive chain ends one by one. During the chain-growth polymerizations, the monomers usually do not react with each other.

Due to their distinct polymer propagation fashions, the polymers resulted from step-growth and chain-growth polymerizations possess very different characteristics. A major difference is in the molecular weight, which is a significant factor that determines the properties of polymeric materials. The molecular weight of the polymers synthesized using step-growth mechanism usually varies from batch to batch and has a wide distribution. According to the theory established by Carothers[54] and Flory,[103] the molecular weight distribution resulted from step-growth mechanism approaches to 2. A broad molecular weight distribution is not desirable because the low molecular weight portion will cause problems in the material properties. For instance, the low molecular weight polymers/oligomers in the polymeric material can act as a plasticizer that will soften the material and affect its mechanical properties.[104] For

semiconducting polymers, it was reported that even small amounts of low molecular weight polymer are detrimental to charge transport within the material.[105] Nevertheless, the chain-growth polymerizations produce polymers with controlled molecular weight and a narrow molecular weight distribution which theoretically approaches to 1 at high DPs.[53,106] Owing to the ability to control the molecular weight, many properties of the polymeric product are tunable by adjusting the parameters in the chain-growth polymerization. In addition, the chain-growth polymerizations are also able to generate the polymers with explicit end group identity and well-defined structures, such as block and graft copolymers, which are difficult to achieve via step-growth polymerizations.

Normally, polymerizations for the synthesis of semiconducting polymers proceed in a step-growth manner, except for Kumada catalyst transfer polymerization (KCPT).[107,108] It was demonstrated in Chapter 4 that Pd/Ag cocatalytic CDC polymerization, even with the AB type monomer, proceeds in a step-growth manner. In the past decade, a lot of effort was made to convert step-growth polymerizations, including Suzuki, Stille, and Negishi polymerizations, as well as DArP, into chain-growth polymerizations for the synthesis of semiconducting polymers.[101,109–123] However, to date there has been no report on converting a step-growth CDC polymerization into a chain-growth one. In general, there are two approaches: i) Intramolecular catalyst transfer, where the catalytic species stays attached to the propagating chain end after the reductive elimination to form an associative π-complex, and the catalytic species intramolecularly migrates along the polymer backbone as the chain extends (Scheme 5.1);[107,108] ii) Inactive monomer and reactive chain ends, also called the intramolecular deactivation, where the formation of the associative π-complex is not required. It is required that the inactive functional group on the monomer becomes reactive once the other functional group on the

monomer reacts with the active polymer chain end or an initiator, which is commonly observed in the AB type condensative chain polymerizations (Scheme 5.2).[109–111] We can see that the communal purpose of both approaches is to avoid the reactions between monomers. In the intramolecular catalyst transfer approach, by keeping the catalytic species near the propagating chain ends, the catalytic species has no chance to catalyze the coupling between two individual monomers. In the intramolecular deactivation approach, the prevention of the reactions between monomers is accomplished by manipulating the reactivity of the functional groups. By forcing monomers only react with the polymer chain ends but not themselves, addition of monomers onto the propagating chain one at a time can be achieved.

Scheme 5.1 Intramolecular catalyst transfer polymerization process

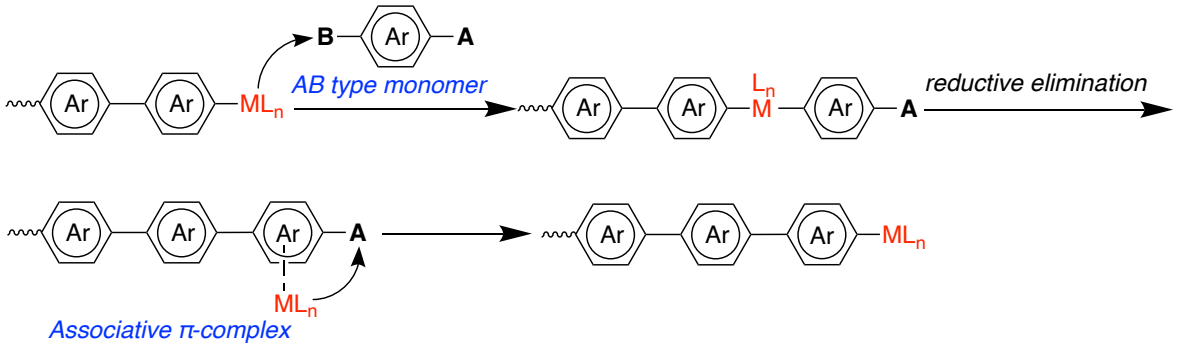

Scheme 5.2 A schematic illustration of intramolecular deactivation concept in condensative chain polymerizations

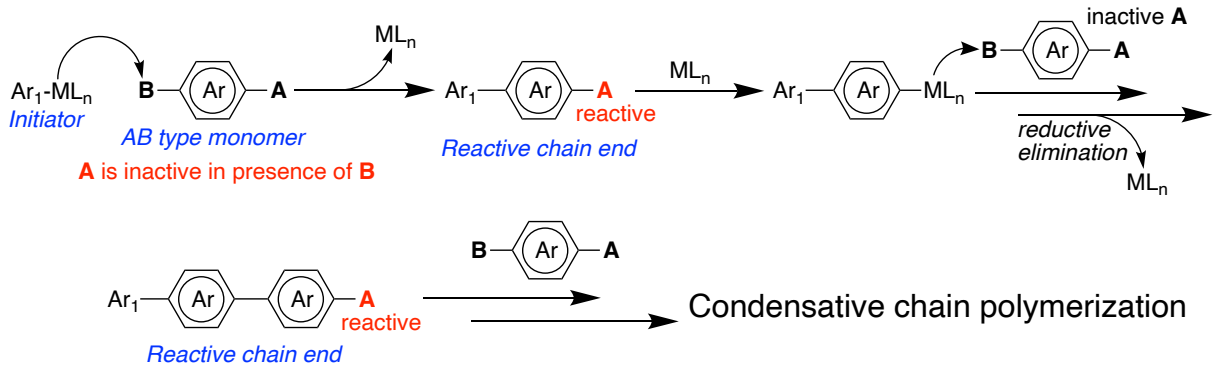

The generation pathway of the catalytically active species from the corresponding pre-catalyst has a huge impact on the polymerization and resulted polymers. There are generally two kinds of metallic pre-catalysts based on the ligand type, L_nM complexes and their $L_nM(Ar)_x$ counterparts. Although L_nM pre-catalysts are generally more available and easier to synthesize, their activation rate is usually slower. The slow activation rate of pre-catalysts has been considered as the main cause of broad molecular weight distributions.[124] $L_nM(Ar)_x$ pre-catalysts, on the other hand, can be activated faster and provide an end-capping group Ar on the polymer, which endows the polymerization with better end group tunability.[112] In addition, in the case of AB type polymerization where Ar is unreactive to the condensation reaction, the introduction of the end-capping group Ar can minimize the occurrence of undesired chain combinations which would widen the molecular weight distribution of the resulted polymer. Therefore, in order to make a polymerization more controlled and eventually proceed in a chain-growth fashion, $L_nM(Ar)_x$ pre-catalysts are considered as the better option.

In this Chapter, three $L_nM(Ar)_x$ pre-catalysts, *t*Bu_3P-PdBr-benzene, $(PPh_3)_2$-Pd-(pentafluorobenzene)$_2$, and $(PPh_3)_2$-Pd-(thienyl tetrafluorobenzene)$_2$, were developed and tested in the Pd/Ag cocatalytic AB type CDC polymerization (Scheme 5.3). Out of the three pre-catalysts, it was discovered that $(PPh_3)_2$-Pd-(thienyl tetrafluorobenzene)$_2$ has the highest potential to produce narrow molecular weight distributions, since it provided complete and fast pre-catalyst activation.

Scheme 5.3 Pd/Ag cocatalytic AB type CDC polymerization (top) with the three $L_nM(Ar)_x$ pre-catalysts (bottom)

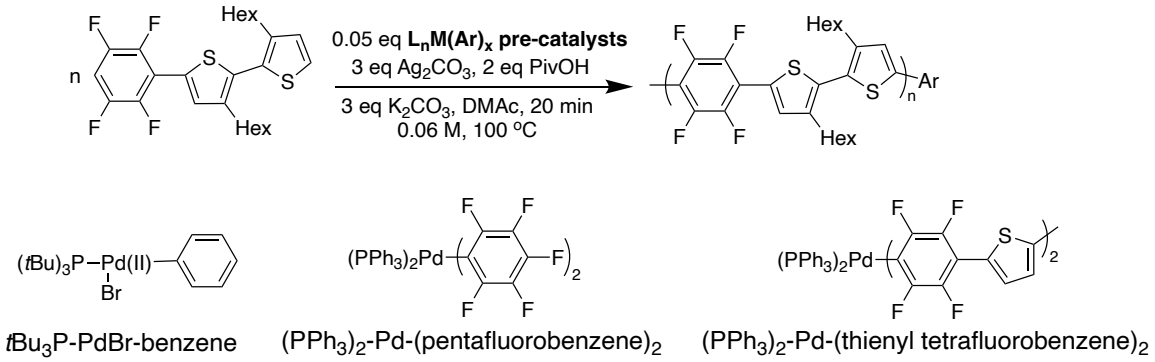

5.2 Results and Discussion

5.2.1 *tBu₃P-PdBr-benzene*

*t*Bu$_3$P-PdBr-benzene was synthesized in bulk bromobenzene, and the reaction solution (0.5 M) was directly added to the polymerization without further workup due to the air-sensitivity of *t*Bu$_3$P-PdBr-benzene. After the polymerization, the resulted polymer was isolated by precipitation in hexanes and analyzed with NMR. ^{1}H NMR spectrum (Figure 5.1) shows that only thiophene end group was detected. No signals from end-capping group benzene were observed. DP and % conv. were calculated using the data from ^{19}F NMR spectrum (Figure 5.2). The DP is 4.3 and % conv. is 72 %. The low values of DP and % conv. and the fact that no benzene end group was detected indicated that the activation of *t*Bu$_3$P-PdBr-benzene pre-catalyst did not occur efficiently. Moreover, it was speculated that the presence of a large amount of bromobenzene in the polymerization might poison the Pd catalyst, which leads to low DP and % conv.

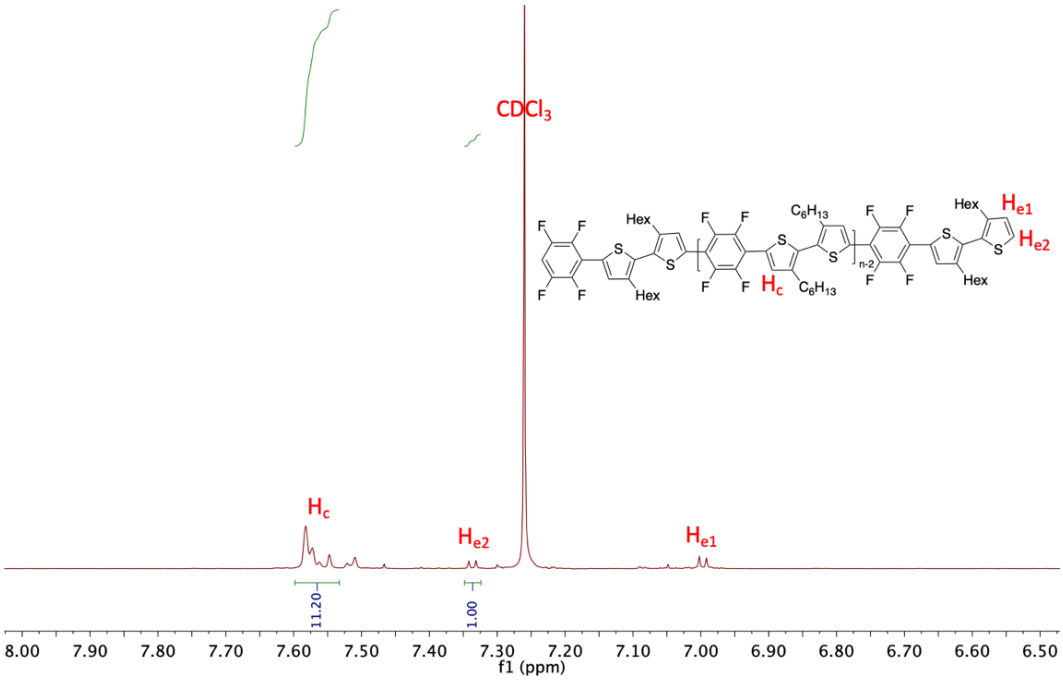

Figure 5.1 The aromatic region in ^{1}H NMR spectrum of polymer synthesized with *t*Bu_3P-PdBr-benzene pre-catalyst.

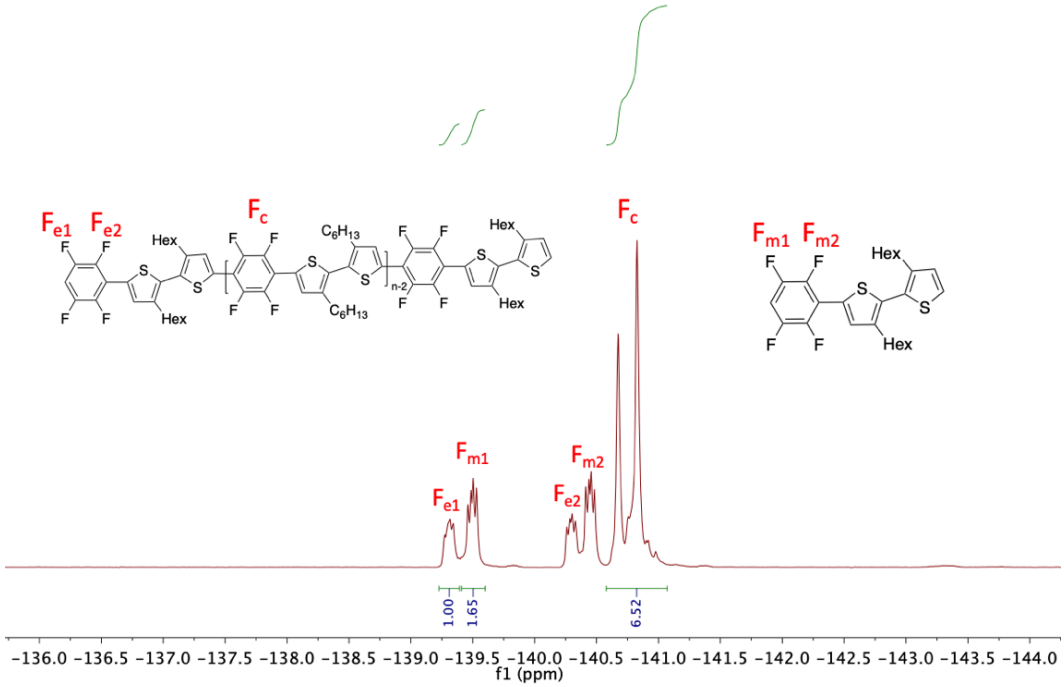

Figure 5.2 The aromatic region in ^{19}F NMR spectrum of polymer synthesized with *t*Bu_3P-PdBr-benzene pre-catalyst.

5.2.2 *$(PPh_3)_2$-Pd-(pentafluorobenzene)$_2$*

$(PPh_3)_2$-Pd-(pentafluorobenzene)$_2$ was synthesized and purified before being used in polymerizations. After the polymerization, the resulted polymer and monomer mixture was analyzed with ^{19}F NMR. ^{19}F NMR spectrum (Figure 5.3) shows that the end-capping pentafluorobenzne group is only 5 %. However, DP and % conv. are a lot higher compared to the ones with *t*Bu$_3$P-PdBr-benzene pre-catalyst, which are 7.1 and 98 %, respectively. It was suspected that $(PPh_3)_2$-Pd-(pentafluorobenzene)$_2$ might be too stable to be efficiently activated. If the release of catalytically active species from the pre-catalyst occurs simultaneously as the chain extension, most polymer chains will not have the end-capping group. To confirm this hypothesis, we reacted AB type monomer **H** with the $(PPh_3)_2$-Pd-(pentafluorobenzene)$_2$ pre-catalyst at a 1:1 ratio for 20 min. The ^{19}F NMR shows that polymers were generated, and the DP was 13.0. This demonstrates that the activation rate of $(PPh_3)_2$-Pd-(pentafluorobenzene)$_2$ pre-catalyst is too slow compared to the chain extension rate, ascribed to its high stability.

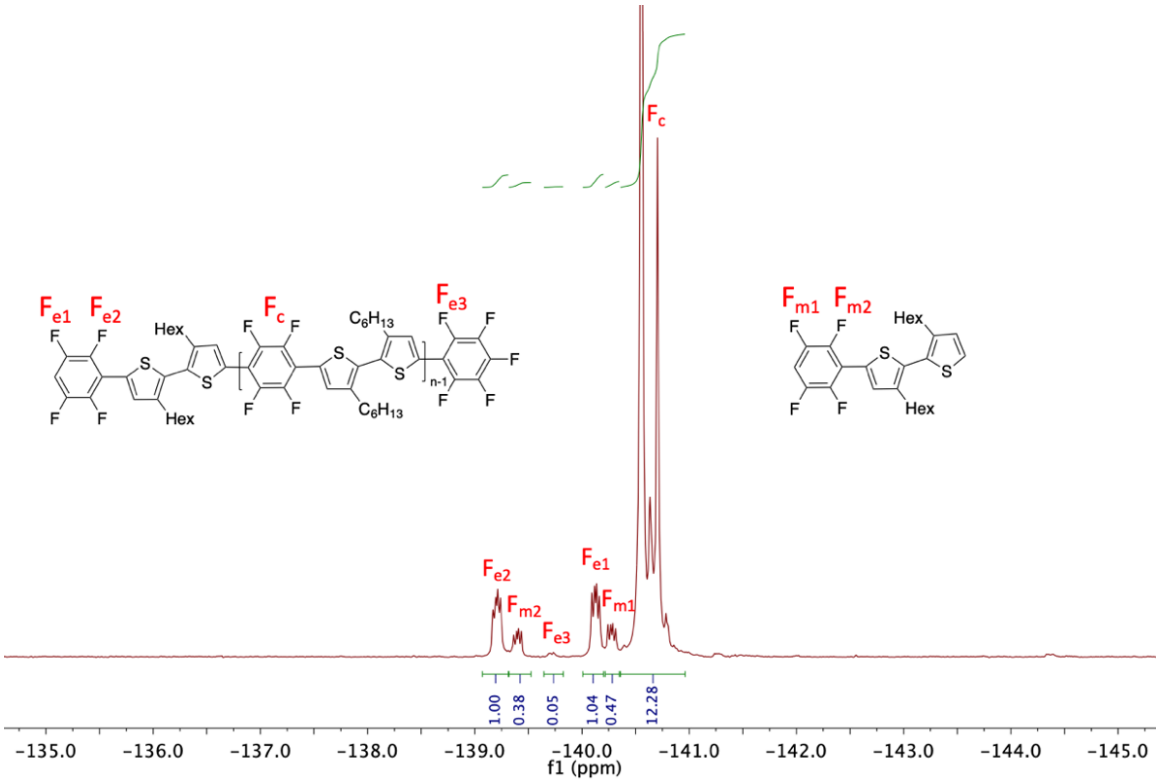

Figure 5.3 The aromatic region in ^{19}F NMR spectrum of polymer synthesized with $(PPh_3)_2$-Pd-(pentafluorobenzene)$_2$ pre-catalyst.

5.2.3 *$(PPh_3)_2$-Pd-(thienyl tetrafluorobenzene)$_2$*

$(PPh_3)_2$-Pd-(thienyl tetrafluorobenzene)$_2$ was synthesized and purified before being used in polymerizations. After the polymerization, the resulted polymer and monomer mixture was analyzed with ^{19}F NMR. 100 % Thienyl tetrafluorobenzene end-capping group were detected in ^{19}F NMR spectrum (Figure 5.4). The DP and % conv. were 11.2 and 100 %. The reaction between $(PPh_3)_2$-Pd-(thienyl tetrafluorobenzene)$_2$ and monomer **H** at 1:1 ratio did not generate polymers, indicating that the activation rate of $(PPh_3)_2$-Pd-(thienyl tetrafluorobenzene)$_2$ pre-catalyst is faster than the chain extension rate. Therefore, $(PPh_3)_2$-Pd-(thienyl tetrafluorobenzene)$_2$ pre-catalyst has the potential to produce polymers with a narrow molecular weight distribution. The kinetic experiment on the Pd/Ag cocatalytic AB type CDC

polymerization with $(PPh_3)_2$-Pd-(thienyl tetrafluorobenzene)$_2$ pre-catalyst was also carried out. The DP vs. % conv. plot still suggests that the polymerization with $(PPh_3)_2$-Pd-(thienyl tetrafluorobenzene)$_2$ pre-catalyst proceeded in a step-growth manner (Figure 5.5).

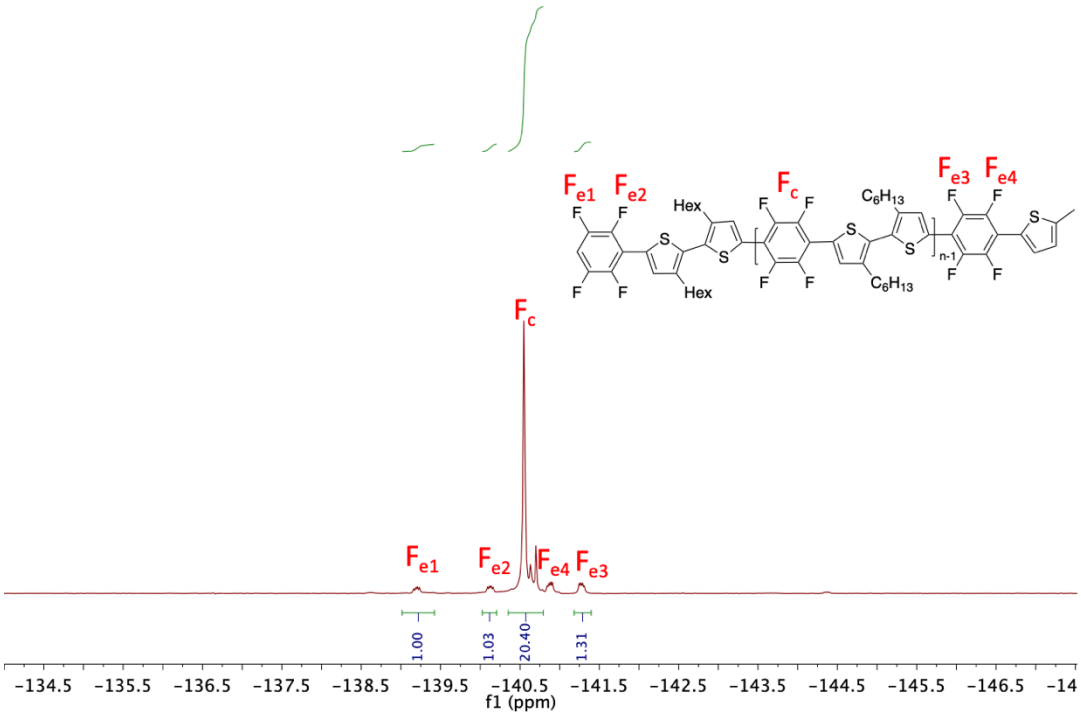

Figure 5.4 The aromatic region in ^{19}F NMR spectrum of polymer synthesized with $(PPh_3)_2$-Pd-(thienyl tetrafluorobenzene)$_2$ pre-catalyst.

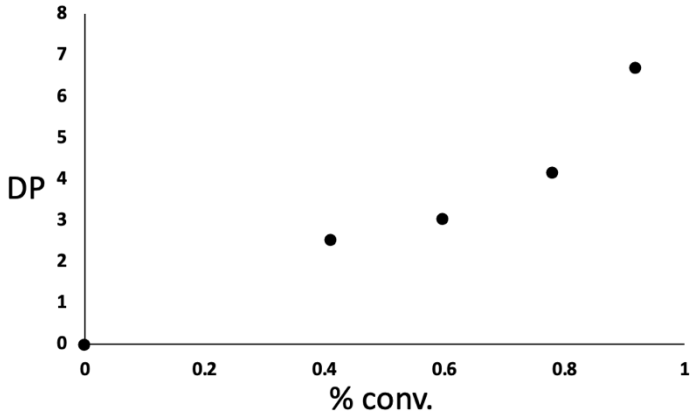

Figure 5.5 Number-average degree of polymerization (DP) versus monomer conversion (% conv.) plot of CDC polymerization with $(PPh_3)_2$-Pd-(thienyl tetrafluorobenzene)$_2$ pre-catalyst.

5.3 Conclusions

Three $L_nM(Ar)_x$ pre-catalysts, *t*Bu_3P-PdBr-benzene, $(PPh_3)_2$-Pd-(pentafluorobenzene)$_2$, and $(PPh_3)_2$-Pd-(thienyl tetrafluorobenzene)$_2$, were developed and tested in the Pd/Ag cocatalytic AB type CDC polymerization. It was discovered that out of the three pre-catalysts, only $(PPh_3)_2$-Pd-(thienyl tetrafluorobenzene)$_2$ was able to give 100 % end-capping group, owing to its complete and fast pre-catalyst activation. Although the CDC polymerization with $(PPh_3)_2$-Pd-(thienyl tetrafluorobenzene)$_2$ still proceeded in a step-growth manner, $(PPh_3)_2$-Pd-(thienyl tetrafluorobenzene)$_2$ has the potential to act as an initiator in the pursuit of chain-growth mechanism.

5.4 Supplementary Information

5.4.1 *General Information*

All reactions were carried out under nitrogen atmosphere using standard Schlenk techniques unless otherwise noted. NMR spectra were recorded on Bruker AV-300 and AV-500 spectrometers operating at 300 and 500 MHz, respectively. NMR chemical shifts (δ) are reported in parts per million (ppm) downfield of tetramethylsilane and are referenced relative to the residual solvent signal for ^{1}H NMR ($CDCl_3$ (7.26 ppm)). Anhydrous solvents such as 1,4-dioxane, N,N-dimethylacetamide (DMAc) and tetrahydrofuran (THF) were used as purchased from Sigma Aldrich. Deuterated solvents were stored over 4 Å molecular sieves. *t*Bu_3P-PdBr-benzene was synthesized using previously reported methods.[125] All other reagents and chemicals were purchased from Sigma-Aldrich or Tokyo Chemical International and used without further purification.

5.4.2 *Synthesis of $(PPh_3)_2$-Pd-(pentafluorobenzene)$_2$ Pre-catalyst*

A 50 mL round bottom flask equipped with an acid-washed stir bar was oven dried overnight. The round bottom flask was sealed with a rubber septum and evacuated and refilled with nitrogen three times. Pentafluorobenzene (168 mg, 1.00 mmol) and anhydrous THF (3 mL) were injected into the round bottom flask under nitrogen. The solution was cooled to -78 °C, and under nitrogen pressure, n-butyllithium solution (2.5 M in hexanes) (0.4 mL, 1.00 mmol) was injected into the reaction flask dropwise. The mixture was stirred at -78 °C for 10 min, and a suspension of bis(triphenylphosphine)palladium(II) dichloride (281 mg, 0.40 mmol) in THF (2 mL) was injected into the reaction mixture. After that, the reaction mixture was stirred at -78 °C for another hour. The reaction mixture was slowly warmed up to room temperature and stirred at room temperature for 2 h. A light purple suspension was obtained. The solid was removed by filtration and washed with acetone. The solution was concentrated under reduced pressure. Toluene was added, and the insoluble solid was removed by filtration. The solution was then concentrated under reduced pressure again. A white solid (132 mg, 34 %) was obtained after the precipitation in hexanes and dried under vacuum overnight. ^{1}H NMR (500 MHz, 298 K, chloroform-*d*): δ 7.64 (dtd, *J* = 8.6, 5.7, 1.3 Hz, 12H), 7.39 (m, 6H), 7.31 (m, 12H). ^{19}F NMR (470 MHz, 298 K, chloroform-*d*): δ -116.92 (dd, *J* = 29.9, 7.3 Hz, 4F), -162.41 (t, *J* = 19.7 Hz, 2F), -162.73 (t, *J* = 22.5 Hz, 4F).

5.4.3 *Synthesis of $(PPh_3)_2$-Pd-(thienyl tetrafluorobenzene)$_2$ Pre-catalyst*

A 50 mL round bottom flask equipped with an acid-washed stir bar was oven dried overnight. The round bottom flask was sealed with a rubber septum and evacuated and refilled with nitrogen three times. **3a** from Chapter 3 (61.4 mg, 0.250 mmol) and anhydrous THF (2 mL) were injected into the round bottom flask under nitrogen. The solution was cooled to -78 °C, and

under nitrogen pressure, n-butyllithium solution (2.5 M in hexanes) (0.1 mL, 0.250 mmol) was injected into the reaction flask dropwise. The mixture was stirred at -78 °C for 10 min, and a suspension of bis(triphenylphosphine)palladium(II) dichloride (70.2 mg, 0.100 mmol) in THF (2 mL) was injected into the reaction mixture. After that, the reaction mixture was stirred at -78 °C for another hour. The reaction mixture was slowly warmed up to room temperature and stirred at room temperature for 2 h. The solid in the resulted suspension was removed by filtration and washed with acetone. The solution was concentrated under reduced pressure. Toluene was added, and the insoluble solid was removed by filtration. The solution was concentrated under reduced pressure again. A white solid (65.7 mg, 59 %) was obtained after the precipitation in hexanes and dried under vacuum overnight. The ^{1}H NMR and ^{19}F NMR show that the white solid contains both monosubstituted Pd complex ($(PPh_3)_2$-Pd-(thienyl tetrafluorobenzene)) (82 %) and disubstituted Pd complex ($(PPh_3)_2$-Pd-(thienyl tetrafluorobenzene)$_2$) (18 %). $(PPh_3)_2$-Pd-(thienyl tetrafluorobenzene): ^{1}H NMR (500 MHz, 298 K, chloroform-*d*): δ 7.64 (dtd, *J* = 8.6, 5.7, 1.3 Hz, 12H), 7.39 (m, 6H), 7.31 (m, 12H), 6.86 (d, *J* = 3.6 Hz, 1H), 6.71 (d, *J* = 3.6 Hz, 1H). ^{19}F NMR (470 MHz, 298 K, chloroform-*d*): δ -118.53 (dd, *J* = 27.5, 6.7 Hz, 2F), -142.29 (dd, *J* = 30.7, 11.4 Hz, 2F). $(PPh_3)_2$-Pd-(thienyl tetrafluorobenzene)$_2$: ^{1}H NMR (500 MHz, 298 K, chloroform-*d*): δ 7.64 (dtd, *J* = 8.6, 5.7, 1.3 Hz, 12H), 7.39 (m, 6H), 7.31 (m, 12H), 7.03 (d, *J* = 3.6 Hz, 2H), 6.69 (d, *J* = 3.6 Hz, 2H). ^{19}F NMR (470 MHz, 298 K, chloroform-*d*): δ -116.87 (d, *J* = 27.3, 4F), -142.50 (d, *J* = 31.3 Hz, 4F).

Chapter 6. Conclusions and Future Recommendations

6.1 Development of New CDC Polymerizations

Two dual catalytic systems for CDC polymerizations, Au/Ag and Pd/Ag systems were investigated here as presented in Chapters 2 and 3. The fact that both Au/Ag and Pd/Ag systems successfully produced D-A semiconducting polymers reinforced that the dual catalytic systems, where more than one metal catalyst activates the C-H bonds of monomers, have a higher potential in CDC polymerization than the mono-catalytic systems, because the catalysts in mono-catalytic CDCs often have insufficient selectivity to distinguish the donor and acceptor monomers. However, not all combinations of two transition metal catalysts would work, certain prerequisites need to be met: 1) Each metal catalyst only selectively activates one substrate over the other (orthogonality); 2) Ligand transfer is able to occur smoothly from one metal to the other (transmetalation); 3) Two metal catalysts are redox compatible.[60] Copper has been reported to be a good C-H bond activating reagent for fluoroaryl species.[126] In that case, Pd/Cu cocatalyzed CDC polymerization seems to be a feasible option for future work.

The polymerization behaviors of the Au/Ag and Pd/Ag catalytic systems are very different. Au/Ag system displayed a high cross-coupling yield in the small molecule model reaction but generated polymers with low molecular weight and high homo-coupling defects content. Whereas the small molecule model reaction catalyzed by Pd/Ag system proceeded inefficiently, but the CDC polymerization catalyzed by Pd/Ag system generated high molecular weight polymers with minimal homo-coupling defects. These two dual catalytic polymerization systems both defy the Carothers equation because they violate the equal reactivity assumption of the functional groups. The functional groups (C-H bonds) in Pd/Ag catalyzed CDC

polymerizations appear to be more reactive as the polymerization proceeds, and the functional groups (C-H bonds) in Au/Ag catalyzed CDC polymerizations appear to be less reactive after the 1st cross coupling reaction between monomers. Therefore, the classic Carothers equation is not suitable to be used here to predict the polymerization behaviors of the Au/Ag and Pd/Ag catalytic CDC systems based on their small molecule model reactions.

With this knowledge, in the future pursuit of developing new CDC polymerizations, we must be aware of the possible significant change in the reactivity of the functional groups as the polymerizations proceed. High cross-coupling yields in the small molecule model reactions do not always map directly to polymerizations. When focusing on the results of the initial step CDC (1st cross-coupling), the conditions generating high cross-coupling yields sometimes does not yield defect-free and high-molecular weight semiconducting polymers. The more prominent indicator for a successful polymerization is the chain extension steps (e.g., 2nd and/or 3rd cross-coupling) as the 1st coupling reaction only occurs at the beginning of the polymerization before creating the polymer chain. The chain extension step occurs throughout the polymerization and therefore determines the length and chemical structure of the resulting semiconducting polymer.

Finally, the results in this study have implications beyond polymerizations and can be used to ease the synthesis of a wide range of molecules where C-H bond activation may be the limiting factor.

6.2 Development of CDC Condensative Chain Polymerizations

As it was discussed in Chapter 5, there are generally two pathways to realize CDC condensative chain polymerizations, intramolecular catalyst transfer and intramolecular deactivation (Schemes 5.1 and 5.2). For the current Pd/Ag cocatalytic AB type CDC

polymerization using the monomer **H**, the intramolecular deactivation pathway is not feasible because the monomer **H** itself is reactive. During the polymerization, if Pd catalytic species detaches from the chain-end after the reductive elimination and oxidation, it can catalyze the coupling reaction between two monomers, leading to step-growth mechanism. The other pathway, intramolecular catalyst transfer, also seems to be challenging for converting the current Pd/Ag cocatalytic step-growth polymerization into a condensative chain polymerization. Firstly, the AB type monomer **H** is not perfectly planar (the thiophene-thiophene dihedral angle is at least 87°),[69] which presents difficulty in formation of associative π-complexes. In addition, the monomer **H** consists of three connected arenes, which can be too long to allow the efficient "ring walking" of the Pd catalyst. Secondly, the Pd/Ag cocatalytic cycle shows that after reductive elimination, the Pd(0) species needs to be oxidized by Ag(I) first before it can react with the new chain end. This oxidation step can cause the detachment of Pd catalyst from the polymer chain end.

To achieve CDC condensative chain polymerizations, much more research need to be carried out. Based on the discussion above, the chemical structure of the current monomer **H** causes many issues. It is obvious that we need to redesign the AB type monomer to make it inactive by itself and able to be activated after its reaction with the chain end. We can also make it smaller and planar so that the formation of associative π-complexes with the Pd catalyst is more favorable. In that case, a monomer screening study is essential to learn about the monomer scope of this Pd/Ag cocatalytic CDC polymerization. For instance, if it was discovered by performing the monomer screening study that apart from thiophene species, pyrrole derivatives are also great electron-rich monomers for the Pd/Ag cocatalytic CDC polymerization, an AB

type monomer consisting of a 1,2,4,5-tetrafluorobenzene and an alkylated pyrrole could become useful to achieve intramolecular catalyst transfer (Scheme 6.1).

Scheme 6.1 Hypothetic design of new AB type monomer

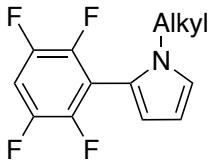

References

(1) Chiang, C. K.; Fincher, C. R.; Park, Y. W.; Heeger, A. J.; Shirakawa, H.; Louis, E. J.; Gau, S. C.; MacDiarmid, A. G. Electrical Conductivity in Doped Polyacetylene. *Phys. Rev. Lett.* **1977**, *39*, 1098–1101.

(2) Shirakawa, H.; Louis, E. J.; MacDiarmid, A. G.; Chiang, C. K.; Heeger, A. J. Synthesis of Electrically Conducting Organic Polymers: Halogen Derivatives of Polyacetylene, (CH) x. *J. Chem. Soc. Chem. Commun.* **1977**, No. 16, 578.

(3) Chiang, C. K.; Druy, M. A.; Gau, S. C.; Heeger, A. J.; Louis, E. J.; MacDiarmid, A. G.; Park, Y. W.; Shirakawa, H. Synthesis of Highly Conducting Films of Derivatives of Polyacetylene, (CH)x. *J. Am. Chem. Soc.* **1978**, *100*, 1013–1015.

(4) Liu, C.; Wang, K.; Gong, X.; Heeger, A. J. Low Bandgap Semiconducting Polymers for Polymeric Photovoltaics. *Chem. Soc. Rev.* **2016**, *45*, 4825–4846.

(5) Holliday, S.; Li, Y.; Luscombe, C. K. Recent Advances in High Performance Donor-Acceptor Polymers for Organic Photovoltaics. *Prog. Polym. Sci.* **2017**, *70*, 34–51.

(6) Borges, B. G. A. L.; Gioti, M.; Correa, R. S.; Andreopoulou, A. K.; Veiga, A. G.; Laskarakis, A.; Kallitsis, J. K.; Logothetidis, S.; Rocco, M. L. M. Surface, Interface and Electronic Studies on Anthracene Derived Polymeric Thin Films for OLED Applications. *Opt Mater (Amst)* **2021**, *117*, 111145.

(7) Ahmad, V.; Shukla, A.; Sobus, J.; Sharma, A.; Gedefaw, D.; Andersson, G. G.; Andersson, M. R.; Lo, S.; Namdas, E. B. High-Speed OLEDs and Area-Emitting Light-Emitting Transistors from a Tetracyclic Lactim Semiconducting Polymer. *Adv. Opt. Mater.* **2018**, *6*, 1800768.

(8) Chaudhry, M. U.; Muhieddine, K.; Wawrzinek, R.; Li, J.; Lo, S.-C.; Namdas, E. B. Nano-Alignment in Semiconducting Polymer Films: A Path to Achieve High Current Density and Brightness in Organic Light Emitting Transistors. *ACS Photonics* **2018**, *5*, 2137–2144.

(9) Yang, J.; Zhao, Z.; Wang, S.; Guo, Y.; Liu, Y. Insight into High-Performance Conjugated Polymers for Organic Field-Effect Transistors. *Chem* **2018**, *4*, 2748–2785.

(10) Chen, H.; Hurhangee, M.; Nikolka, M.; Zhang, W.; Kirkus, M.; Neophytou, M.; Cryer, S. J.; Harkin, D.; Hayoz, P.; Abdi-Jalebi, M.; McNeill, C. R.; Sirringhaus, H.; McCulloch, I. Dithiopheneindenofluorene (**TIF**) Semiconducting Polymers with Very High Mobility in Field-Effect Transistors. *Adv. Mater.* **2017**, *29*, 1702523.

(11) Riera-Galindo, S.; Leonardi, F.; Pfattner, R.; Mas-Torrent, M. Organic Semiconductor/Polymer Blend Films for Organic Field-Effect Transistors. *Adv. Mater. Technol.* **2019**, *4*, 1900104.

(12) Sirringhaus, H. 25th Anniversary Article: Organic Field-Effect Transistors: The Path Beyond Amorphous Silicon. *Adv. Mater.* **2014**, *26*, 1319–1335.

(13) Nambiar, S.; Yeow, J. T. W. Conductive Polymer-Based Sensors for Biomedical Applications. *Biosens. Bioelectron.* **2011**, *26*, 1825–1832.

(14) Martin, D. C. Molecular Design, Synthesis, and Characterization of Conjugated Polymers for Interfacing Electronic Biomedical Devices with Living Tissue. *MRS Commun.* **2015**, *5*, 131–152.

(15) Gibson, G. L.; McCormick, T. M.; Seferos, D. S. Atomistic Band Gap Engineering in Donor–Acceptor Polymers. *J. Am. Chem. Soc.* **2012**, *134*, 539–547.

(16) Beaujuge, P. M.; Amb, C. M.; Reynolds, J. R. Spectral Engineering in π-Conjugated Polymers with Intramolecular Donor−Acceptor Interactions. *Acc. Chem. Res.* **2010**, *43*, 1396–1407.
(17) Müllen, K.; Pisula, W. Donor–Acceptor Polymers. *J. Am. Chem. Soc.* **2015**, *137*, 9503–9505.
(18) Scharber, M. C.; Mühlbacher, D.; Koppe, M.; Denk, P.; Waldauf, C.; Heeger, A. J.; Brabec, C. J. Design Rules for Donors in Bulk-Heterojunction Solar Cells—Towards 10 % Energy-Conversion Efficiency. *Adv. Mater.* **2006**, *18*, 789–794.
(19) Hendriks, K. H.; Li, W.; Heintges, G. H. L.; van Pruissen, G. W. P.; Wienk, M. M.; Janssen, R. A. J. Homocoupling Defects in Diketopyrrolopyrrole-Based Copolymers and Their Effect on Photovoltaic Performance. *J. Am. Chem. Soc.* **2014**, *136*, 11128–11133.
(20) Vangerven, T.; Verstappen, P.; Drijkoningen, J.; Dierckx, W.; Himmelberger, S.; Salleo, A.; Vanderzande, D.; Maes, W.; Manca, J. v. Molar Mass versus Polymer Solar Cell Performance: Highlighting the Role of Homocouplings. *Chem. Mater.* **2015**, *27*, 3726–3732.
(21) Stille, J. K. The Palladium-Catalyzed Cross-Coupling Reactions of Organotin Reagents with Organic Electrophiles[New Synthetic Methods(58)]. *Angew. Chem. Int. Ed. Engl.* **1986**, *25*, 508–524.
(22) Miyaura, N.; Yamada, K.; Suzuki, A. A New Stereospecific Cross-Coupling by the Palladium-Catalyzed Reaction of 1-Alkenylboranes with 1-Alkenyl or 1-Alkynyl Halides. *Tetrahedron Lett.* **1979**, *20*, 3437–3440.
(23) Kanimozhi, C.; Balraju, P.; Sharma, G. D.; Patil, S. Synthesis of Diketopyrrolopyrrole Containing Copolymers: A Study of Their Optical and Photovoltaic Properties. *J. Phys. Chem. B* **2010**, *114*, 3095–3103.
(24) Kettle, J.; Horie, M.; Majewski, L. A.; Saunders, B. R.; Tuladhar, S.; Nelson, J.; Turner, M. L. Optimisation of PCPDTBT Solar Cells Using Polymer Synthesis with Suzuki Coupling. *Sol. Energy Mater. Sol. Cells* **2011**, *95*, 2186–2193.
(25) Osedach, T. P.; Andrew, T. L.; Bulović, V. Effect of Synthetic Accessibility on the Commercial Viability of Organic Photovoltaics. *Energy Environ. Sci.* **2013**, *6*, 711.
(26) Marrocchi, A.; Facchetti, A.; Lanari, D.; Petrucci, C.; Vaccaro, L. Current Methodologies for a Sustainable Approach to π-Conjugated Organic Semiconductors. *Energy Environ. Sci.* **2016**, *9*, 763–786.
(27) Po, R.; Bernardi, A.; Calabrese, A.; Carbonera, C.; Corso, G.; Pellegrino, A. From Lab to Fab: How Must the Polymer Solar Cell Materials Design Change? – An Industrial Perspective. *Energy Environ. Sci.* **2014**, *7*, 925.
(28) Trost, B. The Atom Economy—A Search for Synthetic Efficiency. *Science (1979)* **1991**, *254*, 1471–1477.
(29) Kuwabara, J. Direct Arylation Polycondensation for Synthesis of Optoelectronic Materials. *Polymer Journal* **2018**, *50*, 1099–1106.
(30) Nakabayashi, K. Direct Arylation Polycondensation as Conjugated Polymer Synthesis Methodology. *Polymer Journal* **2018**, *50*, 475–483.
(31) Wakioka, M.; Morita, H.; Ichihara, N.; Saito, M.; Osaka, I.; Ozawa, F. Mixed-Ligand Approach to Palladium-Catalyzed Direct Arylation Polymerization: Synthesis of Donor–Acceptor Polymers Containing Unsubstituted Bithiophene Units. *Macromolecules* **2020**, *53*, 158–164.

(32) Wakioka, M.; Yamashita, N.; Mori, H.; Nishihara, Y.; Ozawa, F. Synthesis of a 1,2-Dithienylethene-Containing Donor-Acceptor Polymer via Palladium-Catalyzed Direct Arylation Polymerization (DArP). *Molecules* **2018**, *23*, 981.
(33) Shi, Q.; Tatum, W.; Zhang, J.; Scott, C.; Luscombe, C. K.; Marder, S. R.; Blakey, S. B. The Direct Arylation Polymerization (DArP) of Well-Defined Alternating Copolymers Based On 5,6-Dicyano[2,1,3]Benzothiadiazole (DCBT). *Asian J. Org. Chem.* **2018**, *7*, 1419–1425.
(34) Gobalasingham, N. S.; Thompson, B. C. Direct Arylation Polymerization: A Guide to Optimal Conditions for Effective Conjugated Polymers. *Prog. Polym. Sci.* **2018**, *83*, 135–201.
(35) Leclerc, M.; Brassard, S.; Beaupré, S. Direct (Hetero)Arylation Polymerization: Toward Defect-Free Conjugated Polymers. *Polymer Journal* **2020**, *52*, 13–20.
(36) Wakioka, M.; Ozawa, F. Highly Efficient Catalysts for Direct Arylation Polymerization (DArP). *Asian J. Org. Chem.* **2018**, *7*, 1206–1216.
(37) Lapointe, D.; Fagnou, K. Overview of the Mechanistic Work on the Concerted Metallation–Deprotonation Pathway. *Chem. Lett.* **2010**, *39*, 1118–1126.
(38) Stuart, D. R.; Fagnou, K. The Catalytic Cross-Coupling of Unactivated Arenes. *Science (1979)* **2007**, *316*, 1172–1175.
(39) Pankow, R. M.; Thompson, B. C. Approaches for Improving the Sustainability of Conjugated Polymer Synthesis Using Direct Arylation Polymerization (DArP). *Polym. Chem.* **2020**, *11*, 630–640.
(40) Mooney, M.; Nyayachavadi, A.; Rondeau-Gagné, S. Eco-Friendly Semiconducting Polymers: From Greener Synthesis to Greener Processability. *J. Mater. Chem. C* **2020**, *8*, 14645–14664.
(41) Kuwabara, J.; Kanbara, T. Facile Synthesis of π-Conjugated Polymers via Direct Arylation Polycondensation. *Bull. Chem. Soc. Jpn.* **2019**, *92*, 152–161.
(42) Huang, Y.; Luscombe, C. K. Towards Green Synthesis and Processing of Organic Solar Cells. *Chem. Rec.* **2019**, *19*, 1039–1049.
(43) Kuwabara, J.; Kanbara, T. Step-Economical Synthesis of Conjugated Polymer Materials Composed of Three Components: Donor, Acceptor, and π Units. *Macromol. Rapid Commun.* **2021**, *42*, 2000493.
(44) Stepek, I. A.; Itami, K. Recent Advances in C–H Activation for the Synthesis of π-Extended Materials. *ACS Mater. Lett.* **2020**, *2*, 951–974.
(45) Liu, J.-R.; Duan, Y.-Q.; Zhang, S.-Q.; Zhu, L.-J.; Jiang, Y.-Y.; Bi, S.; Hong, X. C–H Acidity and Arene Nucleophilicity as Orthogonal Control of Chemoselectivity in Dual C–H Bond Activation. *Org. Lett.* **2019**, *21*, 2360–2364.
(46) Kang, L. J.; Xing, L.; Luscombe, C. K. Exploration and Development of Gold- and Silver-Catalyzed Cross Dehydrogenative Coupling toward Donor–Acceptor π-Conjugated Polymer Synthesis. *Polym. Chem.* **2019**, *10*, 486–493.
(47) Aoki, H.; Saito, H.; Shimoyama, Y.; Kuwabara, J.; Yasuda, T.; Kanbara, T. Synthesis of Conjugated Polymers Containing Octafluorobiphenylene Unit via Pd-Catalyzed Cross-Dehydrogenative-Coupling Reaction. *ACS Macro Lett.* **2018**, *7*, 90–94.
(48) Zhang, Q.; Chang, M.; Lu, Y.; Sun, Y.; Li, C.; Yang, X.; Zhang, M.; Chen, Y. A Direct C–H Coupling Method for Preparing π-Conjugated Functional Polymers with High Regioregularity. *Macromolecules* **2018**, *51*, 379–388.

(49) Shimoyama, Y.; Kuwabara, J.; Kanbara, T. Mechanistic Study of Pd/Ag Dual-Catalyzed Cross-Dehydrogenative Coupling of Perfluoroarenes with Thiophenes. *ACS Catal.* **2020**, *10*, 3390–3397.
(50) Li, J.; Han, D.; Zhang, Q.; He, Z.; Lu, Y. Synthesis and Properties of Fluorinated Benzotriazole-Based Donor-Acceptor-Type Conjugated Polymers via Pd-Catalyzed Direct C-H/C-H Coupling Polymerization. *J Polym Sci.* **2021**, *59*, 240–250.
(51) Saito, H.; Kuwabara, J.; Yasuda, T.; Kanbara, T. Synthesis of Pyrrole-Based Poly(Arylenevinylene)s via Rh-Catalyzed Dehydrogenative Direct Alkenylation. *Polym. Chem.* **2016**, *7*, 2775–2779.
(52) Saito, H.; Kuwabara, J.; Yasuda, T.; Kanbara, T. Synthesis of Polyfluoro Arylene-Based Poly(Arylenevinylene)s via Pd-Catalyzed Dehydrogenative Direct Alkenylation. *Macromol. Rapid Commun.* **2018**, *39*, 1800414.
(53) Odian, G. *PRINCIPLES OF POLYMERIZATION Fourth Edition*; Wiley: New York, 2004.
(54) Carothers, W. H. Polymers and Polyfunctionality. *Trans. Faraday Soc.* **1936**, *32*, 39–49.
(55) Iimori, H.; Shibasaki, Y.; Ando, S.; Ueda, M. Nonstoichiometric Polycondensation I. Synthesis of Polythioether from Dibromomethane and 4,4′-Thiobisbenzenethiol. *Macromol. Symp.* **2003**, *199*, 23–36.
(56) Matyjaszewski, K.; Möller, M. *Polymer Science: A Comprehensive Reference, Volume 5*; Elsevier: Amsterdam, 2013.
(57) Miyatake, K.; Hlil, A. R.; Hay, A. S. High Molecular Weight Aromatic Polyformals Free of Macrocyclic Oligomers. A Condensative Chain Polymerization Reaction. *Macromolecules* **2001**, *34*, 4288–4290.
(58) Kihara, N.; Komatsu, S.; Takata, T.; Endo, T. Significance of Stoichiometric *Imbalance* in Step Polymerization via Reactive Intermediate. *Macromolecules* **1999**, *32*, 4776–4783.
(59) Goto, E.; Ando, S.; Ueda, M.; Higashihara, T. Nonstoichiometric Stille Coupling Polycondensation for Synthesizing Naphthalene-Diimide-Based π-Conjugated Polymers. *ACS Macro Lett.* **2015**, *4*, 1004–1007.
(60) Ackerman, L. K. G.; Lovell, M. M.; Weix, D. J. Multimetallic Catalysed Cross-Coupling of Aryl Bromides with Aryl Triflates. *Nature* **2015**, *524*, 454–457.
(61) Cambeiro, X. C.; Ahlsten, N.; Larrosa, I. Au-Catalyzed Cross-Coupling of Arenes via Double C–H Activation. *J. Am. Chem. Soc.* **2015**, *137*, 15636–15639.
(62) He, C.-Y.; Min, Q.-Q.; Zhang, X. Palladium-Catalyzed Aerobic Dehydrogenative Cross-Coupling of Polyfluoroarenes with Thiophenes: Facile Access to Polyfluoroarene–Thiophene Structure. *Organometallics* **2012**, *31*, 1335–1340.
(63) Li, R.; Jiang, L.; Lu, W. Intermolecular Cross-Coupling of Simple Arenes via C−H Activation by Tuning Concentrations of Arenes and TFA. *Organometallics* **2006**, *25*, 5973–5975.
(64) Wei, Y.; Su, W. $Pd(OAc)_2$ -Catalyzed Oxidative C−H/C−H Cross-Coupling of Electron-Deficient Polyfluoroarenes with Simple Arenes. *J. Am. Chem. Soc.* **2010**, *132*, 16377–16379.
(65) Masui, K.; Ikegami, H.; Mori, A. Palladium-Catalyzed C−H Homocoupling of Thiophenes: Facile Construction of Bithiophene Structure. *J. Am. Chem. Soc.* **2004**, *126*, 5074–5075.
(66) Bay, K. L.; Yang, Y.-F.; Houk, K. N. Multiple Roles of Silver Salts in Palladium-Catalyzed C–H Activations. *Journal of Organometallic Chemistry* **2018**, *864*, 19–25.

(67) Lotz, M. D.; Camasso, N. M.; Canty, A. J.; Sanford, M. S. Role of Silver Salts in Palladium-Catalyzed Arene and Heteroarene C–H Functionalization Reactions. *Organometallics* **2017**, *36*, 165–171.
(68) Whitaker, D.; Burés, J.; Larrosa, I. Ag(I)-Catalyzed C–H Activation: The Role of the Ag(I) Salt in Pd/Ag-Mediated C–H Arylation of Electron-Deficient Arenes. *J. Am. Chem. Soc.* **2016**, *138*, 8384–8387.
(69) Pomerantz, M.; Amarasekara, A. S.; Dias, H. V. R. Synthesis and Solid-State Structures of Dimethyl 2,2‘-Bithiophenedicarboxylates. *J. Org. Chem.* **2002**, *67*, 6931–6937.
(70) Pilati, T.; Metrangolo, P.; Resnati, G. 4,4′-Dibromo-2,2′,3,3′,5,5′,6,6′-Octafluorobiphenyl. *Acta Crystallogr. C* **2001**, *57*, 113–114.
(71) Ahlsten, N.; Perry, G. J. P.; Cambeiro, X. C.; Boorman, T. C.; Larrosa, I. A Silver-Free System for the Direct C–H Auration of Arenes and Heteroarenes from Gold Chloride Complexes. *Catal. Sci. Technol.* **2013**, *3*, 2892.
(72) Edwards, D. A.; Harker, R. M.; Mahon, M. F.; Molloy, K. C. Aerosol-Assisted Chemical Vapour Deposition (AACVD) of Silver Films from Triorganophosphine Adducts of Silver Carboxylates, Including the Structure of [Ag(O2CC3F7)(PPh3)2]. *Inorganica Chim. Acta* **2002**, *328*, 134–146.
(73) García-Domínguez, P.; Nevado, C. Au–Pd Bimetallic Catalysis: The Importance of Anionic Ligands in Catalyst Speciation. *J. Am. Chem. Soc.* **2016**, *138*, 3266–3269.
(74) Blaskovits, J. T.; Johnson, P. A.; Leclerc, M. Mechanistic Origin of β-Defect Formation in Thiophene-Based Polymers Prepared by Direct (Hetero)Arylation. *Macromolecules* **2018**, *51*, 8100–8113.
(75) Blackmond, D. G. Reaction Progress Kinetic Analysis: A Powerful Methodology for Mechanistic Studies of Complex Catalytic Reactions. *Angew. Chem. Int. Ed.* **2005**, *44*, 4302–4320.
(76) Burés, J. Variable Time Normalization Analysis: General Graphical Elucidation of Reaction Orders from Concentration Profiles. *Angew. Chem. Int. Ed.* **2016**, *55*, 16084–16087.
(77) Fujinami, Y.; Kuwabara, J.; Lu, W.; Hayashi, H.; Kanbara, T. Synthesis of Thiophene- and Bithiophene-Based Alternating Copolymers via Pd-Catalyzed Direct C–H Arylation. *ACS Macro Lett.* **2012**, *1*, 67–70.
(78) Wang, L.; Carrow, B. P. Oligothiophene Synthesis by a General C–H Activation Mechanism: *Electrophilic* Concerted Metalation–Deprotonation (*e* CMD). *ACS Catal.* **2019**, *9*, 6821–6836.
(79) Xing, L.; Liu, J.-R.; Hong, X.; Houk, K. N.; Luscombe, C. K. An Exception to the Carothers Equation Caused by the Accelerated Chain Extension in a Pd/Ag Cocatalyzed Cross Dehydrogenative Coupling Polymerization. *J. Am. Chem. Soc.* **2022**, *144*, 2311–2322.
(80) Petit, A.; Flygare, J.; Miller, A. T.; Winkel, G.; Ess, D. H. Transition-State Metal Aryl Bond Stability Determines Regioselectivity in Palladium Acetate Mediated C–H Bond Activation of Heteroarenes. *Org. Lett.* **2012**, *14*, 3680–3683.
(81) Gaussian 16, Revision A.03, Frisch, M. J., Trucks, G. W., Schlegel, H. B., Scuseria, G. E., Robb, M. A., Cheeseman, J. R., Scalmani, G., Barone, V., Petersson, G. A., Nakatsuji, H., Li, X., Caricato, M., Marenich, A. V., Bloino, J., Janesko, B. G., Gomperts, R., Mennucci, B., Hratchian, H. P., Ortiz, J. V., Izmaylov, A. F., Sonnenberg, J. L., Williams-Young, D., Ding, F., Lipparini, F., Egidi, F., Goings, J., Peng, B., Petrone, A., Henderson, T.,

Ranasinghe, D., Zakrzewski, V. G., Gao, J., Rega, N., Zheng, G., Liang, W., Hada, M., Ehara, M., Toyota, K., Fukuda, R., Hasegawa, J., Ishida, M., Nakajima, T., Honda, Y., Kitao, O., Nakai, H., Vreven, T., Throssell, K., Montgomery, J. A. Jr., Peralta, J. E., Ogliaro, F., Bearpark, M. J., Heyd, J. J., Brothers, E. N., Kudin, K. N., Staroverov, V. N., Keith, T. A., Kobayashi, R., Normand, J., Raghavachari, K., Rendell, A. P., Burant, J. C., Iyengar, S. S., Tomasi, J., Cossi, M., Millam, J. M., Klene, M., Adamo, C., Cammi, R., Ochterski, J. W., Martin, R. L., Morokuma, K., Farkas, O., Foresman, J. B. & Fox, D. J., Gaussian, Inc., Wallingford CT, 2016.

(82) Lee, C.; Yang, W.; Parr, R. G. Development of the Colle-Salvetti Correlation-Energy Formula into a Functional of the Electron Density. *Phys. Rev. B: Condens. Matter Mater. Phys.* **1988**, *37*, 785–789.

(83) Becke, A. D. Density-functional Thermochemistry. III. The Role of Exact Exchange. *J. Chem. Phys.* **1993**, *98*, 5648–5652.

(84) Grimme, S.; Antony, J.; Ehrlich, S.; Krieg, H. A Consistent and Accurate *Ab Initio* Parametrization of Density Functional Dispersion Correction (DFT-D) for the 94 Elements H-Pu. *J. Chem. Phys.* **2010**, *132*, 154104.

(85) Grimme, S.; Ehrlich, S.; Goerigk, L. Effect of the Damping Function in Dispersion Corrected Density Functional Theory. *J. Comp. Chem.* **2011**, *32*, 1456–1465.

(86) Dunning Jr., T. H.; Hay, P. J. *Modern Theoretical Chemistry*, Ed. H. F. Schaefer III, Vol. 3 (Plenum, New York, 1977) 1-28.

(87) Hay, P. J.; Wadt, W. R. *Ab Initio* Effective Core Potentials for Molecular Calculations. Potentials for the Transition Metal Atoms Sc to Hg. *J. Chem. Phys.* **1985**, *82*, 270–283.

(88) Wadt, W. R.; Hay, P. J. *Ab Initio* Effective Core Potentials for Molecular Calculations. Potentials for Main Group Elements Na to Bi. *J. Chem. Phys.* **1985**, *82*, 284–298.

(89) Hay, P. J.; Wadt, W. R. *Ab Initio* Effective Core Potentials for Molecular Calculations. Potentials for K to Au Including the Outermost Core Orbitals. *J. Chem. Phys.* **1985**, *82*, 299–310.

(90) Häussermann, U.; Dolg, M.; Stoll, H.; Preuss, H.; Schwerdtfeger, P.; Pitzer, R. M. Accuracy of Energy-Adjusted Quasirelativistic *Ab Initio* Pseudopotentials. *Molecular Physics* **1993**, *78*, 1211–1224.

(91) Igel-Mann, G.; Stoll, H.; Preuss, H. Pseudopotentials for Main Group Elements (IIIa through VIIa). *Molecular Physics* **1988**, *65*, 1321–1328.

(92) Bergner, A.; Dolg, M.; Küchle, W.; Stoll, H.; Preuß, H. *Ab Initio* Energy-Adjusted Pseudopotentials for Elements of Groups 13–17. *Molecular Physics* **1993**, *80*, 1431–1441.

(93) Marenich, A. v.; Cramer, C. J.; Truhlar, D. G. Universal Solvation Model Based on Solute Electron Density and on a Continuum Model of the Solvent Defined by the Bulk Dielectric Constant and Atomic Surface Tensions. *J. Phys. Chem. B* **2009**, *113*, 6378–6396.

(94) Legault, C. Y. *CYLView, 1.0b*; Universitéde Sherbrooke: Québec, Montreal, Canada, 2009; (http://www.cylview.org).

(95) Weigend, F.; Ahlrichs, R. Balanced Basis Sets of Split Valence, Triple Zeta Valence and Quadruple Zeta Valence Quality for H to Rn: Design and Assessment of Accuracy. *Phys. Chem. Chem. Phys.* **2005**, *7*, 3297.

(96) Zhao, Y.; Truhlar, D. G. The M06 Suite of Density Functionals for Main Group Thermochemistry, Thermochemical Kinetics, Noncovalent Interactions, Excited States,

and Transition Elements: Two New Functionals and Systematic Testing of Four M06-Class Functionals and 12 Other Functionals. *Theor. Chem. Acc.* **2008**, *120*, 215–241.
(97) Adamo, C.; Barone, V. Toward Reliable Density Functional Methods without Adjustable Parameters: The PBE0 Model. *J. Chem. Phys.* **1999**, *110*, 6158–6170.
(98) Chai, J.-D.; Head-Gordon, M. Long-Range Corrected Hybrid Density Functionals with Damped Atom–Atom Dispersion Corrections. *Phys. Chem. Chem. Phys.* **2008**, *10*, 6615.
(99) Xing, L.; Luscombe, C. K. Advances in Applying C–H Functionalization and Naturally Sourced Building Blocks in Organic Semiconductor Synthesis. *J. Mater. Chem. C* **2021**, *9*, 16391–16409.
(100) Li, C.-J.; Trost, B. M. Green Chemistry for Chemical Synthesis. *Proc. Natl. Acad. Sci.* **2008**, *105*, 13197–13202.
(101) Zhang, K.; Tkachov, R.; Ditte, K.; Kiriy, N.; Kiriy, A.; Voit, B. AB- Versus AA+BB-Suzuki Polycondensation: A Palladium/Tris(Tert-Butyl)Phosphine Catalyst Can Outperform Conventional Catalysts. *Macromol. Rapid Commun.* **2020**, *41*.
(102) Yokozawa, T.; Yokoyama, A. Chain-Growth Condensation Polymerization for the Synthesis of Well-Defined Condensation Polymers and π-Conjugated Polymers. *Chem. Rev.* **2009**, *109*, 5595–5619.
(103) Flory, P. J. Fundamental Principles of Condensation Polymerization. *Chem. Rev.* **1946**, *39*, 137–197.
(104) Nunes, R. W.; Martin, J. R.; Johnson, J. F. Influence of Molecular Weight and Molecular Weight Distribution on Mechanical Properties of Polymers. *Polym. Eng. Sci.* **1982**, *22*, 205–228.
(105) Himmelberger, S.; Vandewal, K.; Fei, Z.; Heeney, M.; Salleo, A. Role of Molecular Weight Distribution on Charge Transport in Semiconducting Polymers. *Macromolecules* **2014**, *47*, 7151–7157.
(106) Szwarc, M.; Levy, M.; Milkovich, R. Polymerization Initiated by Electron Transfer to Monomer. A New Method of Formation of Block Polymers. *J. Am. Chem. Soc.* **1956**, *78*, 2656–2657.
(107) Iovu, M. C.; Sheina, E. E.; Gil, R. R.; McCullough, R. D. Experimental Evidence for the Quasi-"Living" Nature of the Grignard Metathesis Method for the Synthesis of Regioregular Poly(3-Alkylthiophenes). *Macromolecules* **2005**, *38*, 8649–8656.
(108) Miyakoshi, R.; Yokoyama, A.; Yokozawa, T. Catalyst-Transfer Polycondensation. Mechanism of Ni-Catalyzed Chain-Growth Polymerization Leading to Well-Defined Poly(3-Hexylthiophene). *J. Am. Chem. Soc.* **2005**, *127*, 17542–17547.
(109) Yokozawa, T.; Yokoyama, A. Chain-Growth Condensation Polymerization for the Synthesis of Well-Defined Condensation Polymers and π-Conjugated Polymers. *Chem. Rev.* **2009**, *109*, 5595–5619.
(110) Verswyvel, M.; Steverlynck, J.; Hadj Mohamed, S.; Trabelsi, M.; Champagne, B.; Koeckelberghs, G. All-Conjugated ABC- *Block* -Copolymer Formation with a Varying Sequence via an Unassociated Catalyst. *Macromolecules* **2014**, *47*, 4668–4675.
(111) Yokoyama, A.; Yokozawa, T. Converting Step-Growth to Chain-Growth Condensation Polymerization. *Macromolecules* **2007**, *40*, 4093–4101.
(112) Grisorio, R.; Suranna, G. P. Intramolecular Catalyst Transfer Polymerisation of Conjugated Monomers: From Lessons Learned to Future Challenges. *Polym. Chem.* **2015**, *6*, 7781–7795.

(113) Lee, J. A.; Luscombe, C. K. Dual-Catalytic Ag–Pd System for Direct Arylation Polymerization to Synthesize Poly(3-Hexylthiophene). *ACS Macro Lett.* **2018**, *7*, 767–771.
(114) Willot, P.; Govaerts, S.; Koeckelberghs, G. The Controlled Polymerization of Poly(Cyclopentadithiophene)s and Their All-Conjugated Block Copolymers. *Macromolecules* **2013**, *46*, 8888–8895.
(115) Bryan, Z. J.; McNeil, A. J. Conjugated Polymer Synthesis via Catalyst-Transfer Polycondensation (CTP): Mechanism, Scope, and Applications. *Macromolecules* **2013**, *46*, 8395–8405.
(116) Kang, S.; Ono, R. J.; Bielawski, C. W. Controlled Catalyst Transfer Polycondensation and Surface-Initiated Polymerization of a *p* -Phenyleneethynylene-Based Monomer. *J. Am. Chem. Soc.* **2013**, *135*, 4984–4987.
(117) Yokozawa, T.; Kohno, H.; Ohta, Y.; Yokoyama, A. Catalyst-Transfer Suzuki−Miyaura Coupling Polymerization for Precision Synthesis of Poly(*p*-Phenylene). *Macromolecules* **2010**, *43*, 7095–7100.
(118) Sui, A.; Shi, X.; Wu, S.; Tian, H.; Geng, Y.; Wang, F. Controlled Synthesis of Polyfluorenes via Kumada Catalyst Transfer Polycondensation with $Ni(Acac)_2$/Dppp as the Catalyst. *Macromolecules* **2012**, *45*, 5436–5443.
(119) Bryan, Z. J.; Smith, M. L.; McNeil, A. J. Chain-Growth Polymerization of Aryl Grignards Initiated by a Stabilized NHC-Pd Precatalyst. *Macromol. Rapid Commun.* **2012**, *33*, 842–847.
(120) Bridges, C. R.; McCormick, T. M.; Gibson, G. L.; Hollinger, J.; Seferos, D. S. Designing and Refining Ni(II)Diimine Catalysts Toward the Controlled Synthesis of Electron-Deficient Conjugated Polymers. *J. Am. Chem. Soc.* **2013**, *135*, 13212–13219.
(121) Yokozawa, T.; Suzuki, R.; Nojima, M.; Ohta, Y.; Yokoyama, A. Precision Synthesis of Poly(3-Hexylthiophene) from Catalyst-Transfer Suzuki−Miyaura Coupling Polymerization. *Macromol. Rapid Commun.* **2011**, *32*, 801–806.
(122) Willot, P.; Steverlynck, J.; Moerman, D.; Leclère, P.; Lazzaroni, R.; Koeckelberghs, G. Poly(3-Alkylthiophene) with Tuneable Regioregularity: Synthesis and Self-Assembling Properties. *Polym. Chem.* **2013**, *4*, 2662.
(123) Okamoto, K.; Luscombe, C. K. Controlled Polymerizations for the Synthesis of Semiconducting Conjugated Polymers. *Polym. Chem.* **2011**, *2*, 2424.
(124) Lee, S. R.; Bloom, J. W. G.; Wheeler, S. E.; McNeil, A. J. Accelerating Ni(II) Precatalyst Initiation Using Reactive Ligands and Its Impact on Chain-Growth Polymerizations. *Dalton Trans.* **2013**, *42*, 4218.
(125) Yokoyama, A.; Suzuki, H.; Kubota, Y.; Ohuchi, K.; Higashimura, H.; Yokozawa, T. Chain-Growth Polymerization for the Synthesis of Polyfluorene via Suzuki−Miyaura Coupling Reaction from an Externally Added Initiator Unit. *J. Am. Chem. Soc.* **2007**, *129*, 7236–7237.
(126) Lesieur, M.; Lazreg, F.; Cazin, C. S. J. A Cooperative Pd–Cu System for Direct C–H Bond Arylation. *Chem. Commun.* **2014**, *50*, 8927–8929.

Vita

PROFESSIONAL EXPERIENCE

2017 – Present **PhD Graduate Research Assistant with Prof. Christine Luscombe**

University of Washington, Seattle, WA

- Dual-catalytic systems for cross dehydrogenative coupling (CDC) toward donor-acceptor π-conjugated polymer synthesis

2015 – 2017 **Master's Graduate Research Assistant with Prof. Coleen Pugh**

University of Akron, Akron, OH

- Photo and thermo-crosslinking of polystyrene containing 1-functionalized benzocyclobutenes

AWARDS & FELLOWSHIPS

2021 Data Intensive Research Enabling Clean Technologies (DIRECT) Program

2020 NSF Center for C-H Functionalization International Research Experience Fellowship

2019 Torrance Foundation Tech Due Diligence Fellowship

2019 Clean Energy Institute Graduate Fellowship

LEADERSHIP & CIVIC ACTIVITIES

2020 – Present **Communications Lead** *Students in Clean Energy, Clean Energy Institute*

2020 **Outreach Volunteer** *Climate Change // Curiosity Expo, Pacific Science Center, Seattle, WA*

2019 **Outreach Volunteer** *Understanding the Principles of Fuel Cell, Einstein Middle School, Shoreline, WA*

2019 – Present **Research Mentor** *University of Washington*

Luscombe Group

- Shan Zhang, Applied Master's Program
- Erin Mee, Undergraduate Research
- Tabatha de la Rosa, Undergraduate Research

2017 **Research Mentor** *University of Akron*

Pugh Group

- Ted Hammer, First Year PhD Research

COMMUNICATION

Presentations

2022 71st SPSJ Annual Meeting (virtual) – Japan

2021 13th Annual Frontiers in C–H Functionalization Conference (virtual) – Atlanta, GA

2019 11th Annual Frontiers in C–H Functionalization Conference – Atlanta, GA

2018 10th Annual Frontiers in C-H Functionalization Conference – Atlanta, GA

Publications

2022 Xing, L.; Liu, J. -R.; Hong, X.; Houk, K. N.; Luscombe, C. K. An exception to Carothers equation caused by the accelerated chain extension in a Pd/Ag co-catalyzed cross dehydrogenative coupling polymerization. *J. Am. Chem. Soc.* **2022**, *144*, 2311–2322.

2021 Xing, L.; Luscombe, C. K. Advances in Applying C-H Functionalization and Naturally Sourced Building Blocks for Organic Semiconductor Synthesis. *J. Mater. Chem. C* **2021**, *9*, 16391-16409.

2019 Kang, L. J.; Xing, L.; Luscombe, C. K. Exploration and Development of Gold- and Silver Catalyzed Cross Dehydrogenative Coupling Toward Donor–Acceptor π-Conjugated Polymer Synthesis. *Polym. Chem*. **2019**, *10*, 486-493.